Constitutive laws of composite materials via multi-axial testing and numerical optimization
by Dongfang Huang

A thesis submitted in partial fulfillment of the requirements for the degree of Master of Science in Mechanical Engineering
Montana State University

Abstract:
The use of composite materials in structural components has increased dramatically in recent years. As applications become more demanding, the need for reliable prediction of their mechanical properties is increasing as well.

Four different loading paths were applied with multi-axial testing, and the corresponding FEM modeling was created. After carrying out optimization, the optimum engineering constants were obtained. This set of optimum properties is very close to those obtained with standard unidirectional testing. Fewer tests are required, less time is taken, and more precise properties are gained with this procedure.

CONSTITUTIVE LAWS OF COMPOSITE MATERIALS VIA MULTI-AXIAL TESTING AND NUMERICAL OPTIMIZATION

by

Dongfang Huang

A thesis submitted in partial fulfillment
of the requirements for the degree

of

Master of Science

in

Mechanical Engineering

MONTANA STATE UNIVERSITY – BOZEMAN
Bozeman, Montana

September 2003

APPROVAL

Of a thesis submitted by

Dongfang Huang

This thesis has been read by each member of the thesis committee and has been found to be satisfactory regarding content, English usage, format, citations, bibliographic style, and consistency, and is ready for submission to the College of Graduate Studies.

Dr. Douglas Cairns _____ (Signature) 9/2/03 Date

Approved for the Department of Mechanical Engineering

Dr. Vic Cundy _____ (Signature) 9/2/03 Date

Approved for the college of Graduate Studies

Dr. Bruce McLeod _____ (Signature) 9-8-03 Date

STATEMENT OF PERMISSION TO USE

In presenting this thesis in partial fulfillment of the requirements for a master's degree at Montana State University-Bozeman, I agree that the Library shall make it available to borrowers under rules of the Library.

If I have indicated my intention to copyright this thesis by including a copyright notice page, copying is allowable only for scholarly purposes, consistent with "fair use" as prescribed in the U.S. Copyright Law. Requests for permission for extended quotation from or reproduction of this thesis in whole or in parts may be granted only by copyright holder.

Signature Dongfang Huang

Date 09/02/03

ACKNOWLEDGEMENT

First and foremost I would like to thank my parents for their encouragement and patience throughout this process.

This project would not have been possible without the guidance and direction provided by my advisor, Dr. Cairns. I would also like to thank the MSU composites group who extended a helping hand in my study.

TABLE OF CONTENTS

TABLE OF CONTENTS – CONTINUED

TABLE OF CONTENTS – CONTINUED

TABLE OF CONTENTS – CONTINUED

LIST OF TABLES

LIST OF TABLES – CONTINUED

LIST OF TABLE – CONTINUED

LIST OF FIGURES

LIST OF FIGURE – CONTINUED

LIST OF FIGURE – CONTINUED

LIST OF FIGURE – CONTINUED

Figure Page

ABSTRACT

The use of composite materials in structural components has increased dramatically in recent years. As applications become more demanding, the need for reliable prediction of their mechanical properties is increasing as well.

Four different loading paths were applied with multi-axial testing, and the corresponding FEM modeling was created. After carrying out optimization, the optimum engineering constants were obtained. This set of optimum properties is very close to those obtained with standard unidirectional testing. Fewer tests are required, less time is taken, and more precise properties are gained with this procedure.

CHAPTER 1

INTRODUCTION

The use of composite materials in structural components has increased dramatically in recent years as their cost of production continues to decline and advances in composite design methodology become increasingly widespread. As applications become more demanding, the need for reliable prediction of their mechanical properties and behavior is becoming ever more important [1].

As a result of the increased demands on the structural applications of composites, efforts have been made to investigate the mechanical properties in composite materials at structural levels [1]. However, familiarity with orthotropic behaviors is needed to characterize the material behavior of composites. These behaviors require detailed and well organized test methods to determine the associated laminate properties.

The Montana State University (MSU) composite team built an In Plane Loader (or IPL). The IPL is designed and built for gaining a better understanding of material properties, especially composite material properties. The IPL is a highly computerized automatic machine which can collect the reaction forces and displacements at specific points when applying a variety of pre-selected loading paths. Moreover, the IPL built by MSU allows the low cost, simple, and easy experiments to be used for acquiring composite properties. The IPL in MSU composite lab is illustrated in Figure 1.01.

On the other hand, there are some numerical approaches for predicting composite properties as well. Finite element method (FEM) modeling is an appropriate way to gain

the knowledge of material behavior by means of simulation. ANSYS, the powerful computer program, was selected to accomplish FEM modeling. [3] Besides the FEM model, two numerical techniques, bounding techniques and optimization, were also used to determine the composite properties.

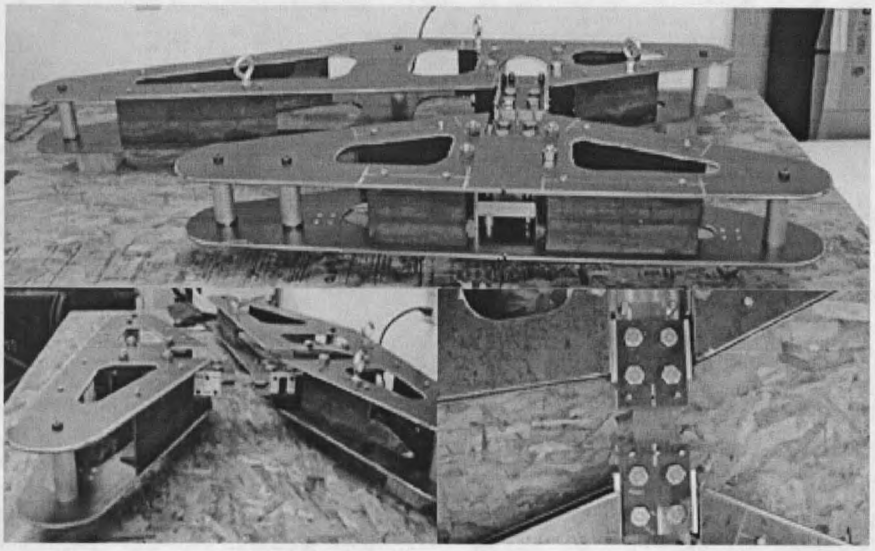

Figure 1.01 The In-Plane Loader machine

Although many numerical approaches have been developed to predict composite properties, these may not be accurate and must be verified with experimental results. Namely, the FEM modeling results have to be compared with the experimental data obtained by the IPL machine. If both data match, the FEM modeling results can be considered accurate. If not, an optimization procedure can be carried out in order to find values that optimize the difference between FEM modeling and experimental data.

This methodology may be a more effective approach than the traditional ones used to estimate a composite's properties. The current research provides an investigation into the efficiency, cost, and precision of this methodology to determine composite properties.

Motivation

Conventional approaches for determining the constitutive law of composites require conducting multiple experiments. Significant time is often spent collecting and analyzing the experimental data in order to estimate the material constitutive properties. However, convention characterization procedure is time-consuming, tedious, labor-intensive, inaccurate, and often prohibitive to complete characterization.

A more practical approach, which is more efficient and accurate, is strongly desired. This more desirable approach would involve limited experiments and would yield a more precise constitutive law by employing multiple loadings on a simple sample combined with numerical techniques, such as finite element analysis, optimization, and bounding techniques.

The constitutive behavior of a composite laminate in structural components is complicated. The lamina properties can be estimated by micromechanical analysis procedures, and lamina properties can be measured by physical means in a macromechanical analysis of the structure. In this work, micromechanical analysis deals with the individual constituent materials mechanical response to determine the equivalent combined continuum mechanical response. Real design power is realized when the micromechanical estimate of the properties of a lamina agree with the measured properties. However, it should be noted that a micromechanical analysis has inherent limitations. The micromechanical theories must be validated by careful experimental work [2].

Because this discrepancy exists between the micro-structure of the composites in practical analysis and the assumed perfect micro-structure of composites in theoretical analysis, it is inevitable that the engineering constants of composites estimated by micromechanical analysis will not agree with the experimental data of the physical tests. The purpose of this study is to find more accurate engineering constants which agree well with the experimental data. Several numerical analysis techniques are employed to explore whether or not the approach is feasible.

Objective and Approach

Our goal of this research is to find an appropriate methodology to determine the composite laminate properties. Note that this research is restricted to linear elastic behavior.

Micromechanical analysis and macromechanical analysis are used in numerical modeling and experimental approaches respectively. Furthermore, the mechanics of materials approach and elasticity approach are employed to estimate the engineering constants of a composite, to examine the feasibility of the technique, and determine the upper and lower bounds of each engineering constant.

Coupons with a notch were selected to determine the composite constitutive law by means of the IPL tests and mathematical modeling.

As mentioned above, the MSU composite team has built the IPL in the materials lab. The IPL machine is used to conduct the tests and to obtain the reaction forces and displacements of a specific point in each test specimen.

FEM modeling is used to simulate the experiments on the IPL and to gain the corresponding reaction forces and displacements at a specific point. ANSYS was the program used for the FEM modeling.

The IPL is a testing machine capable of providing any combination of in-plane loads on a sample. Four loading paths were designed and applied to the coupons in this research. These were tensile (open/close), tensile + shear (sliding), rotation (moment), and tensile + shear + rotation. Upon applying the loading sequences to the coupons, data of reaction forces and displacements were acquired. Meanwhile, the FEM model was used to calculate the corresponding reaction forces and displacements as well. The optimization procedure was needed if there was a discrepancy between the results of FEM modeling and experiments.

The reaction forces and displacements depend on the composite properties, geometry and the specific loadings. The following function depicts the relationship.

$$F_n^r, \delta_n^r = F_n^r, \delta_n^r (E, G, \upsilon, g, f, \delta) \qquad (1.01)$$

where E, G and υ are the elastic moduli of fiber reinforced composite, g stands for the specific geometry of the sample, f and δ are respectively the applied forces and applied displacements, and F_n^r and δ_n^r are the reaction forces and displacements at the specific nodes respectively.

The optimization is accomplished by minimizing the discrepancy between the FEM modeling results and the experimental results.

$$\left| \left(F_n^r, \delta_n^r\right)_{Computer} - \left(F_n^r, \delta_n^r\right)_{Experiment} \right| = e \qquad (1.02)$$

where $\left(F_n^r, \delta_n^r\right)_{Computer}$ is the data of reaction forces and displacement obtained by computer modeling, $\left(F_n^r, \delta_n^r\right)_{Experiment}$ is the reaction forces and displacement obtained by experiments, and e is the error to be minimized.

The objective of this research is to determine the constitutive law (or engineering constants) of composites by means of several numerical analysis techniques and experimental data by IPL. The operation procedure is illustrated in Figure 1.02.

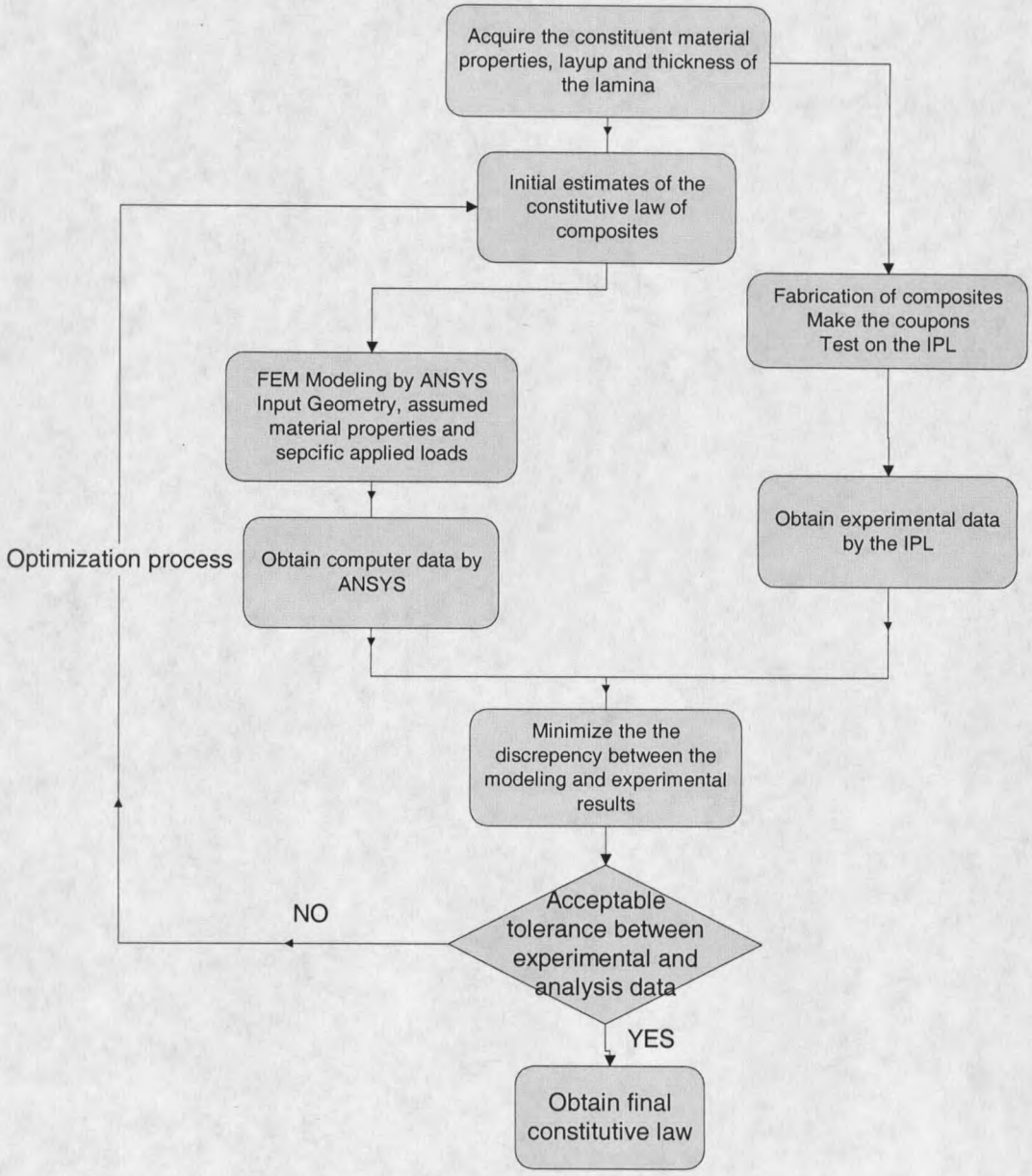

Chart 1.02 Flow chart of determining the composite constitutive properties

Organization of Thesis

In Chapter 2, theories of elasticity and mechanics of composite materials are introduced briefly as these theories are used to determine the initial constitutive law of composites with the aid of the numerical analysis techniques. In chapter 3, the fabrication of composite samples and experimental procedures are described. In Chapter 4, the details of numerical approaches of composite engineering constants are demonstrated, and finite element analysis modeling, optimization and bounding techniques are described. In chapter 5, experimental results are presented, numerical results and experimental data are compared. In chapter 6, the conclusions from this study are presented as well as a list of items that should be included in future studies.

CHAPTER 2

BACKGROUND

This research involves elasticity theory and focuses upon composite materials. The theory of elasticity and mechanics of composite materials are introduced briefly in this chapter. A key concept is that the micromechanical estimation of the engineering constants of a composite must agree with the experimental data, thus leading to an approach of determining more accurate engineering constants by means of a combined empirical and numerical analysis technique. The In-Plane Loader machine, which is designed to facilitate the testing of mechanical behaviors of composites is described in this chapter as well.

Introduction to Linear Elastic Solids

Concepts and Definitions

The current research is limited to linear elastic behavior. Generalized anisotropic Hooke's constitutive law states [3]

$$\sigma_{ij} = C_{ijkl}\varepsilon_{kl} \tag{2.01}$$

$$\varepsilon_{ij} = S_{ijkl}\sigma_{kl} \tag{2.02}$$

where, C_{ijkl} is the elastic stiffness tensor,
S_{ijkl} is the elastic compliance tensor,
σ_{ij} is the second order stress tensor,
ε_{kl} is the second order strain tensor.

The relationship between elastic stiffness and compliance can be expressed as:

$$S_{ijkl} = C_{ijkl}^{-1} \tag{2.03}$$

Hooke's law written in matrix from Eq.(2.01) becomes:

$$\begin{pmatrix} \sigma_{11} \\ \sigma_{22} \\ \sigma_{33} \\ \sigma_{23} \\ \sigma_{31} \\ \sigma_{12} \\ \sigma_{32} \\ \sigma_{13} \\ \sigma_{21} \end{pmatrix} = \begin{pmatrix} C_{1111} & C_{1122} & C_{1133} & C_{1123} & C_{1131} & C_{1112} & C_{1132} & C_{1113} & C_{1121} \\ C_{2211} & C_{2222} & C_{2233} & C_{2223} & C_{2231} & C_{2212} & C_{2232} & C_{2213} & C_{2221} \\ C_{3311} & C_{3322} & C_{3333} & C_{3323} & C_{3331} & C_{3312} & C_{3332} & C_{3313} & C_{3321} \\ C_{2311} & C_{2322} & C_{2333} & C_{2323} & C_{2331} & C_{2312} & C_{2332} & C_{2313} & C_{2321} \\ C_{3111} & C_{3122} & C_{3133} & C_{3123} & C_{3131} & C_{3112} & C_{3132} & C_{3113} & C_{3121} \\ C_{1211} & C_{1222} & C_{1233} & C_{1223} & C_{1231} & C_{1212} & C_{1232} & C_{1213} & C_{1221} \\ C_{3211} & C_{3222} & C_{3233} & C_{3223} & C_{3231} & C_{3212} & C_{3232} & C_{3213} & C_{3221} \\ C_{1311} & C_{1322} & C_{1333} & C_{1323} & C_{1331} & C_{1312} & C_{1332} & C_{1313} & C_{1321} \\ C_{2111} & C_{2122} & C_{2133} & C_{2123} & C_{2131} & C_{2112} & C_{2132} & C_{2113} & C_{2121} \end{pmatrix} \cdot \begin{pmatrix} \varepsilon_{11} \\ \varepsilon_{22} \\ \varepsilon_{33} \\ \varepsilon_{23} \\ \varepsilon_{31} \\ \varepsilon_{12} \\ \varepsilon_{32} \\ \varepsilon_{13} \\ \varepsilon_{21} \end{pmatrix}$$

(2.04)

In this model, σ_{ij} and ε_{ij} are the second order stress and strain tensors, and C_{ijkl} and S_{ijkl} are referred to as fourth order stiffness and compliance tensors. Young's moduli, shear moduli, and Poisson ratios, (E, G and υ), which are the physical interpreters of materials and are useful in engineering analysis. Hence, the stiffness and compliance in terms of engineering constants represent the characterized properties of material, and are referred to as the constitutive parameters of a solid material [3].

Fortunately, there is no need to deal with these fourth order tensors and 81 elastic constants because various symmetry conditions simplify the equations considerably in practice. As shown in any mechanics of materials book, both stresses and strains are symmetric (i.e., $\sigma_{ij} = \sigma_{ji}$, and $\varepsilon_{ij} = \varepsilon_{ji}$), so that there are only six independent stress components and six independent strain components. This means that the elastic constants

must be symmetric with respect to the first two subscripts and with respect to the last two subscripts (i.e., $C_{ijkl} = C_{jikl}$ and $C_{ijkl} = C_{ijlk}$ where $i, j, k, l = 1,2,3$), and that the number of nonzero elastic constants is now reduced to 36. Furthermore, since $C_{ijkl} = C_{klij}$, the number of independent constants is reduced to 21. These simplifications lead to a contracted notation. With this contracted notation the generalized Hook's law can be written as:

$$\sigma_i = C_{ij}\varepsilon_j \qquad i, j = 1,2,...,6 \qquad \text{or} \qquad \{\sigma\} = [C]\{\varepsilon\} \tag{2.05}$$

$$\varepsilon_i = S_{ij}\sigma_j \qquad i, j = 1,2,...,6 \qquad \text{or} \qquad \{\varepsilon\} = [S]\{\sigma\} \tag{2.06}$$

where the stiffness and compliance matrices (or elastic constant matrices) are now 6 x 6 with 21 independent components and the stresses and strains are column vectors.

Further simplifications of the stiffness and compliance matrices are possible if the material properties have some forms of symmetry. If a linearly elastic solid has two mutually perpendicular planes of symmetry, say plane 1 with unit e_1 and plane 2 with unit e_2, then automatically the plane 3 with a normal in the direction of e_3 is also a plane of material symmetry. The material is called an <u>*orthotropic material*</u>. (see Figure 2.01).

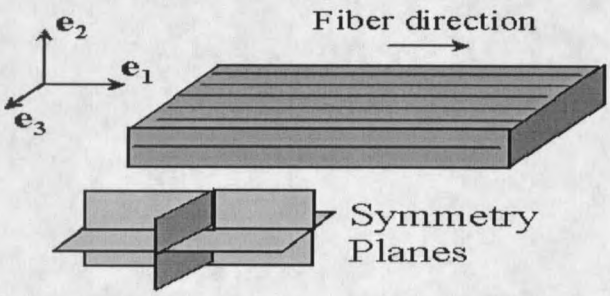

Figure 2.01 Illustration of the orthotropic material (Three planes of symmetry)

The stiffness and compliance matrices of orthotropic materials are expressed by equation (2.07) and (2.08), where C_{ij} and S_{ij} are all 6 x 6 matrices and the number of independent components is nine.

$$C_{ij} = \begin{pmatrix} C_{11} & C_{12} & C_{13} & 0 & 0 & 0 \\ C_{12} & C_{22} & C_{23} & 0 & 0 & 0 \\ C_{13} & C_{23} & C_{33} & 0 & 0 & 0 \\ 0 & 0 & 0 & C_{44} & 0 & 0 \\ 0 & 0 & 0 & 0 & C_{55} & 0 \\ 0 & 0 & 0 & 0 & 0 & C_{66} \end{pmatrix} \tag{2.07}$$

$$S_{ij} = \begin{pmatrix} S_{11} & S_{12} & S_{13} & 0 & 0 & 0 \\ S_{12} & S_{22} & S_{23} & 0 & 0 & 0 \\ S_{13} & S_{23} & S_{33} & 0 & 0 & 0 \\ 0 & 0 & 0 & S_{44} & 0 & 0 \\ 0 & 0 & 0 & 0 & S_{55} & 0 \\ 0 & 0 & 0 & 0 & 0 & S_{66} \end{pmatrix} \tag{2.08}$$

If there exists a plane, say plane 3, such that every plane perpendicular to it is a plane of material symmetry, then the material is called a <u>*transversely isotropic material*</u>. For example, the properties of materials along the direction 2 are the same as those along the direction 3; then this material is regarded as a transversely isotropic material with respect to 2-3 plane. For such a material we would expect that $C_{22} = C_{33}$, $C_{12} = C_{13}, C_{55} = C_{66}$, and that C_{44} would not be independent from the other stiffness. The complete stiffness and compliance matrices for a specially orthotropic, transversely isotropic material are of the form [3]:

$$C_{ij} = \begin{pmatrix} C_{11} & C_{12} & C_{12} & 0 & 0 & 0 \\ C_{12} & C_{22} & C_{23} & 0 & 0 & 0 \\ C_{12} & C_{23} & C_{22} & 0 & 0 & 0 \\ 0 & 0 & 0 & \frac{C_{22} - C_{23}}{2} & 0 & 0 \\ 0 & 0 & 0 & 0 & C_{66} & 0 \\ 0 & 0 & 0 & 0 & 0 & C_{66} \end{pmatrix} \tag{2. 09}$$

$$S_{ij} = \begin{bmatrix} S_{11} & S_{12} & S_{12} & 0 & 0 & 0 \\ S_{12} & S_{22} & S_{23} & 0 & 0 & 0 \\ S_{12} & S_{23} & S_{22} & 0 & 0 & 0 \\ 0 & 0 & 0 & 2(S_{22} - S_{23}) & 0 & 0 \\ 0 & 0 & 0 & 0 & S_{66} & 0 \\ 0 & 0 & 0 & 0 & 0 & S_{66} \end{bmatrix} \tag{2.10}$$

Equations (2.09) and (2.10) have five independent elastic constants. When a material is characterized experimentally, the engineering constants such as Young's modulus E, shear modulus G, and Poisson's ratio υ are usually measured instead of the C_{ij} or S_{ij}. These engineering constants are used in analysis and design because they are easily defined and interpreted in terms of simple states of stress and strain.

$$\begin{pmatrix} \varepsilon_{11} \\ \varepsilon_{22} \\ \varepsilon_{33} \\ \gamma_{23} \\ \gamma_{31} \\ \gamma_{12} \end{pmatrix} = \begin{pmatrix} \frac{1}{E_1} & \frac{-\nu_{12}}{E_1} & \frac{-\nu_{13}}{E_1} & 0 & 0 & 0 \\ \frac{-\nu_{21}}{E_2} & \frac{1}{E_2} & \frac{-\nu_{23}}{E_2} & 0 & 0 & 0 \\ \frac{-\nu_{31}}{E_3} & \frac{-\nu_{32}}{E_3} & \frac{1}{E_3} & 0 & 0 & 0 \\ 0 & 0 & 0 & \frac{1}{G_{23}} & 0 & 0 \\ 0 & 0 & 0 & 0 & \frac{1}{G_{13}} & 0 \\ 0 & 0 & 0 & 0 & 0 & \frac{1}{G_{12}} \end{pmatrix} \cdot \begin{pmatrix} \sigma_{11} \\ \sigma_{22} \\ \sigma_{33} \\ \tau_{23} \\ \tau_{13} \\ \tau_{12} \end{pmatrix} \tag{2.11}$$

where E_1, E_2 and E_3 are the longitudinal moduli with respect to directions 1, 2 and 3 respectively; $\upsilon_{21}, \upsilon_{23}$ and υ_{13} are the Poisson ratios along with plane 2-1, plane 2-3, and plane 1-3, respectively; G_{12}, G_{23} and G_{13} are the shear moduli associated with the plane 1-2, plane 2-3 and plane 1-3, respectively.

The stress-strain relationship of the orthotropic materials in terms of engineering constants can be expressed as equation (2.11).

The stress-strain relationship of transversely isotropic material with respect of plane 2-3 in terms of engineering constants can be expressed as

$$\begin{pmatrix} \varepsilon_{11} \\ \varepsilon_{22} \\ \varepsilon_{33} \\ \gamma_{23} \\ \gamma_{31} \\ \gamma_{12} \end{pmatrix} = \begin{pmatrix} \frac{1}{E_1} & \frac{-\nu_{21}}{E_2} & \frac{-\nu_{21}}{E_2} & 0 & 0 & 0 \\ \frac{-\nu_{21}}{E_2} & \frac{1}{E_2} & \frac{-\nu_{23}}{E_2} & 0 & 0 & 0 \\ \frac{-\nu_{21}}{E_2} & \frac{-\nu_{23}}{E_2} & \frac{1}{E_2} & 0 & 0 & 0 \\ 0 & 0 & 0 & \frac{1}{G_{23}} & 0 & 0 \\ 0 & 0 & 0 & 0 & \frac{1}{G_{12}} & 0 \\ 0 & 0 & 0 & 0 & 0 & \frac{1}{G_{12}} \end{pmatrix} \cdot \begin{pmatrix} \sigma_{11} \\ \sigma_{22} \\ \sigma_{33} \\ \tau_{23} \\ \tau_{13} \\ \tau_{12} \end{pmatrix} \tag{2.12}$$

where

$$G_{23} = \frac{E_2}{2(1+\upsilon_{32})} \tag{2.13}$$

(Note: the stress-strains relationship with the stiffness matrix $[C]$ can be gained accordingly.)

Restrictions on Engineering Constants

For an orthotropic material, the symmetric stiffness matrix with nine coefficients can be expressed as equation (2.12). Then, the relationships between C_{ij} and the engineering constants are given by: [2]

$$C_{11} = \frac{1-\upsilon_{23}\upsilon_{32}}{E_2E_3\Delta}, \qquad C_{12} = \frac{\upsilon_{12}+\upsilon_{31}\upsilon_{23}}{E_2E_3\Delta}, \qquad C_{23} = \frac{\upsilon_{31}+\upsilon_{21}\upsilon_{32}}{E_2E_3\Delta}$$

$$C_{22} = \frac{1-\upsilon_{13}\upsilon_{31}}{E_1E_3\Delta}, \qquad C_{23} = \frac{\upsilon_{32}+\upsilon_{12}\upsilon_{31}}{E_1E_3\Delta}, \qquad C_{33} = \frac{1-\upsilon_{12}\upsilon_{21}}{E_1E_2\Delta} \tag{2.14}$$

$$C_{44} = G_{23}, \qquad C_{55} = G_{31}, \qquad C_{66} = G_{12} \tag{2.15}$$

where

$$\Delta = \frac{1-\upsilon_{12}\upsilon_{21}-\upsilon_{23}\upsilon_{32}-\upsilon_{31}\upsilon_{13}-2\upsilon_{21}\upsilon_{32}\upsilon_{13}}{E_1E_2E_3} \tag{2.16}$$

The relationships among engineering constants are more complex. Those relationships must be investigated thoroughly in order to avoid the pitfalls of an intuition built up on the basis of working with isotropic materials. Thus, it is required that the elements of both the stiffness and compliance matrices must be numerically positive.

This mathematical condition can be replaced by the following physical argument. [1]

$$S_{11}, S_{22}, S_{33}, S_{44}, S_{55}, S_{66} > 0 \tag{2.17}$$

or in terms of the engineering constants,

$$E_1, E_2, E_3, G_{23}, G_{31}, G_{12} > 0 \tag{2.18}$$

We note also that the compliance matrix is symmetric so that

$$\frac{\upsilon_{12}}{E_1} = \frac{\upsilon_{21}}{E_2}, \quad \frac{\upsilon_{13}}{E_1} = \frac{\upsilon_{31}}{E_3}, \quad \frac{\upsilon_{23}}{E_2} = \frac{\upsilon_{32}}{E_3} \tag{2.19}$$

The determinant of a matrix and all sub-determinants must be positive definiteness. For positive definiteness, with these criteria, the restrictions for the engineering constants are as follows [2]

$$\upsilon_{21}^2 < \left(\frac{E_2}{E_1}\right);\ \upsilon_{12}^2 < \left(\frac{E_1}{E_2}\right);\ \upsilon_{32}^2 < \left(\frac{E_3}{E_2}\right)$$

$$\upsilon_{23}^2 < \left(\frac{E_2}{E_3}\right);\ \upsilon_{13}^2 < \left(\frac{E_1}{E_3}\right);\ \upsilon_{31}^2 < \left(\frac{E_3}{E_1}\right) \tag{2.20}$$

Also,

$$1 - \upsilon_{12}\upsilon_{21} - \upsilon_{23}\upsilon_{32} - \upsilon_{31}\upsilon_{13} - 2\upsilon_{21}\upsilon_{32}\upsilon_{13} > 0 \tag{2.21}$$

For a transversely isotropic material, the compliance matrix in terms of engineering constants is shown as equation (2.14). Because the compliance matrix is positive definite, the diagonal elements are positive definite. That is, [2]

$$E_1, E_2, G_{23}, G_{12} > 0 \tag{2.22}$$

Also,

$$\det\begin{bmatrix} \frac{1}{E_1} & \frac{-\upsilon_{21}}{E_2} \\ \frac{-\upsilon_{21}}{E_2} & \frac{1}{E_2} \end{bmatrix} = \frac{1}{E_1 E_2}\left(1 - \frac{E_1}{E_2}\upsilon_{21}^2\right) > 0 \tag{2.23}$$

i.e.,

$$\upsilon_{21}^2 < \frac{E_2}{E_1} \quad \text{or} \quad \upsilon_{12}\upsilon_{21} < 1 \tag{2.24}$$

$$\det\begin{bmatrix} \frac{1}{E_2} & \frac{-\upsilon_{23}}{E_2} \\ \frac{-\upsilon_{23}}{E_2} & \frac{1}{E_2} \end{bmatrix} = \frac{1}{E_2^2}\left(1 - \upsilon_{23}^2\right) > 0 \tag{2.25}$$

i.e.,

$$-1 < \upsilon_{23} < 1 \tag{2.26}$$

Also,

$$\det\begin{bmatrix} \frac{1}{E_1} & \frac{-\upsilon_{21}}{E_2} & \frac{-\upsilon_{21}}{E_2} \\ \frac{-\upsilon_{21}}{E_2} & \frac{1}{E_2} & \frac{-\upsilon_{23}}{E_2} \\ \frac{-\upsilon_{21}}{E_2} & \frac{-\upsilon_{23}}{E_2} & \frac{1}{E_2} \end{bmatrix} = \frac{1}{E_1 E_2^2}(1+\upsilon_{23})\left(1-\upsilon_{23}-2\left(\frac{E_1}{E_2}\right)\upsilon_{21}^2\right) \tag{2.27}$$

Since $1+\upsilon_{23} > 0$, therefore,

$$1-2\upsilon_{21}^2\left(\frac{E_1}{E_2}\right) > \upsilon_{23} \quad \text{or} \quad 1-2\upsilon_{21}\upsilon_{12} > \upsilon_{23} \tag{2.28}$$

The assumed engineering constants have to agree with the restrictions.

Coordinate Transformation

If the material coordinate system is rotated about any axis, the material parameters vary significantly. The rotation matrix is as follows [3]:

$$a_{i'k} = \cos(i',k) = \cos(\theta) \tag{2.29}$$

$$A = \begin{bmatrix} a_{x'x} & a_{x'y} & a_{x'z} \\ a_{y'x} & a_{y'y} & a_{y'z} \\ a_{z'x} & a_{z'y} & a_{z'z} \end{bmatrix} \tag{2.30}$$

Suppose the coordinate system is rotated about the z-axis by an arbitrary angle θ. To determine the effect on the material parameters, it is necessary to return to the fourth order compliance tensor, S_{ijkl}, and the transformation matrix can be expressed as

$$A = \begin{pmatrix} \cos(\theta) & \sin(\theta) & 0 \\ -\sin(\theta) & \cos(\theta) & 0 \\ 0 & 0 & 1 \end{pmatrix} \tag{2.31}$$

The fourth order tensor's transformation formula is as follows: [3]

$$C_{i'j'k'l'} = a_{i'm} a_{j'n} a_{k'p} a_{l'q} C_{mnpq} \tag{2.32}$$

$$S_{i'j'k'l'} = a_{i'm} a_{j'n} a_{k'p} a_{l'q} S_{mnpq} \tag{2.33}$$

where $C_{i'j'k'l'}$, $S_{i'j'k'l'}$, C_{mnpq} and S_{mnpq} are all fourth order tensors, and $a_{i'k}$ represents cosine of the angle between the rotated and original axis.

Mechanics of Composite Materials

Two levels can be taken to investigate the mechanical behavior of fiber reinforced composite materials, micromechanical and macromechanical analysis. Micromechanics is concerned with the mechanical behavior of constituent materials (fiber and matrix materials), the interaction of these constituents, and the resulting behavior of the basic composite. Macromechanics is concerned with the equivalent homogeneous continuum mechanical behavior of composite materials and structures as equivalent engineering properties without regard for the constituent materials or their interactions.

A composite material is obviously heterogeneous at the constituent material level, with properties possibly changing from point to point. However, the macromechanical stress-strain relationships of the lamina can be expressed in terms of average stresses and strains and effective properties of an equivalent homogeneous material. The properties of

a composite are usually anisotropic. That is, the properties associated with an axis passing through a point in the material generally depend on the orientation of the axis. Fortunately, each type of composite has characteristic material property symmetries associated with various types of composite laminae.

Certain mathematical manipulations will be used to simplify the directional nature of composite properties.

Macromechanical Approach

The properties of composites are referred to as homogeneous and anisotropic, with various kinds of symmetries. The composite material selected for this research is the unidirectional fiber D155 [4]. The D155 composite laminae have directions of 0°, +45°, 90°, and -45°, which are symmetric about the mid-plane. The layup is denoted as [0/+45/90/-45]s. The constitutive properties of each layer are theoretically the same in any direction perpendicular to the fiber.

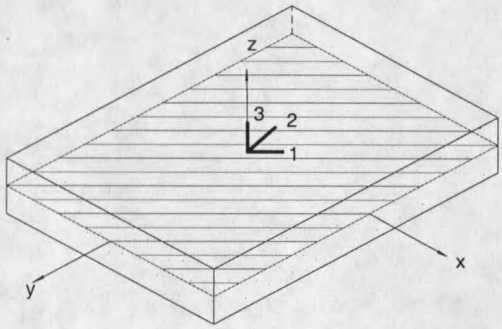

Figure 2.02 Transversely isotropic material associated with plane 2-3

See Figure 2.02 (i.e., the properties along the 2 direction are the same as those along the 3 direction), and the material is transversely isotropic. The composite in this research is a transversely isotropic material with respect to material principal plane 2-3.

The stresses and strains are defined in the principal material directions (or local coordinates) for an orthotropic material. However, the principal directions of orthotropy often do not coincide with coordinate directions that are geometrically natural to the solution of the problem. In this work, the coordinate directions of selected geometry are different from the principal material directions (See the Figure 2.03), which is non-principal direction (or global coordinate). The angles are 0°, +45°, -45°, 90° between the principal (Local) and non-principal direction. (Global)

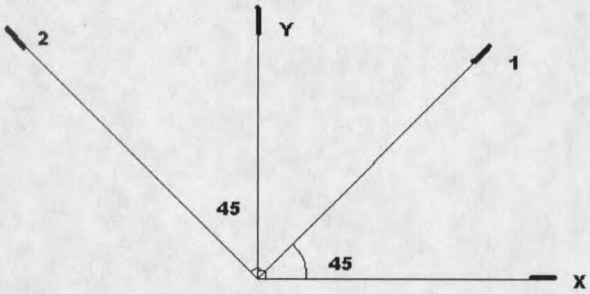

Figure 2.03 Orientation of the global and local coordinate

There, the coordinates natural to the solution of the coupon are X, Y, Z, whereas the principle material coordinates are 1,2,3. The angle between X-1 and Y-2 is 45°, Z is parallel to the principle direction 1. Thus, a relationship is needed between the stresses and strains in the principal material directions and those in the global coordinates. Then, a method of transforming stress-strain relations from one coordinates system to another is also needed.

As discussed in the previous sections, the 6 x 6 stiffness and compliance matrices have to be re-arranged to fourth order tensor form in order to conduct coordinate rotation.

$$\begin{pmatrix} \varepsilon_{11} \\ \varepsilon_{22} \\ \varepsilon_{33} \\ \varepsilon_{23} \\ \varepsilon_{31} \\ \varepsilon_{12} \\ \varepsilon_{32} \\ \varepsilon_{13} \\ \varepsilon_{21} \end{pmatrix} = \begin{bmatrix} \frac{1}{E_1} & \frac{-\nu_{12}}{E_2} & \frac{-\nu_{12}}{E_2} & 0 & 0 & 0 & 0 & 0 & 0 \\ \frac{-\nu_{12}}{E_2} & \frac{1}{E_2} & \frac{-\nu_{23}}{E_2} & 0 & 0 & 0 & 0 & 0 & 0 \\ \frac{-\nu_{12}}{E_2} & \frac{-\nu_{23}}{E_2} & \frac{1}{E_2} & 0 & 0 & 0 & 0 & 0 & 0 \\ 0 & 0 & 0 & \frac{2(1+\nu_{23})}{E_2} & 0 & 0 & \frac{2(1+\nu_{23})}{E_2} & 0 & 0 \\ 0 & 0 & 0 & 0 & \frac{1}{G_{12}} & 0 & 0 & \frac{1}{G_{12}} & 0 \\ 0 & 0 & 0 & 0 & 0 & \frac{1}{G_{12}} & 0 & 0 & \frac{1}{G_{12}} \\ 0 & 0 & 0 & \frac{2(1+\nu_{23})}{E_2} & 0 & 0 & \frac{2(1+\nu_{23})}{E_2} & 0 & 0 \\ 0 & 0 & 0 & 0 & \frac{1}{G_{12}} & 0 & 0 & \frac{1}{G_{12}} & 0 \\ 0 & 0 & 0 & 0 & 0 & \frac{1}{G_{12}} & 0 & 0 & \frac{1}{G_{12}} \end{bmatrix} \cdot \begin{pmatrix} \sigma_{11} \\ \sigma_{22} \\ \sigma_{33} \\ \tau_{23} \\ \tau_{31} \\ \tau_{12} \\ \tau_{32} \\ \tau_{13} \\ \tau_{21} \end{pmatrix} \tag{2.34}$$

Equation (2.34) embodies the stress-strain relationship in terms of engineering constants, with the rearranged fourth order compliance tensor,

where

$$G_{23} = \frac{E_2}{2(1+\upsilon_{23})} \tag{2.35}$$

In this case, the angle of the directions between X-1 and Y-2 is 45°; Z is parallel to the principle direction 3. The transformation matrix mentioned in equation (2.19) can be employed to conduct the coordinate system rotation.

Due to the large amounts of calculation, it is convenient to employ the computer to accomplish the coordinate transformation. The programming in Mathematica is attached in Appendix A, indicating the details of mathematical manipulation. C_{mnpq} and S_{mnpq} stand for the stiffness in the local coordinate system, while $C_{m'n'p'q'}$ and $S_{m'n'p'q'}$ are respectively the stiffness and compliance matrices in global coordinates. The new forms of stiffness and compliance matrices after rotation are as follows:

$$C_{i'j'k'l'} = \begin{pmatrix} C_{1'1'1'1'} & C_{1'1'2'2'} & C_{1'1'3'3'} & 0 & 0 & C_{1'1'1'2'} & 0 & 0 & C_{1'1'2'1'} \\ C_{2'2'1'1'} & C_{2'2'2'2'} & C_{2'2'3'3'} & 0 & 0 & C_{2'2'1'2'} & 0 & 0 & C_{2'2'2'1'} \\ C_{3'3'1'1'} & C_{3'3'2'2'} & C_{3'3'3'3'} & 0 & 0 & C_{3'3'1'2'} & 0 & 0 & C_{3'3'2'1'} \\ 0 & 0 & 0 & C_{2'3'2'3'} & C_{2'3'3'1'} & 0 & C_{2'3'3'2''} & C_{2'3'1'3'} & 0 \\ 0 & 0 & 0 & C_{3'1'2'3'} & C_{3'1'3'1'} & 0 & C_{3'1'3'2'} & C_{3'1'1'3''} & 0 \\ C_{1'2'1'1'} & C_{1'2'2'2'} & C_{1'2'3'3'} & 0 & 0 & C_{1'2'1'2'} & 0 & 0 & C_{1'2'2'1'} \\ 0 & 0 & 0 & C_{3'2'2'3'} & C_{3'2'3'1'} & 0 & C_{3'2'3'2'} & C_{3'2'1'3'} & 0 \\ 0 & 0 & 0 & C_{1'3'2'3'} & C_{1'3'3'1'} & 0 & C_{1'3'3'2'} & C_{1'3'1'3'} & 0 \\ C_{2'1'1'1'} & C_{2'1'2'2'} & C_{2'1'3'3'} & 0 & 0 & C_{2'1'1'2'} & 0 & 0 & C_{2'1'2'1'} \end{pmatrix}$$

(2-36)

$$S_{i'j'k'l'} = \begin{pmatrix} S_{1'1'1'1'} & S_{1'1'2'2'} & S_{1'1'3'3'} & 0 & 0 & S_{1'1'1'2'} & 0 & 0 & S_{1'1'2'1'} \\ S_{2'2'1'1'} & S_{2'2'2'2'} & S_{2'2'3'3'} & 0 & 0 & S_{2'2'1'2'} & 0 & 0 & S_{2'2'2'1'} \\ S_{3'3'1'1'} & S_{3'3'2'2'} & S_{3'3'3'3'} & 0 & 0 & S_{3'3'1'2'} & 0 & 0 & S_{3'3'2'1'} \\ 0 & 0 & 0 & S_{2'3'2'3'} & S_{2'3'3'1'} & 0 & S_{2'3'3'2''} & S_{2'3'1'3'} & 0 \\ 0 & 0 & 0 & S_{3'1'2'3'} & S_{3'1'3'1'} & 0 & S_{3'1'3'2'} & S_{3'1'1'3''} & 0 \\ S_{1'2'1'1'} & S_{1'2'2'2'} & S_{1'2'3'3'} & 0 & 0 & S_{1'2'1'2'} & 0 & 0 & S_{1'2'2'1'} \\ 0 & 0 & 0 & S_{3'2'2'3'} & S_{3'2'3'1'} & 0 & S_{3'2'3'2'} & S_{3'2'1'3'} & 0 \\ 0 & 0 & 0 & S_{1'3'2'3'} & S_{1'3'3'1'} & 0 & S_{1'3'3'2'} & S_{1'3'1'3'} & 0 \\ S_{2'1'1'1'} & S_{2'1'2'2'} & S_{2'1'3'3'} & 0 & 0 & S_{2'1'1'2'} & 0 & 0 & S_{2'1'2'1'} \end{pmatrix}$$

(2.37)

The components of the stiffness and compliance matrices $C_{m'n'p'q'}$ and $S_{m'n'p'q'}$ represent the components of the matrices after performing a coordinate transformation.

Actually, they are functions of the angle (θ) and the engineering constants ($E_1, E_2, G_{12}, G_{23}, \upsilon_{12}$). The detailed procedures are shown in Appendix A.

$$S_{m'n'p'q'} = f_{\mathrm{I}}(\sin(\theta), \cos(\theta), E_{11}, E_{22}, \upsilon_{12}, G_{12}, G_{23}) \tag{2.38}$$

$$C_{m'n'p'q'} = f_{\mathrm{II}}(\sin(\theta), \cos(\theta), E_{11}, E_{22}, \upsilon_{12}, G_{12}, G_{23}) \tag{2.39}$$

Again, because of the symmetry of the matrices, the fourth-order stiffness, $C_{m'n'p'q'}$ and compliance, $S_{m'n'p'q'}$ tensors can be reduced to 6 x 6 matrices $C_{i'j'}$ and $S_{i'j'}$ respectively. Further, $C_{i'j'}$ and $S_{i'j'}$ are still functions of the angle and the set of engineering constants:

$$S_{i'j'} = f_{\mathrm{I}}(\sin(\theta), \cos(\theta), E_{11}, E_{22}, \upsilon_{12}, G_{12}, G_{23}) \tag{2.40}$$

$$C_{i'j'} = f_{\mathrm{II}}(\sin(\theta), \cos(\theta), E_{11}, E_{22}, \upsilon_{12}, G_{12}, G_{23}) \tag{2.41}$$

In this work, one of the laminate orientations is $\theta = 45^o$. By substituting 45°, we obtain the complete compliance $S_{i'j'}$ as follows:

$$S_{i'j'} = \begin{bmatrix} \frac{(S_{11}+2\cdot S_{12}+S_{22}+4\cdot S_{66})}{4} & \frac{(S_{11}+2\cdot S_{12}+S_{22}-4\cdot S_{66})}{4} & \frac{(S_{12}+S_{23})}{2} & 0 & 0 & \frac{(S_{11}-S_{22})}{4} \\ \frac{(S_{11}+2\cdot S_{12}+S_{22}-4\cdot S_{66})}{4} & \frac{(S_{11}+2\cdot S_{12}+S_{22}+4\cdot S_{66})}{4} & \frac{(S_{12}+S_{23})}{2} & 0 & 0 & \frac{(S_{11}-S_{22})}{4} \\ \frac{(S_{12}+S_{23})}{2} & \frac{(S_{12}+S_{23})}{2} & S_{22} & 0 & 0 & \frac{(S_{12}-S_{23})}{2} \\ 0 & 0 & 0 & \left(S_{22}-S_{23}+\frac{S_{66}}{2}\right) & \left(S_{22}+S_{23}+\frac{S_{66}}{2}\right) & 0 \\ 0 & 0 & 0 & \left(S_{22}+S_{23}+\frac{S_{66}}{2}\right) & \left(S_{22}-S_{23}+\frac{S_{66}}{2}\right) & 0 \\ \frac{(S_{11}-S_{22})}{4} & \frac{(S_{11}-S_{22})}{4} & \frac{(S_{12}-S_{23})}{2} & 0 & 0 & \frac{(S_{11}-2\cdot S_{12}+S_{22})}{4} \end{bmatrix} \tag{2.42}$$

Micromechanical Approach

We can predict lamina properties by the procedures of micromechanics. The objective of the micromechanics approaches used here is to determine the elastic moduli or stiffness or compliance of a composite material in terms of the elastic moduli of the constituent materials. For example, the stiffness and compliance of a fiber-reinforced composite can be determined in terms of the properties of the fibers and matrix and in terms of the properties of the relative volumes of fibers and matrix.

$$C_{ij} = C_{ij}(E_f, \upsilon_f, V_f, E_m, \upsilon_m, V_m) \tag{2.43}$$

$$S_{ij} = S_{ij}(E_f, \upsilon_f, V_f, E_m, \upsilon_m, V_m) \tag{2.44}$$

where

E_f and E_m are the Young's moduli of the fiber and matrix respectively,
V_f and V_m are the fraction of fiber and matrix volumes respectively,
υ_f and υ_m are the Poisson's ratios of the fiber and matrix respectively.

For a transversely isotropic composite material, there are five independent engineering constants: E_1, the longitudinal modulus; E_2, transverse modulus; υ_{12}, Poisson ratio; G_{12}, shear modulus associated with the 1-2 plane; and G_{23}, shear modulus associated with 2-3 plane.

Calculation techniques from a material's engineering constants (E_1, E_2, υ_{21}, υ_{23}, G_{12}) have been discussed intensively in the past years [4]. Many formulations have been developed to obtain engineering constants. Some formulations mentioned in the book Composites Mechanics [2] are introduced to estimate the engineering constants of a composite.

However, it must be recognized that a micromechanical analysis has inherent limitations. In order to gain more accurate estimations of the engineering constants, semi-empirical approaches were also used in this research. The empirical solutions were based on curve fitting to elasticity solutions or experimental data, and some of these equations were used along with mechanics of materials equations to formulate a complete set of simple lamina design equations. Therefore, we can carry out this initial estimation just by putting known values of fiber and matrix properties into these formulations. The equations for establishing the elastic moduli of a fiber-reinforced composite are as follows:

Longitudinal Modulus E_1 [5], [6], [7], [8]

$$E_1 = E_f V_f + E_m V_m \tag{2.45}$$

where E_f is the fiber modulus; E_m is the matrix modulus; V_f and V_m are the fiber volume fraction and matrix volume fraction, respectively.

Transverse Modulus E_2 [5], [6], [7], [8]

To improve the estimate of E_2, the semi-empirical Halpin-Tsai formulation is used as follows:

$$\eta = \frac{\frac{E_f}{E_m} - 1}{\frac{E_f}{E_m} + \zeta} \tag{2.46}$$

$$\zeta = 2$$

$$E_2 = E_m \cdot \left(\frac{1+\zeta \cdot \eta \cdot V_f}{1-\eta \cdot V_f} \right) \tag{2.47}$$

where E_2 is the transverse modulus of the composite, and ζ and η are the empirical parameters. ζ is set to 2 based on experience.

Poisson's Ratio υ_{21} [5], [6], [7], [8]

$$\upsilon_{12} = V_m \upsilon_m + V_f \upsilon_f \tag{2.48}$$

where υ_{12} is the major Poisson ratio of the composite.

Shear Modulus Associated with the Plane 1-2 G_{12} [4], [6], [7], [8]

The periodic microstructure model (PPM) formulation can be employed to obtain an improved estimate of G_{12}

$$S_3 = 0.49247 - 0.47603V_f - 0.02748V_f^{\,2} \tag{2.49}$$

$$G_{12} = G_m \left[1 + \frac{V_f (1 - G_m/G_f)}{G_m/G_f + S_3 (1 - G_m/G_f)} \right] \tag{2.50}$$

where G_{12} is the shear modulus associated with the 1-2 plane, G_f is the shear modulus of the fiber, G_m is the shear modulus of the matrix, and S_3 is an empirical parameter.

Shear Modulus Associated with the Plane 2-3 G_{23}. [5], [6], [7], [8]

The inter-laminar shear modulus associated with the 2-3 plane can be computed with the semi-empirical stress-partitioning parameter (SPP) technique.

$$\eta_{23} = \frac{3 - 4\upsilon_m + G_m/G_f}{4(1-\upsilon_m)} \tag{2.51}$$

$$G_{23} = G_m \frac{V_f + \eta_{23}(1-V_f)}{\eta_{23}(1-V_f) + V_f \, G_m/G_f} \tag{2.52}$$

where, G_{23} is the shear modulus associated with the 2-3 plane, and η_{23} is the empirical parameter.

These calculations are used as initial stage values for the optimization technique to be discussed subsequently.

Agreement between Micromechanical and Macromechanical Analysis

Micromechanics is concerned with composite material behavior, wherein the interaction of the constituent materials is examined in detail as part of the definition of the behavior of the macroscopic heterogeneous composite material: Macromechanics is focused upon the composite material behavior wherein the material is presumed homogeneous and the effects of the constituent materials are averaged to provide equivalent continuum mechanical properties of the composite. Hence, lamina properties can be estimated by the procedures of micromechanics.

Knowledge of how to estimate properties is essential to constructing composites that must have certain apparent or macroscopic properties. However, micromechanical analyses have many simplifying assumptions to estimate the complicated combination of constituents. The actual experimental work is a good criterion to determine the consequence of these assumptions. The micromechanical estimation cannot be valid until it agrees with the corresponding experimental works. Once a micromechanical model has

been shown to be sufficiently accurate by comparison with experiments, it can become part of a powerful design methodology that enables us to design the material as well as the structure. Aside from design implications, micromechanical analysis and experimental characterization are both essential if we are to understand composite material mechanical behavior [2].

The focus of this project is to find an appropriate methodology for accurately estimating effective moduli of a composite. As discussed in section 2, the assumption of the effective moduli in micromechanics has to agree with the experimental data in the macromechanical approach. However, there is usually disagreement between the analytical and experimental data in practical situation, because of gaps between the condition of the composites in practical condition and the assumed condition of the composites in the theoretical analysis.

Numerical techniques are used in this work. Finite Element Modeling (FEM) is utilized, and by minimizing the discrepancy between the modeling results and experimental results, optimum engineering constants can be obtained. The details of these techniques are described in Chapter 4.

The In Plane Loader (IPL) machine is used to conduct the tests and collect the experimental data.

Theories and numerical techniques involved in this study is illustrated in Figure 2.04. The work was restricted to linear elastic behaviors, and micromechanical and macromechanical analyses were employed. Three numerical methods were used, FEM model, bounding techniques and numerical optimization. The experimental method was

also used. Note that the numerical techniques and experimental methods are served to the optimization. Optimization is more significant method in this study.

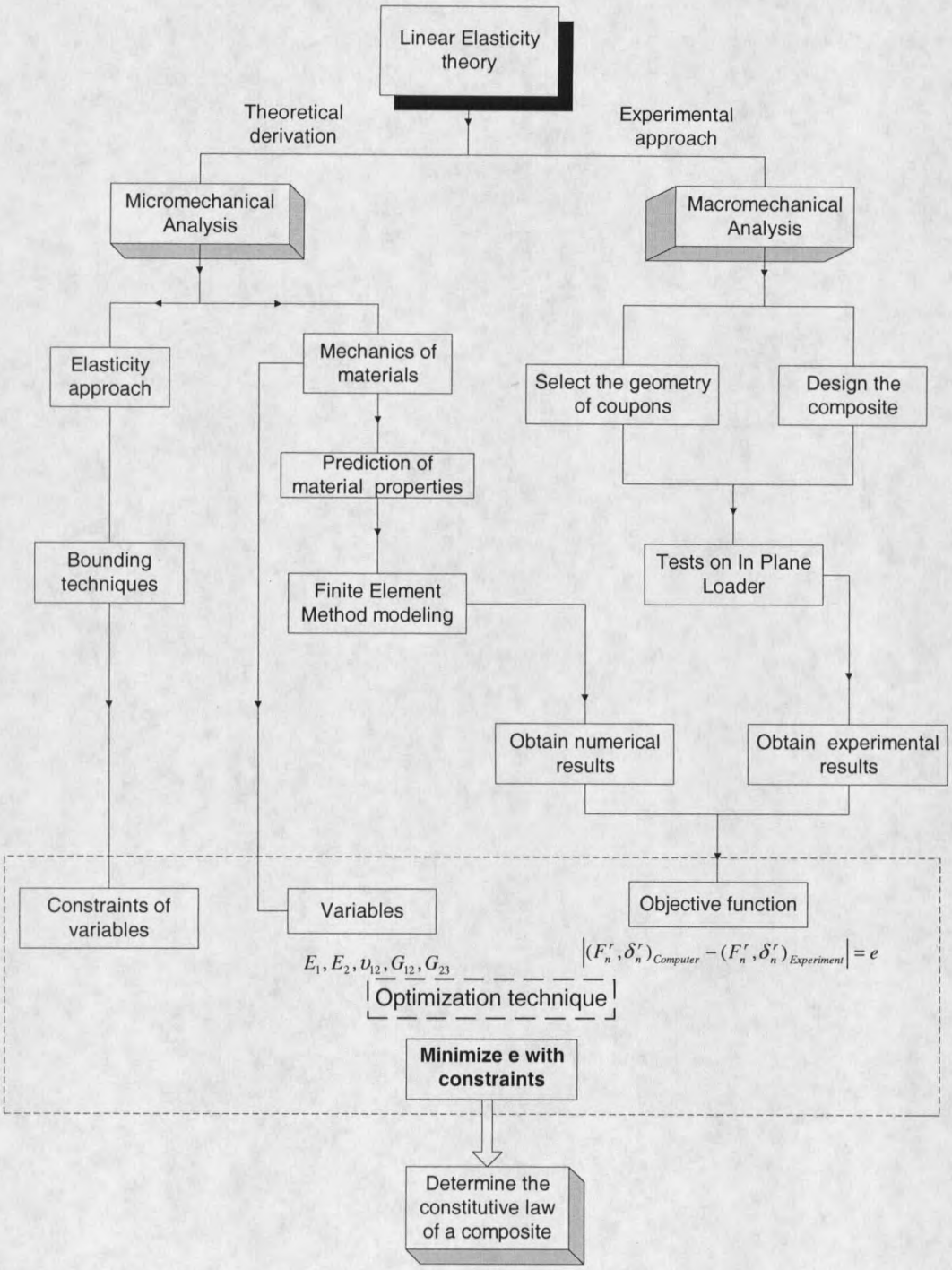

Figure 2.04 Flow chart of theories and numerical techniques in this study

The In-Plane Loader Machine

Determining the effective composite properties usually requires the conduction of an extensive set of experiments. It is desirable to acquire the same results using a reduced set of tests. Under this motivation, the In-Plane Loader (IPL) machine was designed and built by the MSU composite team, based on initial work of the Naval Research Laboratory (NRL). [1] The In Plane Loader (IPL) is a testing machine capable of providing any combination of in-plane loads on a sample. This machine is able to simultaneously load a sample in tension or compression, shear or bending. Some possible loading configurations are illustrated in Figure 2.05 [1], [10].

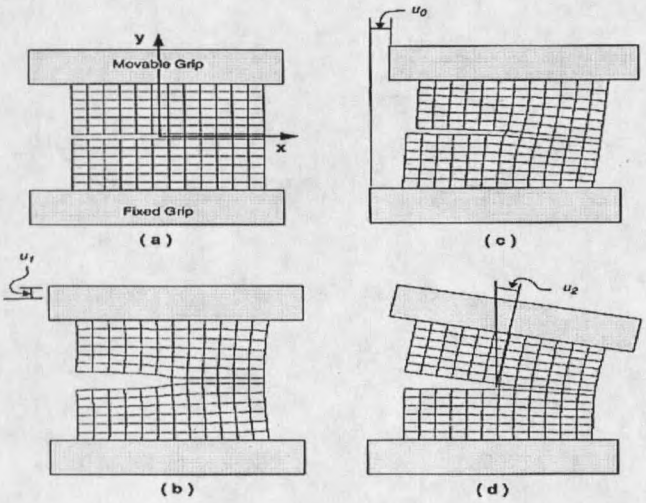

Figure 2.05 a) A composite sample, b) a sample loaded in tension, c) a sample loaded in shear, d) a sample loaded in bending.

The designed IPL system built at NRL is a specialized machine comprised of many custom and expertize parts. The MSU composite team has created an alternative device which is lower cost, more efficient, and more compact testing machine. After going

through many options, the following design was chosen for the initial machine. This testing machine is shown in Figure 2.06 [1], [10].

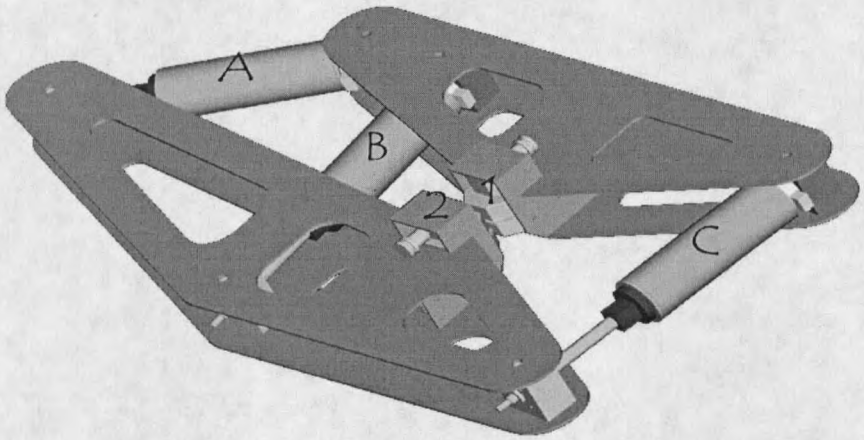

Figure 2.06 Initial IPL design by MSU students

In Figure 2.06, the composite sample is placed in the clamps (Points 1 and 2). The desired displacements are then achieved by changing the lengths of the three actuators (Points A, B, and C). Advantages of this design compared to others is that it is more compact, doesn't require additional structures for stabilization, and it is relatively portable. Computer aided designs were done using Pro/Engineer [5]. The current IPL machine is shown in Figure 2.07 [1], [10].

This testing machine is comprised of linear stepped motor actuators, and grips. The specimen is loaded into the grips, which have the clamps in the heads. The IPL is a computer driven machine. In other words, the selected loading paths are applied to the specimen by means of a computer. Furthermore, the experimental data of a sensor placed

at a specific point can be recorded by the computer. As a consequence, all of the output data can be reviewed on the computer as well.

It is recognized that the structure of this machine is very simple and compact. The specimen can be fixed on the grips by clamping. The computer system instructs the linear actuators to move and the grips moving accordingly until the designed loading paths (displacements) are accomplished.

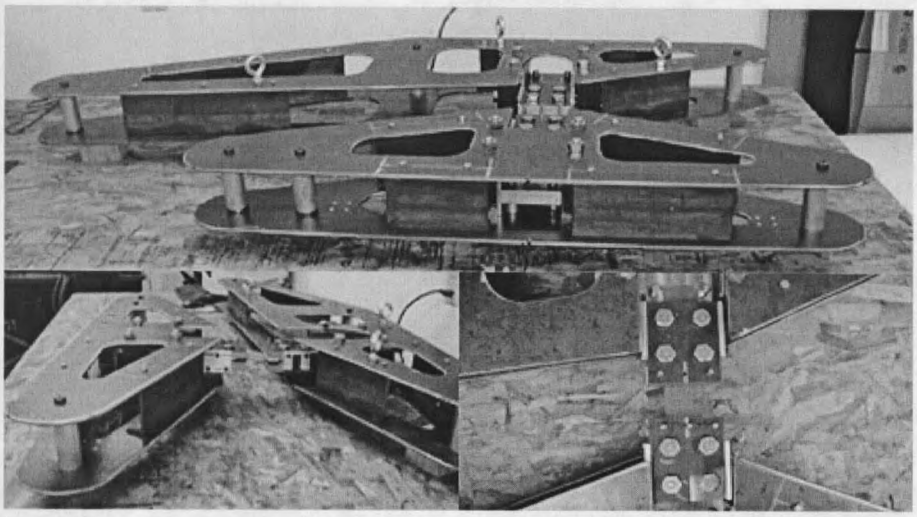

Figure 2.07 The IPL machine built at the MSU composite lab.

To this point, we have established the basis for the research which included micromechanical analysis to determine preliminary estimates for the lamina properties, and the experimental method which utilized the in-plane loader. Chapters 3 and 4 will focus on the details of the experimental techniques and optimization procedures to determine the equivalent in-situ lamina properties to be utilized in preliminary design of composite laminates and structures.

CHAPTER 3

EXPERIMENTAL METHODS

Experiments play a crucial role in this research. The experimental data acquired by the tests are referred to as the norm that verifies the feasibility and accuracy of the numerical estimates. Although there are many numerical approaches to approximate composite properties, nearly all methods must be validated with experimental data. Therefore, care must be taken in obtaining accurate experimental data.

Before conducting experiments, preparation is required. In section 3.1, selection of constituent materials (or the fibers and matrices), a description of the layup of the designed composite, the fabrication equipment and procedure, and the depiction of coupons being used for the experiments are included. Next, the test procedure for the In Plane Loader machine is described in detail. Then, the detailed procedure of the experiments is presented in section 3.2. Finally, the motivation of the experiments is given.

Experimental Design

A composite material is formed by the combination of two or more distinct materials to form a new material with enhanced properties [5]. There is no better way to gain the macroscopic composite properties than actually conducting the experiments. This project was focused upon the study of constitutive parameters of a composite. Both experimental and numerical approaches were used. For the experimental part, the composite was

carefully designed, including the geometry of the coupons. Next, the designed composite was fabricated, the coupons were cut according to the selected geometry and finally, the tests were conducted with the In- Plane Loader machine. The following paragraphs discuss the details.

Design of a Composite Material

Selection of Constituent Materials. The composite material selected in this study is a combination of the constituent materials (fibers and matrices), fibers within a matrix. The glass fiber D155 and ester resin VINYL Ester-DERAKANE 411-C were selected as the constituent materials for fabrication of the designed composite. The properties of the constituent material provided by the manufactures are shown in Tables 3.01 and 3.02. The information was provided by the MSU Composite Database [11]. The layup of the selected composite is $[0°/+45°/90°/-45°]_s$

Table 3.01 The matrix properties [11]

Matrix property	Derakane 411PC-100 Vinyl Ester
Tensile Modulus, Pa E_m	3.21×10^9
Shear Modulus, Pa G_m	0.96×10^9
Nuxy υ_m	0.34

Table 3.02 The fiber properties, D155 [11]

Fiber property	D155
Tensile Modulus, Pa E_f	73.1×10^9
Shear Modulus, Pa G_f	29.959×10^9
Nuxy υ_f	0.22

The selected fabric D155 contains unidirectional fibers. Figure 3.01 illustrates this fabric. White lines are the stitches that hold the fibers parallel to one another before layup.

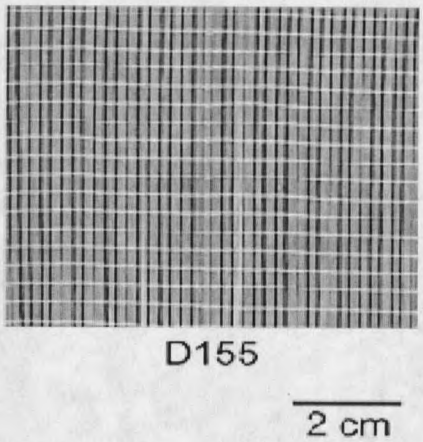

Figure. 3.01 Illustration of fabric D155

Orientation of the Designed Composite. The fibers provide most of the stiffness and strength, and the matrix binds the fibers together providing load transfer between fibers and between the composite and the external loads and supports. Since fibers have a minimal contribution to the strength transverse to the fiber direction and the strength of the matrix is very low, it becomes necessary to add layers with various orientations to support all of the applied loads. One way to achieve this is to create a laminate, stacking layers with various orientations. Most structural applications need reinforcement in other directions [2]. For this case, a composite laminate with the directions in 0°, +45°, 90°, and -45° and a total of eight layers was selected. The composite laminae are symmetric, and the layup of the composite is $[0°/+45°/90°/-45°]_S$. The subscript "S" means of symmetry.

The eight layers of composite carry the loads in different directions. Because of the orientation symmetry of the layers with an equal number of fibers oriented every 45°, this composite is referred to as transversely isotropic in the global x-y plane. The layup of the designed composite is illustrated in Figure 3.02.

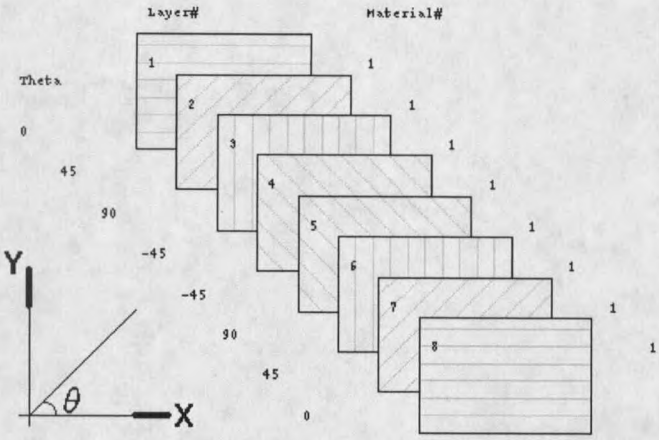

Figure 3.02 Layup of the selected composite

Fabrication Procedure. The choice of manufacturing process depends on the type of matrix and fibers, the cost effectiveness of the process and so on. Often the manufacturing process is the initial consideration in the design of a composite structure.

As described previously, the composite designed for this research is a multi-direction composite with the layer layup of $[0°/+45°/90°/-45°]_s$. Test repeatability requires fabricated high quality composite with sufficient size. To minimize the effects of minor flaws similarly the fabrication process must be suitable for manufacturing relatively large composite laminate [16].

The partial injection Resin Transfer Molding (RTM) method is an appropriate fabrication process to produce the desired composite for this project. This method uses a

two-stage injection process. The first stage injects resin into a vacuum evacuated "pool" outside of the plane of the fabric. Pressure is then applied outside of a flexible film, forcing resin into the fabric in the thickness direction. Resin is not required to flow in the plane of the fabric, thus reducing the dependency on in-plane resin flow, making relatively high volumetric flow rates possible during the injection stage[8],[9]. This method improves the quality of composites dramatically compared to the conventional hand layup method [16].

The remaining procedures of the partial injection RTM process are similar to the typical RTM process. The fibers are cut and oriented according to the designed sizes and layup. Because there is only a single fiber D155 that is used for all of the orientations in 0°, +45°, 90°, and -45° direction, more care needs to be taken while putting the fiber into the mold. It is important to be sure that the directions are sufficiently precise, especially at the directions of +45° and -45°. The process is shown in Figure 3.03.

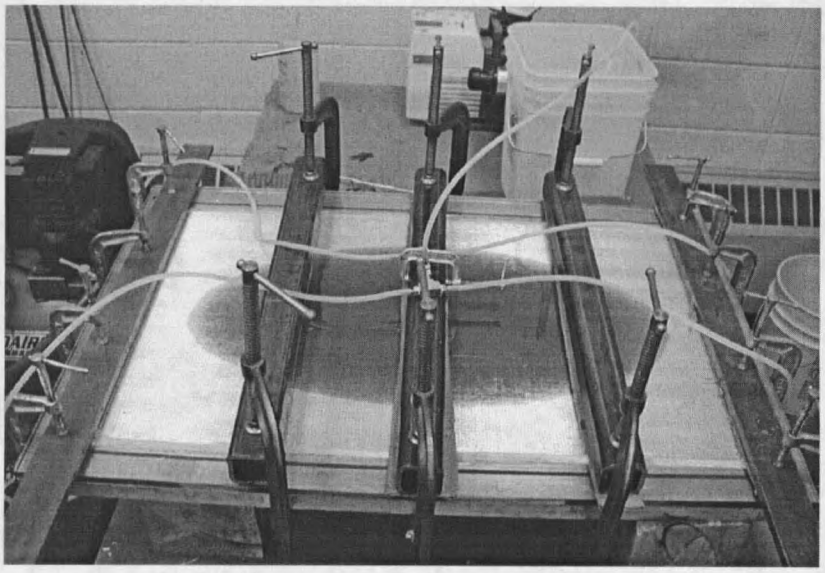

Figure 3.03 Partial injection Resin Transfer Molding (RTM)

In this way, we acquire the desired composite laminate we designed. In the next step, the necessary data such as length, width, and thickness is recorded fro the composite. This composite was then used for the experiments. Post-fabrication processing was needed for the tests. Each laminate was cut into small pieces. The details of making the coupons are presented in the next section.

Preparation of the Coupons

Geometry is one of the important factors in the behavior of structural composite. Upon applying loads, different coupon geometries lead to different reaction forces and displacements at specific points. Notched configuration was selected for the coupons in this project. The coupon dimensions are shown in Figure 3.04.

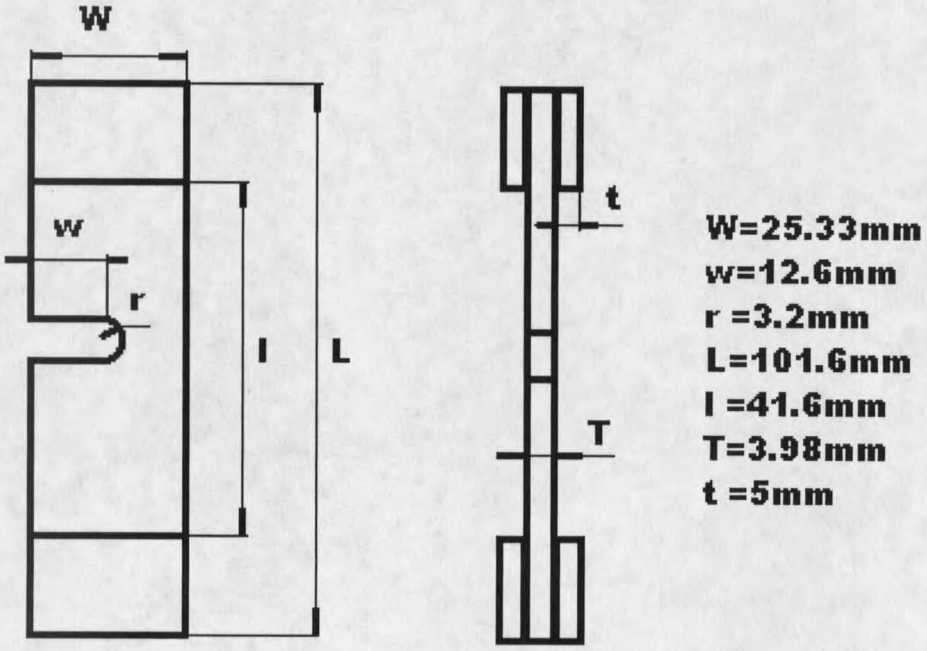

Figure 3.04 The dimension of the notched coupon

One of the reasons why a notched geometry was selected was because stresses and strains concentrate next to the notch under loads perpendicular to the notch. Moreover, since stress and strain next to the grips is much less than next to the notch, the effects of the grips becomes less significant, and the experimental data collected near the notch more accurate. Consequently, this geometry makes the study of a composite constitutive behavior easier.

The coupons are cut according to the selected geometry. Care needs to be taken to keep the original orientation of the composite properly aliened with the coupon geometry. The process of cutting the composite coupons with selected geometry is illustrated in Figure 3.05. There are a total of ten notched coupons and 3 straight coupons to be made.

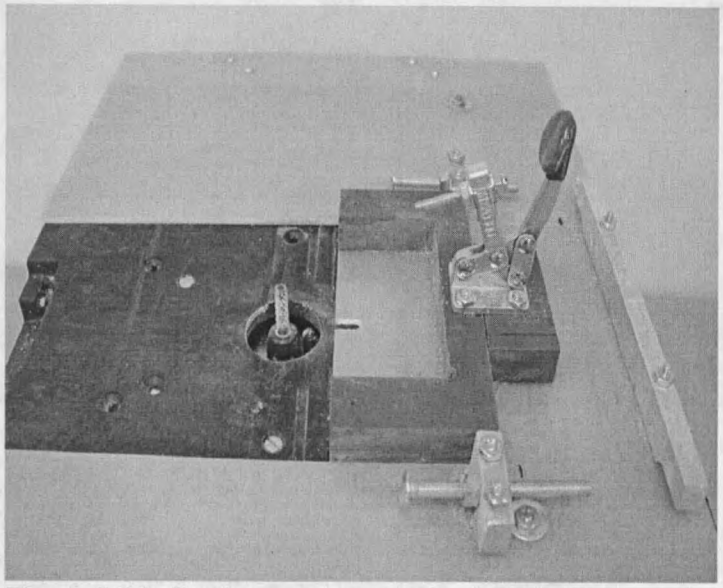

Figure 3.05 Cutting coupons to the designed geometry

The coupons were loaded into the IPL machine for tests. A ready coupon is shown in Figure 3.06.

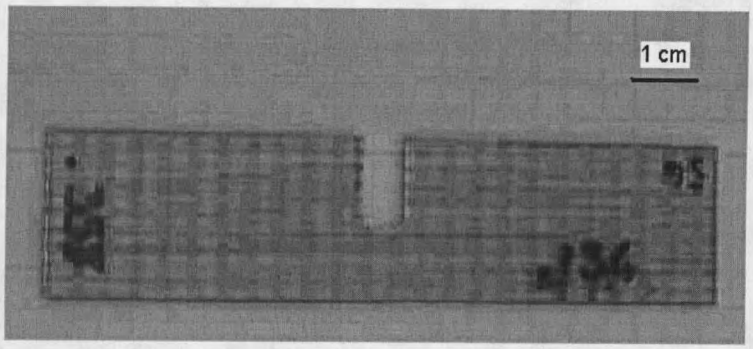

Figure 3.06 A sample cut from the composite

At this point, we have accomplished the preparation of the coupons. The next step is to conduct the experiments using the In-Plane Loader machine. This procedure is introduced in the next section.

In Plane Loader Machine

Introduction of the In-Plane loader Machine

As discussed in the previous Chapter, the test machine used for measuring the reaction forces or displacements at the specific point of the coupons is the In-Plane Loader (IPL) machine. The IPL was designed and built specifically for finding the composite material properties. The primary components of the IPL machine are the fixed and movable grips and the linear stepper motor actuators. Special torque on both in grips is applied to ensure a constant gripping force throughout the test. The objective of the IPL is to control the rigid body motion of the boundary of the coupon that is held by the movable grip. Because the actuators are constrained to move in a plane parallel to the plane of the coupon, the resulting motion involves only three degrees of freedom relative to any frame of reference in that plane [1], [10].

It is important to note here that the grip motion can be resolved into three basic components: sliding u_x, opening/closing u_y, and rotation ω. The IPL is capable of providing any combination of in plane loads on a sample. The basic loading configurations are illustrated in Figure 3.07. The displacements above are denoted as sliding u_o, opening/closing u_1, and rotation u_2 in the figure. These displacements are controlled according to time in the IPL control system [1], [10].

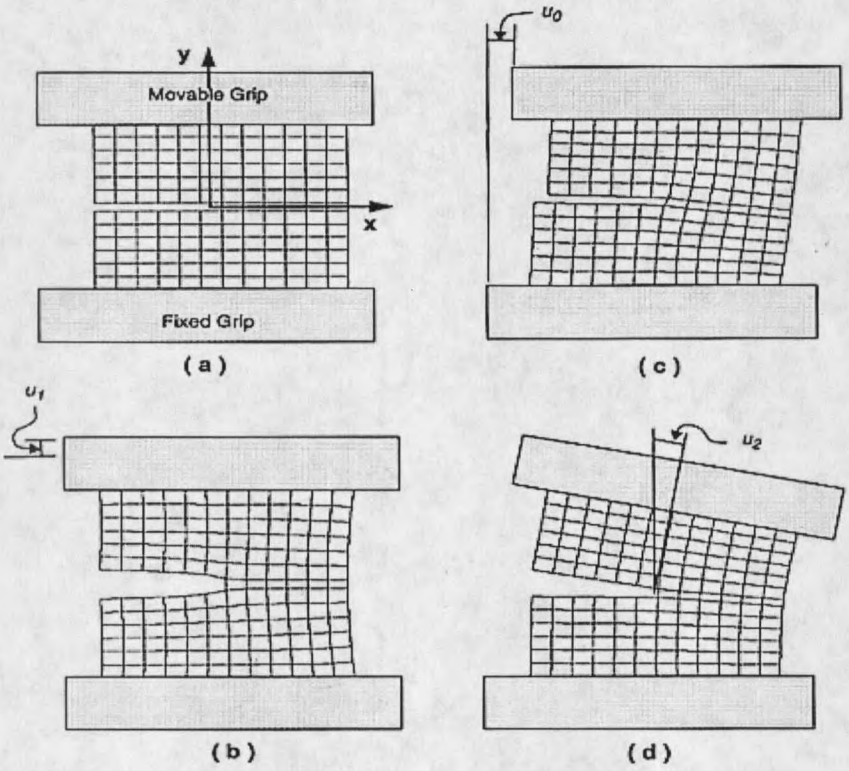

Figure 3.07. a) a composite sample, b) a sample loaded in tension, c) a sample loaded in shear, d) a sample loaded in bending.

Recall, the design of the IPL was discussed in section 3 of Chapter 2 and a design drawing of the IPL is shown in 2.06.

Grips on the IPL

The grips connect to the stepper motors, which provide the motion according to the loading path for the experiment. The grips are used to clamp the coupons by means of the pre-torqued bolts. The assembly of a grip is shown in Figure 3.8. One may see that there are two parts; one connects to the actuator, and the other is the clamp.

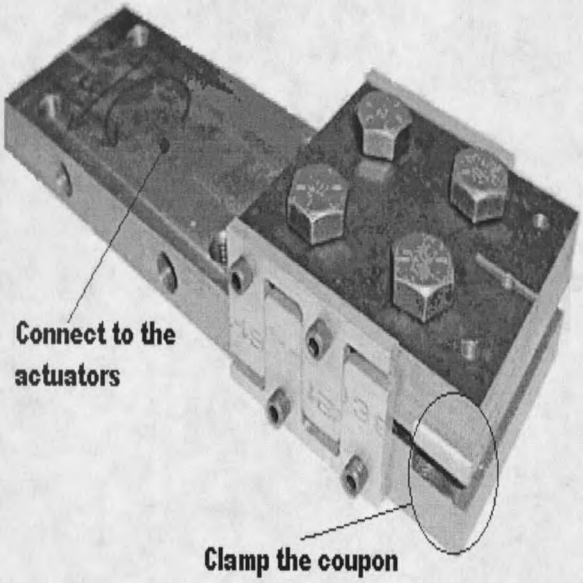

Figure 3.08 (a) Assembly of a grip

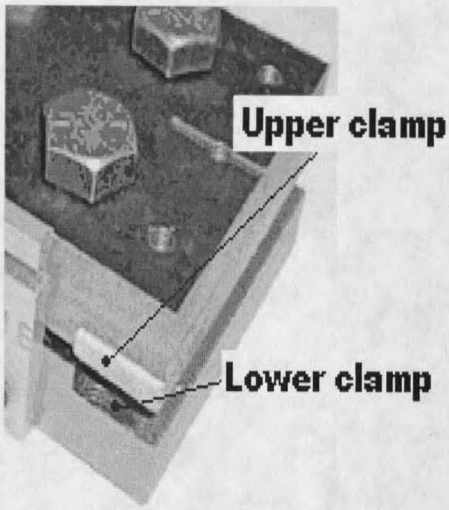

Figure 3.08 (b) Enlarged grip

Bolts are used to tighten the clamps that fix the coupons. The clamp surfaces shown in Figure 3.09 are very rough. Often it is assumed that there is no relative motion between the coupons and the clamps during the actual experiments, as if the coupon were glued to the clamps. Yet the actual condition is a very complicated physical process, and difficult to represent with a simple condition. This condition can be simulated with elements in the Finite Element Modeling, as discussed in Chapter 4.

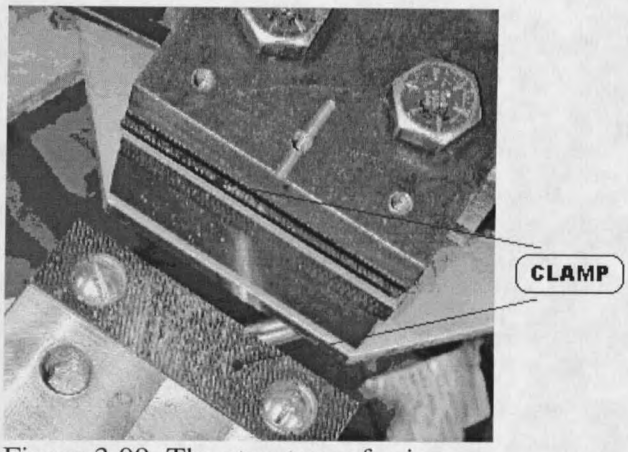

Figure 3.09 The structure of grips.

Carrying Out the Experiments Using the IPL

Design of the Experiments

Recall, the objective of the IPL experiments was to acquire the reaction forces or displacements at a specific point in the test coupons with the notch. Note that all of the experiments are subject to elastic behaviors, and no damage or fracture was apparent during the tests. Four loading conditions were considered for this research. These are:

Tensile (Open/Close) u_y,

Shear (Sliding) u_x + Tensile (Open/Close) u_y,

Moment (Rotation) ω,

Tensile+ Shear + Moment+ (Open/Close+ Sliding + Rotation) $u_y + u_x + \omega$.

The four loading paths designed for notched coupons in this research are depicted in Figure 3.10. The loads are all the displacements in this research. Note that all the displacements are applied to the grips rather than the coupon itself.

Each loading path applied to the notched coupons is illustrated in Figure 3.10.

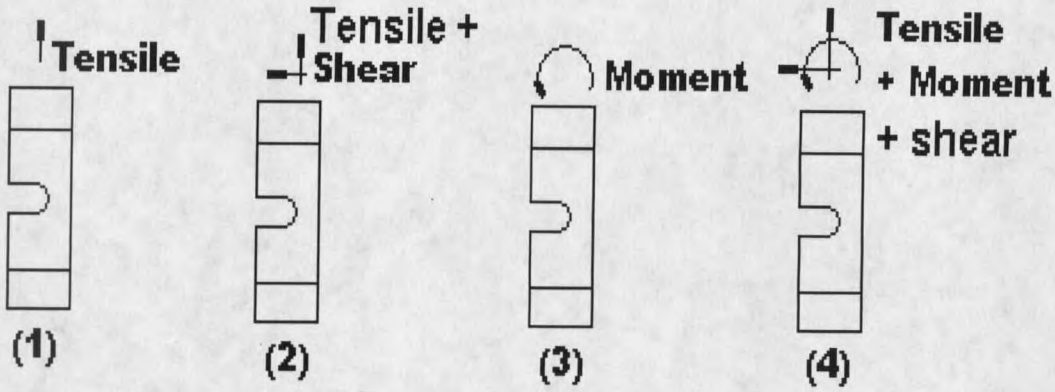

Figure 3.10 Four test load cases applied to notched coupons

Since four loading paths are designed for the notched coupons, and each test was performed twice, a total of 8 notched coupons are needed.

Experiment Procedure

The following sequence of events was repeated for each coupon and each loading sequence: load and clamp the coupon, apply the loads along the specified loading path, display the data of reaction forces and displacements at a specific point.

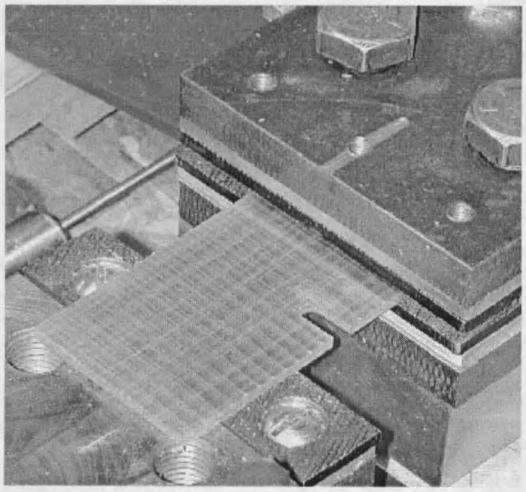

Figure 3.11 Clamping the coupon

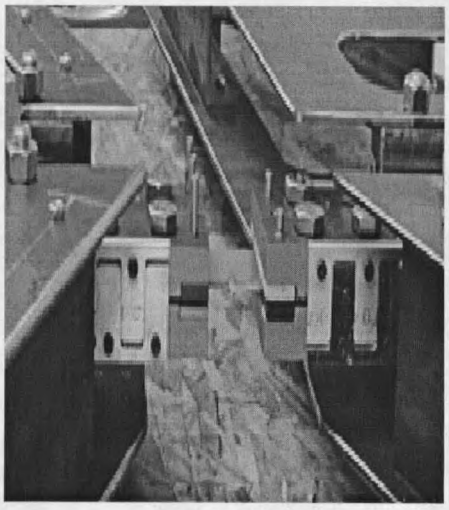

Figure 3.12 Apply the loads to the coupon

The procedure of clamping the coupons in the grips and applying the loads along the specified loading paths is illustrated in Figure 3.11 and Figure 3.12. This procedure was repeated during the tests.

The remainder of the test was performed automatically, with the computer control system controlling the displacement loading path. The system monitored and stored the boundary forces and displacements for each loading step. The automatic load sensors stored the reaction forces and moments at a specific point during the tests. The point selected on the coupon was in the middle of the grip boundary, P (W/2, l, Z). The position of the point where the sensor was located is shown in Figure 3.13. This point corresponds to the point selected for numerical optimization to be discussed in chapter 4.

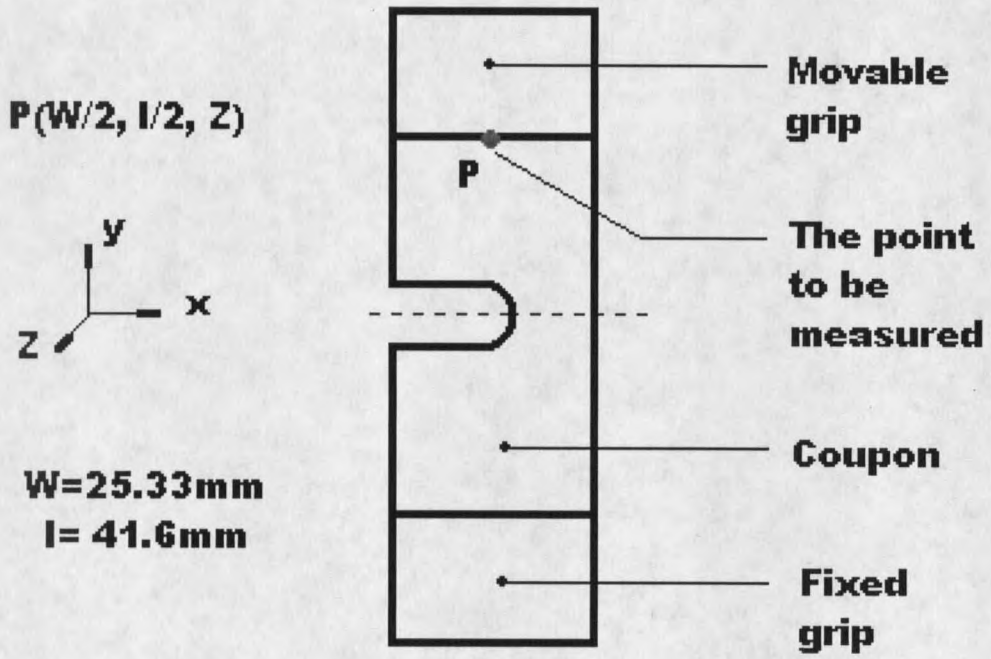

Figure 3.13 The specific point to be measured

Summary of the Motivation of the Experiments

Eight different notched coupons were tested under displacement control in four different loading configurations. These notched specimens were tested to obtain reaction force data at the bottom center edge of the top grip. This data was used to refine estimates of elastic parameters of the composite specimens.

The motivation of each test is shown in Table 3.03.

Table 3.03 Motivation of each test

Loading paths	Notched coupon	Motivation
u_x	2 times, 2 coupons reproducibility	To obtain the reaction forces and displacements at a specific point P under uniaxial loading. The data will be used for *Optimization*.
$u_x + u_y$	2 times, 2 coupons reproducibility	To obtain the reaction forces and displacements at specific point P under combined axial loads. The data will be used for *Optimization*.
ω	2 times, 2 coupons reproducibility	To obtain the reaction forces and displacements at a specific point P under pure rotational loading. The data will be used for *Optimization*.
$u_x + u_x + \omega$	2 times, 2 coupons reproducibility	To obtain the reaction forces and displacements at a specific point P under all three in plane loadings. The data will be used for *Optimization*.

CHAPTER 4

NUMERICAL METHODS

The numerical techniques used to determine the composite properties in the current research are focused upon in this chapter, including the Finite Element Method (FEM), bounding and optimization techniques to match experimental data. Note that the basic restriction of the discussion is to linear elastic behavior.

Finite Element Analysis plays a major role in the mathematical modeling and simulation in this study. Description of the modeling and simulation by ANSYS is provided in the first section. The details about modeling the geometry, mesh, and specified loads and displacements corresponding to the real experimental conditions are illustrated in this section also.

In addition, the bounding techniques of linear elasticity are included in the discussion of determination of the engineering constants. This technique helps to establish the upper and lower bounds of the engineering constants ($E_1, E_2, G_{12}, G_{23}, \upsilon_{12}$) for use in optimization.

ANSYS has an optimization package which was used for this project. The optimization is carried out by comparing the experimental data with the corresponding modeling data,. The optimization technique used to estimate the optimum engineering constants of the composite is introduced. The optimization theories involved in ANSYS are described and the algorithms employed by ANSYS are presented. The applications of

the optimization package are also shown, like the definition of objective function, design variables, and state variables.

Finite Element Method Modeling Using ANSYS

The Finite Element Method (FEM) is a mathematical technique for obtaining approximate numerical solutions to the abstract equations of calculus that model the response of a physical system subjected to external influences [6].

The Finite Element Method has become popular as a result of the computer age, and the application of the method to solve practical problems requires use of computer programs for analysis [14]. All FEM models of this project were performed using ANSYS 6.0. Macros (or command files) are used exclusively to construct and solve all models. A macro can be written to include a description of all of the geometry, loads, and solution information for a given model. They make it possible to run the same model several times with only a single command to start the subroutine each time. Some post-processing was included in the macros but most was done using the Graphical User Interface [6].

FEM modeling is used to simulate the experimental conditions and acquire the corresponding results, such as reaction forces or displacements. These results are employed to carry out optimization by comparing with the experimental data. These two groups of data are supposed to agree with each other. If there is a discrepancy, the optimization procedure is carried out. Hence, more care should be taken to make the FEM model as close as possible to the actual experimental conditions.

Material Properties

Various material properties can be defined for each element type. There are two material types for this case, the composite and the grips (Steel). The composite was modeled as a transversely isotropic laminate, and the grip is an isotropic material.

The material properties are the same in all of the models (see Appendix E). The parameters input into the models are the properties of a single, fiber-reinforced ply. The finite element codes use these parameters to build the laminate properties.

All of the initial elastic properties were obtained by micromechanical estimation techniques as described in chapter 2. The first set of material properties describes the reinforced composite material. These are material properties predominately used in the models. The second set of properties is for the steel grips only.

As listed previously in Chapter 2, the manufactures provided the constituent material properties, which enabled us to estimate the characteristic properties of each lamina of a composite. Meanwhile, it is necessary to know other parameters as well, such as the fiber volume fraction of the designed composite. A sample of the composite was taken and burned, the remaining weight (fibers) was then evaluated relative to the original weight. The fraction of fiber volume and matrix volume were then obtained: $V_f = 0.417$ and $V_m = 0.583$, respectively.

The thickness of the laminate is another parameter which needs to be known for FEM material property modeling. Because only one type of fiber (D155) is used to fabricate the composite, the thickness of each laminate was the same. So the thickness of

each laminate of the composite can be gained simply by dividing the thickness of the composite by eight.

The designed composite has total of eight layers, with the layup of [0°/+45°/90°/-45°/-45°/90°/+45°/0°], illustrated in Figure 4.01. The thickness of the composite was $t_{composite} = 3.98 \times 10^{-3} m$. Then, the calculated thickness of each layer was $t_{DD155} = 4.975 \times 10^{-4} m$.

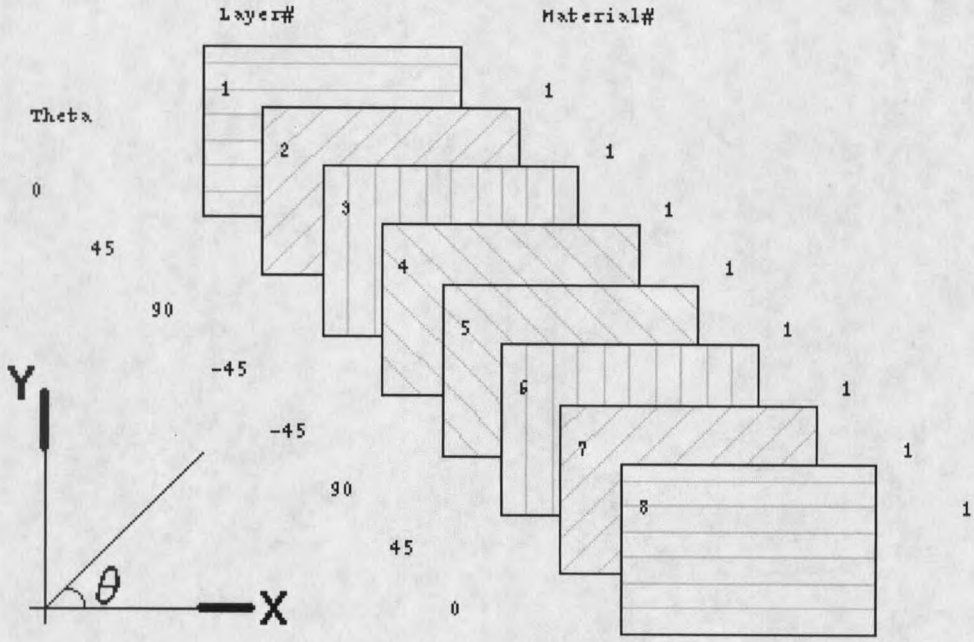

Figure 4.01 Layup of the selected composite in coordinate system

By employing the equations introduced in Chapter 2, the constituent material properties and the parameters obtained above, we are able to estimate the engineering constants of each lamina of composite. The assumed composite material properties are shown in table 4.01.

Table 4.01 The initially assumed engineering constant of transversely isotropic material

Engineering constants	Value	Eq. Reference
Longitudinal Modulus E_1	32.354 x 10^9 Pa	Eq.(2.45)
Transverse Modulus E_2	8.781 x 10^9 Pa	Eq.(2.46); Eq.(2.47)
The major Poisson ratio υ_{12}	0.29	Eq.(4.48)
Poisson ratio associated with 2-3 direction υ_{23}	0.353	See Appendix B
Poisson ratio associated with 1-3 direction υ_{13}	0.29	$\upsilon_{13} = \upsilon_{12}$
Shear modulus associated with the 1-2 plane G_{12}.	2.021 x 10^9 Pa	Eq.(2.49); Eq.(2.50)
Shear modulus associated with the 1-3 plane G_{13}.	2.021 x 10^9 Pa	$G_{13} = G_{12}$
Shear modulus associated with the 2-3 plane G_{23}.	1.973 x 10^9 Pa	Eq.(2.51); Eq.(2.52)

The prediction of the engineering constants has to satisfy the restrictions of elasticity theory as stated in Chapter 2. The assumed engineering constants can be checked and verified simply by substituting these engineering constants into equations (2.21) and (2.22) in Chapter 2. Upon calculation, it is proved to that the assumed engineering constants satisfy the restrictions. The detailed calculation procedure is attached in Appendix C.

The grips are made of steel. The properties of the steel used in this research are listed in Table 4.02.

Table 4.02 Material properties of the grip (Isotropic material)

Engineering constants	Steel
Young's modulus	2 x 10^{11}Pa
Poisson ratio	0.3

Mesh

The mesh is an important feature of FEM modeling. The mesh is a discretization of the structure that allows each element of the structure to be represented with relatively simple relationships. thus enabling us to simulate complicated engineering problems in practical situations. Care must be taken while modeling the complex geometries, since there are a variety of element attributes, real constants and so on. Choosing the appropriate attributes is critical [6].

Mapped Mesh. The procedure for generating a mesh of nodes and elements consists of three main steps: set the element attributes; set mesh controls [10]; and generate the mesh. First, it is necessary to choose either the free mesh or mapped mesh. Since the geometry of the sample modeled is fairly regular, the mapped mesh, which restricts the element shape and mesh pattern to improve accuracy was selected [6].

Element Type. Three element types were used: MESH200, SOLID46, and SOLID45. MESH200 is a mesh only element, and can be used for area-mesh or volume mesh in 3-D space with hexattedral. SOLID46 is a 3-D layered element, and it can be used to model composite laminates. SOLID45 is a 3-D structural solid that dose not model layers, which is used to model the grips. The 8-node hexattedrals were employed for element [6].

Meshing the Coupon. The mesh begins with dividing areas on the sample. The sample was divided into 14 small areas, and then a mesh was created in each area. In order to gain even and uniform elements, the locations of key points on the sample were

carefully selected. Then, the meshed areas were extruded and the meshed volume was obtained. The details about this procedure are demonstrated in Figure 4.02 and Figure 4.03, and the dimension and geometry of each divided area are shown in Figure 4.04. Each element has its own attributes based on element type, real constants, material properties, element coordinate system, and section ID [6].

Real constants are the parameters that provide the opportunities to make model the configuration of each layer. As the composite is the objective in this work, and the layup selected is $[45, 0, 90, -45]_s$ the layer model can be created by defining the real constants. Real constants model is a convenient tool to define the thickness of each layer as well.

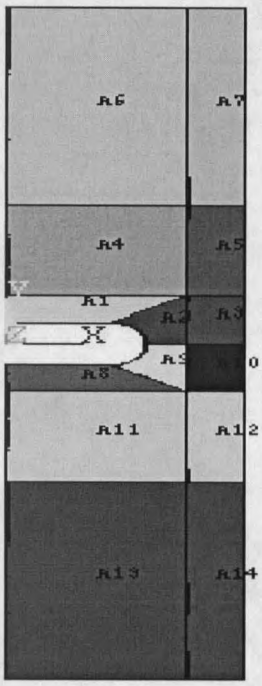

Figure 4.02 Divided areas on the coupon

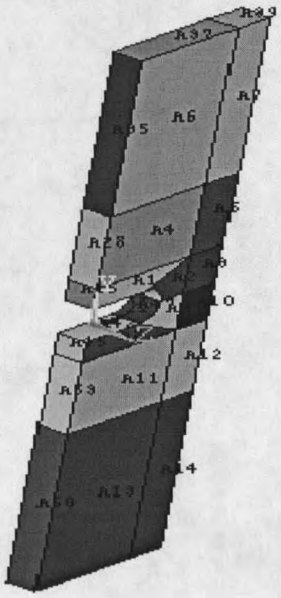

Figure 4.03 Extrude and create the volume

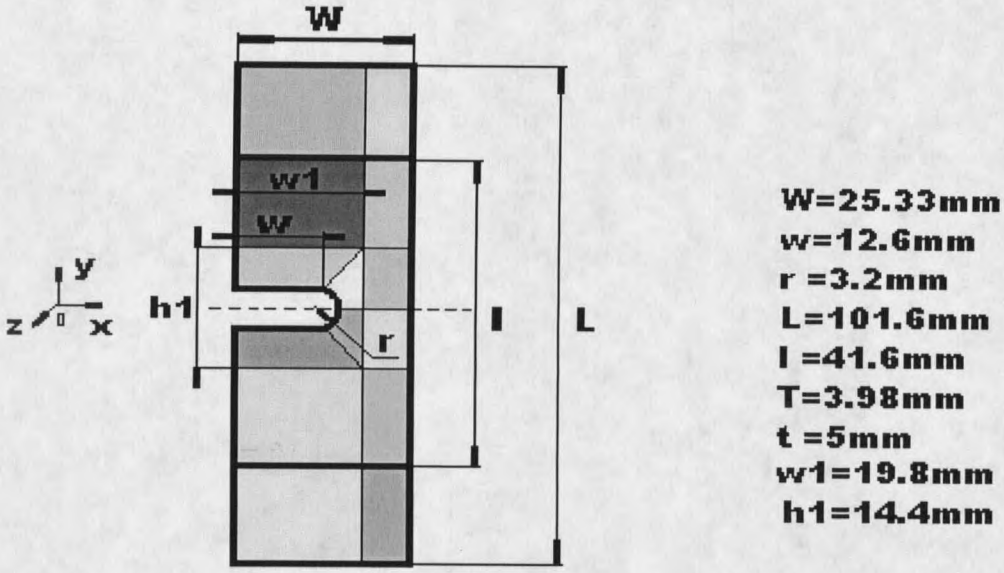

Figure 4.04. Dimension of the divided areas

After carrying out the procedure above, the mesh modeling was completed. The meshed sample is illustrated in Figure 4.05 (a) and Figure 4.06 (b).

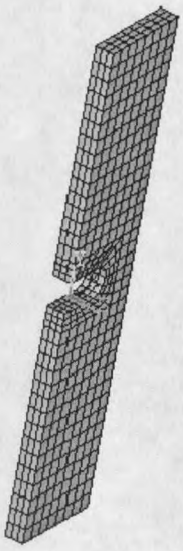

Figure 4.05 (a) Mesh on full specimen

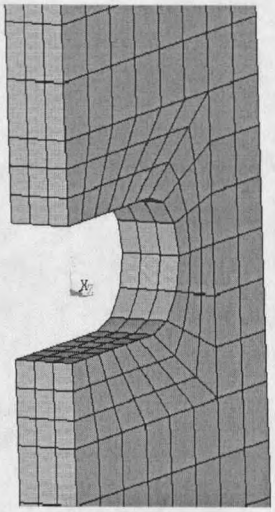

Figure 4.05 (b) Partial illustration

Defining the Layered Configuration. An important characteristic of a composite material is its layered configuration. Each layer may be made of a different orthotropic material with different principle directions. For laminated composites, the fiber directions define the layer orientation. Defining this layered configuration is done by means of specifying individual layer properties. With this method, the material properties, layer orientation angle, and layer thickness are defined. The layer orientation angle defines the orientation of the layer coordinate system with respect to the element coordinate system. The angles of +45, 90, -45, and 0 are specified in the current modeling. The layer orientation angle is illustrated in Figure 4.06 (a). Note that the principle of coordinate transformation is depicted in Chapter 2, and the procedure for evaluating parameters in rotated coordinate system rotation is shown in Appendix A using the Mathematica program.

We consider the selected composite a transversely isotropic material, so we define the material properties in the scope of elastic, and orthogonal material.

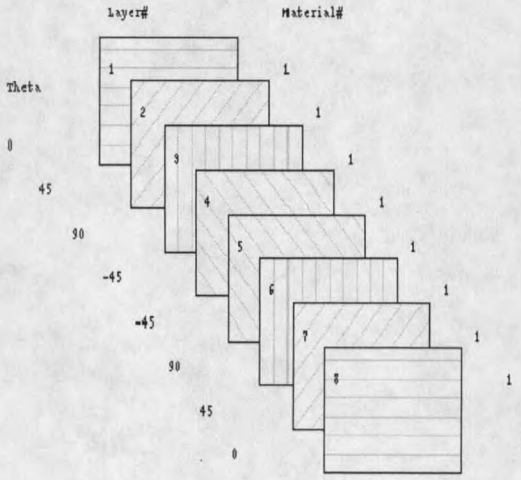

Figure 4.06 (a) Layup of the composite

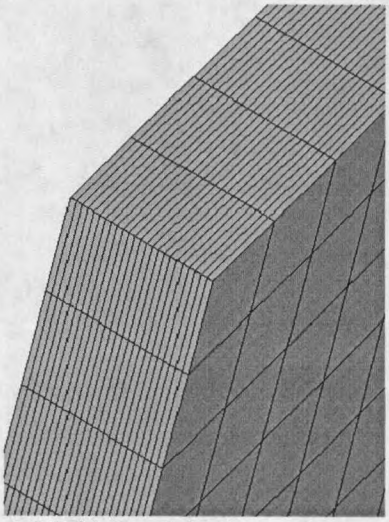

Figure 4.06 (b) Partial illustration

Modeling the Grips (Contact Elements)

As described in Chapter 3, the coupons are clamped with grips during the experiments. The effects of grips need to be taken into consideration for modeling. The clamps are fixed on the grips, and the coupons contact the clamps directly. The surfaces of the clamps are very rough, so that they provide high friction forces when the grips move, and force the coupon to move together with the grips accordingly. The grips affect the experimental results dramatically [6].

This condition was simulated by means of contact elements. Modeling the grips leads us to another subject; contact problem. Contact problems are highly nonlinear and require significant computer resources to solve. Contact problems present two significant difficulties. First, it is necessary to identify the regions of contact. Secondly, most contact problems need to account for friction. There are several friction laws and models to choose from, and all are nonlinear. Frictional responses can be non-deterministic, making solution convergence difficult [6].

As shown in Figure 4.07 and Figure 4.08 (notched coupon), there are four contact surfaces, two are at the top and another two are at bottom of the sample. The friction force is very large, and we imagine that coupons always stick to clamps without any deviations during the experiments. An effort was made to simulate the exact grip conditions of tests with the model, but no results were produced due to non-convergent solutions. As a consequence, an alternate model of grips, a simpler one, was required to accomplish this work. Therefore, in order to simplify this complex physical procedure, "bonded (always)" was selected to model via the Contact Wizard [6] (see Figure 4.09). This condition is similar to the one in which the samples are "glued" on the grips. With

this type of constraint, the contact elements are essentially coupled nodes. The displacement boundary conditions were applied on the grips for numerical/experimental comparisons.

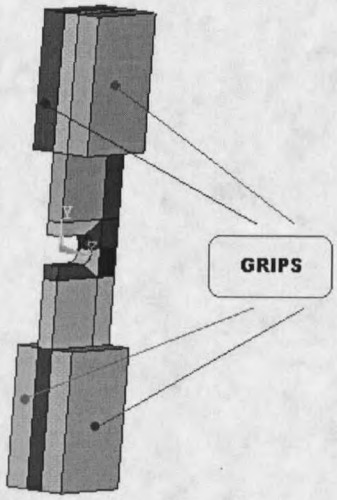

Figure 4.07 Grip modeling

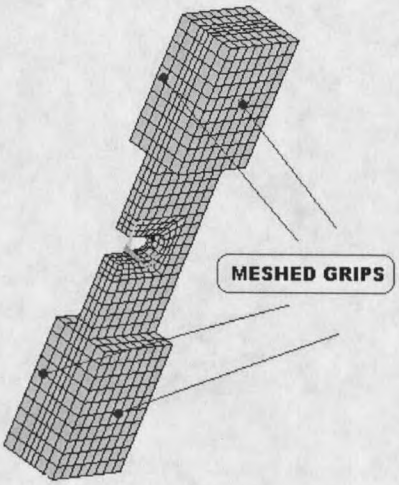

Figure 4.08 Contact element

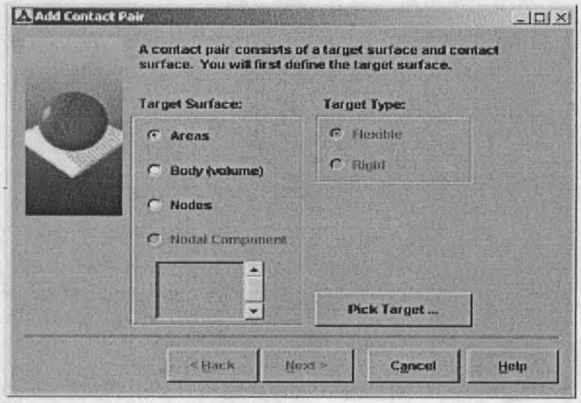

Figure 4.09 Contact Wizard

The MSU composite database provides the accurate characteristic parameters of this composite [7]. In fact, three elements affect the results of the modeling, geometry, characteristic composite properties, and applied loads. Refer to the Eq.(4.53).

Furthermore, we input the standard accurate characteristic properties of composite to ANSYS, and the loads modeled by computer are the same as applied to grips during the experiments. Under the precondition that the simulation of grip conditions in the test is accurate, the modeling results are supposed to match the experimental ones. On the contrary, if the modeling results do not agree with the experimental data, we can diagnose that the grip modeling is not correct.

By comparing the FEM modeling results with the experimental results, the gaps between the two groups of data were identified. In order to make the FEM modeling results fit the experimental ones, several parameters of grip properties are changed, such as the thickness of the grip, the modulus of the grip and so on. This process was to quantify the complex grip conditions during experiments by several parameters. After going through several iterations, the result that the two groups of data satisfy was found. These parameters were subsequently held constant. These parameters of the grip properties were deemed the standard modeling of grip conditions in the lack of accurate and precise contact element modeling. This set of parameters was adopted for all of the optimization studies to determine the transversely isotropic elastic constants.

Boundary Conditions

The main goal of the FEM modeling is to examine how a structure or component responds to certain loading conditions. Therefore, specifying the proper loading conditions is a key step in the analysis. There are a variety of ways to apply loads in the ANSYS program [6].

The word *loads* in ANSYS terminology includes boundary conditions and externally or internally applied forcing functions. For example, loads in structural disciplines are displacements, forces, pressures and so on [6].

This load modeling involves displacements and forces that correspond to the displacements and forces during experiments. According to the experimental loads used, four different loading paths are applied to the samples respectively, tensile (open/close) u_y, tensile plus shear (sliding) $u_y + u_x$, rotation (moment), ω, and tensile plus shear plus rotation, $u_y + u_x + \omega$. These loading paths were applied through the grips by changing the length of hydraulic actuators of the IPL; the following several paragraphs describe the details of each load case. Note that the displacements were used as the control variables rather than forces in this project.

<u>Tensile Load Model.</u> All displacements were applied to the grips rather than the coupon itself. The grips at the bottom of the coupon were fixed, and the top grips were movable. Tensile displacement was then applied on the grips at the top, and the displacements were constrained on the grips at the bottom. Coupled degrees of freedom were used to apply the controlled displacements. Following applied loads in the actual experiments, the displacement in Y direction was applied on the top grips. The tensile load modeling is illustrated in Figure 4.10 and Figure 4.11.

By constraining the displacements of grips at the bottom of the coupon in X, Y and Z directions, the lower part of the coupon was fixed. The tensile response was in the Y direction.

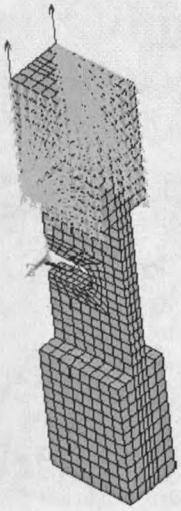

Figure 4.10 Applying tensile displacement

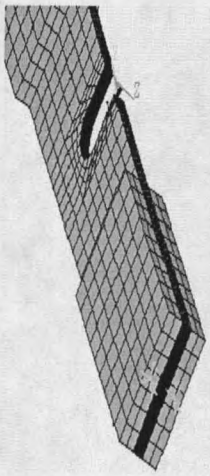

Figure 4.11 Constraining displacement

Shear (Sliding) Load Model. In the same manner, the shear (sliding) model was applied. The only difference between the tensile model and shear model was that applied displacement of the shear model was in the X direction rather than Y direction. The sliding load modeling is shown in Figure 4.12.

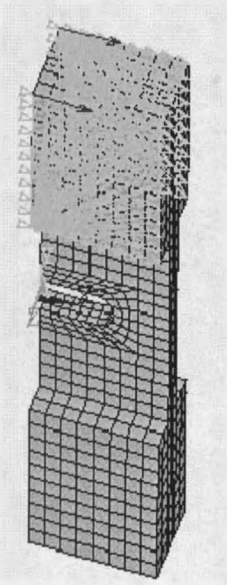

Figure 4.12 Shear load case

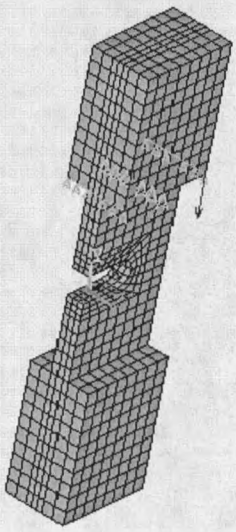

Figure 4.13 Rotation load case

Rotation (Moment) Load Model. This modeling is a bit different. We need to fix an axle located on the line with the coordinate position of X=W/2, Y=(L-l)/2. Refer to Figure 4.04. Then, coupling degrees of freedom on the grips, the displacement in Y direction was applied to one side of the grips, and the displacement in the opposite direction was applied on another side of the grips, to create the rotation (moment) model. This rotation load model is illustrated in Figure 4.13.

Combination Load Model. The combination load modeling of tensile plus moment and shear plus moment are shown in Figure 4.14 and Figure 4.15. The tensile or shear is simply superimposed on the rotation loads.

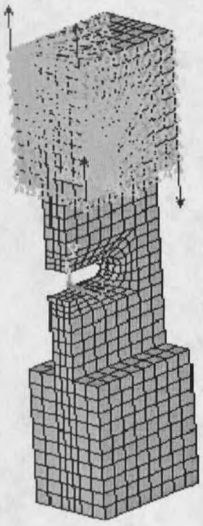

Figure 4.14 Tensile + Moment load case

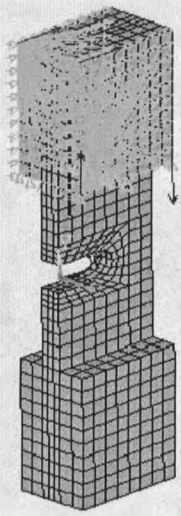

Figure 4.15 Shear + Moment load case

Specific Point to Be Measured

In Chapter 3, the points on the coupon that were measured have been specified. The corresponding specific points of both the notched sample and straight sample were defined in FEM models. Upon the execution of the ANSYS program, we will acquire the

reaction forces of these points. The data of these points by FEM models were compared with the corresponding experimental data.

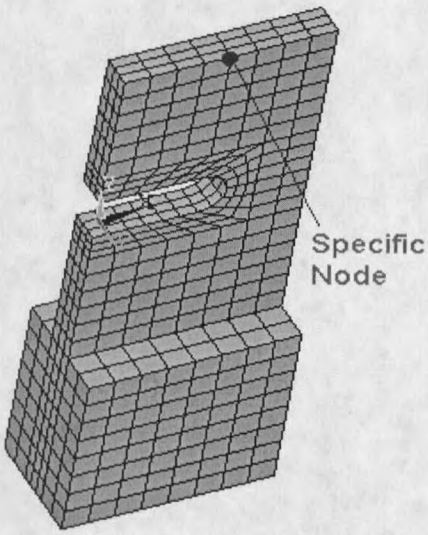

Figure 4.16 (a) Specific point on notched coupon

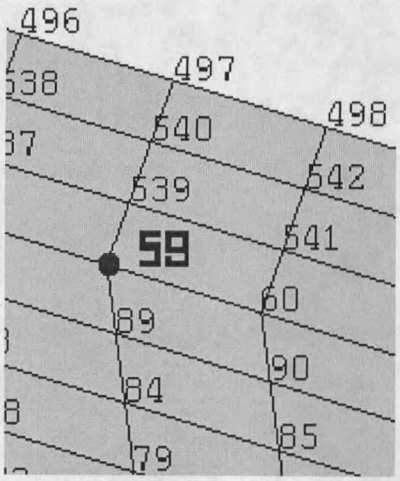

Figure 4.16(b) Enlarged specific point

The specific point on the notched coupon to be measured is illustrated in Figure 4.16 (a) and Figure 4.16 (b).

Obtaining the FEM Model Results

The purpose of using the FEM model is to simulate the experimental data, thus obtaining the corresponding modeling results. To determine reaction forces and moment at the node No.59 is the objective of the FEM model in this project.

As the reaction forces and moment can not be acquired directly from the model, it is necessary to take several steps to obtain them. In the first step, all of the nodes on the selected coupon (Figure 4.19) including node 59 were selected. Performing the FEM model by ANSYS, the forces of all of the selected nodes were added. Yet, the forces and moment distributions at a specific node are required in this project. Secondly, the Node

No.59 was selected, and the elements attached to the Node No.59 were selected. The selected node and elements attached to the node are illustrated in Figure 4.21 and Figure 4.22. Then the nodal force and moment contributions of the selected elements attached to the node were summed. Upon element calculation, the reaction forces and moment of node 59 were obtained.

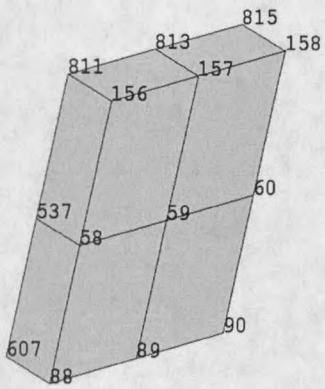

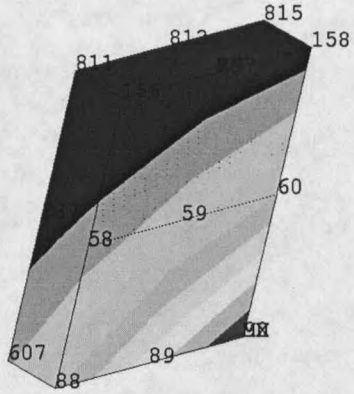

Figure 4.17(a) Select node and elements 01 Figure 4.17 (b) Selected node and element 02

Bounding Techniques

The estimation of the engineering constants of the fiber-reinforced composites was accomplished by means of micromechanical analysis in Chapter 2. The simplest and most intuitive approach, the mechanics of materials approach, was used in this micromechanical model. However, the experience has shown that these simple models are often inaccurate and that there is no substitute for experimental characterization [12].

The elasticity method is another approach to predicting the composite stiffness. Both the mechanics of material and the elasticity approaches have the common objective, estimating the elastic moduli of the composites. The variational energy principles of classical elasticity theory are used to determine upper and lower bounds of the

engineering constants of composites [13]. This approach has limitations as well, and is too theoretical to be used in practical situations. As a result, a semi-empirical method was used to modify the upper and lower bounds of the engineering constants of the composite.

Because the micromechanical theories must be validated by careful experimental work and the assumption of the engineering constants of a composite has to agree with the experimental data, it is necessary to compare the experimental data with the modeled outcomes. Furthermore, in order to find more accurate engineering constants, the optimization technique was employed. The lower and upper bounds of the engineering constants play the crucial roles as the constraints in the classic optimization problem. Minimizing the difference between the experimental data and the computer data is the objective of this optimization, thus gaining more accurate engineering constants.

The (Variational) Energy Method of Elasticity

By means of example, a uniaxial tension test to determine the elastic modulus of the composite material E is chosen for illustrating the bounding techniques with variational principles. The stress and strain states are assumed to be macroscopically uniform which is consistent with the assumption that the composite material is a macroscopically homogeneous continuum. In a uniaxial tension test, the resulting strain energy can be written in two forms [2]:

$$U = \frac{1}{2}\frac{\sigma^2}{E}V \quad \text{[2], [9], [13], [29]} \tag{4.25}$$

$$U = \frac{1}{2}E\varepsilon^2 V \quad \text{[2], [9], [13], [29]} \tag{4.26}$$

where U is strain energy; E is elastic modulus; σ is stress; ε is strain.

The fiber and matrix constituent materials are assumed to be linearly elastic and isotropic and to obey Hooke's law in the form

$$\sigma_x = \frac{\upsilon E}{(1+\upsilon)(1-2\upsilon)}\left(\varepsilon_x + \varepsilon_y + \varepsilon_z\right) + \frac{E}{(1+\upsilon)}\varepsilon_x \quad \text{[2], [13]} \tag{4.27}$$

$$\sigma_y = \frac{\upsilon E}{(1+\upsilon)(1-2\upsilon)}\left(\varepsilon_x + \varepsilon_y + \varepsilon_z\right) + \frac{E}{(1+\upsilon)}\varepsilon_y$$

...

$$\tau_{xy} = G\gamma_{xy} = \frac{E}{2(1+\upsilon)}\gamma_{xy}$$

where σ_x, σ_y, and σ_z are the stress in x, y and z directions respectively (Global coordinate system); ε_x, ε_y, and ε_z are strains in x, y and z directions respectively (Global coordinate system); γ_{xy}, γ_{yz}, and γ_{zx} are shear strains in x-y, y-z and z-x planes; and υ is Poisson's ratio.

The elastic modulus for a composite material may be determined experimentally by a simple unixial tension (or compression) test. The strain energy U absorbed by the specimen is given by

$$U = \frac{1}{2}\int_V \left(\sigma_x\varepsilon_x + \sigma_y\varepsilon_y + \sigma_z\varepsilon_z + \tau_{xy}\gamma_{xy} + \tau_{yz}\gamma_{yz} + \tau_{zx}\gamma_{zx}\right)dV \quad \text{[2], [9], [13], [29]} \tag{4.28}$$

where V is volume.

The application of the principle of minimum complementary energy via calculus of variations can be used to determine a lower bound on the apparent Young's modulus, while the application of minimum potential energy can be used to determine the lower bound of the apparent Young's modulus.

<u>The Lower and Upper Bounds of Transverse Young's Modulus,</u> E_2. To find a lower bound on the apparent Young's modulus, E_2, the basic uniaxial test specimen with normal stress on the ends is utilized. Applying the principles of minimum potential and complementary energy result in:

$$E_2 \geq \frac{E_m E_f}{V_m E_f + V_f E_m} \quad [2], [13], [29] \tag{4.29}$$

for the lower bound and:

$$E_2 \leq \left(\frac{1-\upsilon_f - 4\upsilon_f \upsilon + 2\upsilon^2}{1-\upsilon_f - 2\upsilon_f^2} E_f V_f + \frac{1-\upsilon_m - 4\upsilon_m \upsilon + 2\upsilon^2}{1-\upsilon_m - 2\upsilon_m^2} E_m V_m \right) \quad [2], [13], [29] \tag{4.30}$$

for the upper bound.

This work is primarily applicable to isotropic composites, but it can be interpreted in terms of fibrous composites. Eq. (4.29) is the lower bounds on the transverse modulus E_2, whereas Eq.(4.30) is the upper bound. [2]

The value of Poisson's ratio, υ, for the composite material is unknown at this point. Also, the upper bound on E is unspecified. Applying the principle of minimum potential energy, the expression for the strain energy U is minimized with respect to υ to determint the bound on E. The minimization procedure consists of establishing the point at which: [2], [27]

$$\frac{\partial U}{\partial \upsilon} = 0 \tag{4.31}$$

where U is the strain energy; υ is Poisson's ratio of a composite.

and at the same time

$$\frac{\partial^2 U}{\partial \upsilon^2} > 0 \tag{4.32}$$

resulting in:

$$\frac{\partial U}{\partial \upsilon} = \frac{\varepsilon^2 V}{2}\left(\frac{-4\upsilon_f + 4\upsilon}{1-\upsilon_f - 2\upsilon_f^2}E_f V_f + \frac{-4\upsilon_m + 4\upsilon}{1-\upsilon_m - 2\upsilon_m^2}E_m V_m\right) \tag{4.33}$$

which is zero when

$$\upsilon = \frac{\left(1-\upsilon_m - 2\upsilon_m^2\right)\upsilon_f E_f V_f + \left(1-\upsilon_f - 2\upsilon_f^2\right)\upsilon_m E_m V_m}{\left(1-\upsilon_m - 2\upsilon_m^2\right)E_f V_f + \left(1-\upsilon_f - 2\upsilon_f^2\right)E_m V_m} \quad \text{[2], [27], [28]} \tag{4.34}$$

The matrix and fiber material are assumed to be isotropic and hence, $\upsilon_m < \frac{1}{2}$ and $\upsilon_f < \frac{1}{2}$. This establishes the bounds.

<u>The Lower and Upper Bounds of Shear Modulus Associated with Plane 1-2, G_{12}.</u>

The same procedure to determine the bounds on E can be used to determine the equivalent modulus of elasticity in shear G from a knowledge of the constituent shear moduli G_f and G_m, which are a fiber shear modulus and matrix shear modulus respectively. The only significant difference is that the test specimen of the composite material should be thought of as being subjected to a macroscopically uniform simple shear stress τ, which produces the macroscopically uniform shear strain γ. After application of the variation principles to complementary energy and strain energy

$$G \geq \frac{G_m G_f}{V_m G_f + V_f G_m} \quad \text{[13], [30]} \tag{4.35}$$

for the lower bound on G and:

$$G \leq G_m V_m + G_f V_f \quad \text{[13], [30]} \tag{4.36}$$

for the upper bound on G.

Semi-Empirical Method for Predicting the Bounds of Engineering Constants

Because of the inherent limitation of micromechanical approach to the stiffness characteristic of composites, empirical approaches become indispensable. Semi-empirical method is based on considerable experiments. Then, by means of the numerical analysis, one may find appropriate ways to fit the experimental data. The following approaches of determination of the bounds of the elastic moduli involve the semi-empirical method.

The Lower and Upper Bounds of the Longitudinal Modulus, E_1. The semi-empirical method is used to determine the bounds of E_1. Data has indicated that the lower and upper bounds of the longitudinal modulus E_1 can be 10% lower and higher respectively than the estimated value based on the micromechanical approach [11].

$$E_1^- = (1-10\%)(E_f V_f + E_m V_m) \tag{4.37}$$

$$E_1^+ = (1+10\%)(E_f V_f + E_m V_m) \tag{4.38}$$

Hence, obtaining the bounds of Young's modulus

$$0.9(E_f V_f + E_m V_m) \le E_1 \le 1.1(E_f V_f + E_m V_m) \tag{4.39}$$

The Lower and Upper Bounds of Poisson Ratio υ_{12}. Again, the semi-empirical method is employed to establish the bounds of Poisson ratio υ_{12}. Many experiences have indicated that the lower and upper bounds are 10% lower or higher respectively than the estimation by micromechanical analysis [13].

$$\upsilon_{12}^{-} = (1-10\%)(\upsilon_f V_f + \upsilon_m V_m) \tag{4.40}$$

$$\upsilon_{12}^{+} = (1+10\%)(\upsilon_f V_f + \upsilon_m V_m) \tag{4.41}$$

Thus, obtaining

$$0.9 \cdot (\upsilon_f V_f + \upsilon_m V_m) \le \upsilon_{12} \le 1.1(\upsilon_f V_f + \upsilon_m V_m) \tag{4.42}$$

The Lower and Upper Bounds of the Shear Modulus G_{23}. In order to determine the shear modulus associated with plane 2-3 G_{23}, the Poisson ratio in direction 2, υ_{23} has to be assumed first based on the elasticity theory. As stated previously in Chapter 2, the Poisson ratio has to satisfy [13], [30]

$$|\upsilon_{23}| < \left(\frac{E_2}{E_3}\right)^{1/2} \tag{4.43}$$

Since the Young's moduli have been established in the direction 2 and 3, one may estimate the lower and upper Poisson ratio υ_{23}

$$|\upsilon_{23}|^{-} = \left(\frac{E_2^{-}}{E_3^{+}}\right)^{1/2} \tag{4.44}$$

$$|\upsilon_{23}|^{+} = \left(\frac{E_2^{+}}{E_3^{-}}\right)^{1/2} \tag{4.45}$$

For a transversely isotropic material, there exists the relationship among shear modulus, Young's modulus and Poisson ratio

$$G_{23} = \frac{E_2}{2(1+\upsilon_{23})} \tag{4.46}$$

Thus, we can establish the lower and upper bounds of G_{23}

$$G_{23}^{-} = \frac{E_2^{-}}{2(1+\upsilon_{23}^{+})} \tag{4.47}$$

$$G_{23}^{+} = \frac{E_2^{+}}{2(1+\upsilon_{23}^{-})} \tag{4.48}$$

List the Upper and Lower Bounds of the Engineering Constants

By substituting the known parameters of constituent materials into the equations above, Eq.(4.29), Eq.(4.30), Eq.(4.35), Eq.(4.36), Eq.(4.37), Eq.(4.38), Eq.(4.40), Eq.(4.41), Eq.(4.44), Eq.(4.45), Eq.(4.47), and Eq.(4.48), the upper and lower bounds of each engineering constant can be derived. The values of upper and lower bounds of the engineering constants are listed in Table 4.03.

Table 4.03 The lower and upper bounds of engineering constants of the composite

Engineering constants	Lower and upper bounds
Longitudinal Modulus E_1	$29.119GPa < E_1 < 35.589GPa$
Transverse Modulus E_2	$5.338GPa < E_2 < 32.469GPa$
The major Poisson ratio υ_{12}	$0.261 < \upsilon_{12} < 0.319$
Shear modulus associated with the 1-2 plane G_{12}	$1.61GPa < G_{12} < 13.053GPa$
Shear modulus associated with the 2-3 plane G_{23}	$0.769GPa < G_{23} < 11.555GPa$

Modification of the Assumed Bounds of the Engineering Constants

As previously stated, the principles of minimum potential energy and minimum complementary energy have been used to establish the upper and lower bounds of effective elastic moduli. While the treatment is based on arbitrary phase geometry, the

bounds obtained are generally not close enough to provide a good estimate for the effective elastic moduli.

After reviewing the lower and upper bounds of the elastic moduli in the table above, it was recognized that the bounds of the engineering constants G_{12}, E_2 and G_{23} were too loose to be practical in the application. Therefore, it was considered appropriate to use the empirical data as an aid to establish tighter bounds on these effective elastic moduli.

However, estimation of the bounds of the effective elastic moduli was used only as a constraint for the optimization procedure. Our concern was to find the reasonable bounds for optimization rather than a profound study of determination for the bounds of effective elastic moduli.

<u>The Upper and Lower Bounds of Shear Modulus</u> G_{23}. Many experimental data have indicated that Poisson's ratio is insensitive to the determination of the bounds of shear modulus. In that case, neglecting Poisson's ratio yields the following:

$$G_{23}^{-} = \frac{E_2^{-}}{2(1+\upsilon_{23})} \tag{4.49}$$

$$G_{23}^{+} = \frac{E_2^{+}}{2(1+\upsilon_{23})} \tag{4.50}$$

whereas $\upsilon_{23} = 0.352$, the calculation procedure is shown in Appendix B.

<u>The Upper and Lower Bounds of Young's Modulus,</u> E_2. The upper bound of E_2 was not very close to the effective modulus. Again, the empirical method was used to estimate the upper bound of E_2, 10% higher than the effective modulus.

The revised lower and upper bounds of elastic moduli are shown in Table 4.04.

Table 4.04 The revised bounds of the engineering constants of the composite

Engineering constants	Lower and upper bounds
Longitudinal Modulus E_1	$29.119GPa < E_1 < 35.589GPa$
Transverse Modulus E_2	$5.338GPa < E_2 < 9.659GPa$
The major Poisson ratio υ_{12}	$0.261 < \upsilon_{12} < 0.319$
Shear modulus associated with the 1-2 plane G_{12}	$1.61GPa < G_{12} < 13.053GPa$
Shear modulus associated with the 2-3 plane G_{23}	$2.053GPa < G_{23} < 12.488GPa$

Description of Optimization

Overview Optimization

Optimization is an important tool in decision science and in the analysis of physical systems. To use it, we must first identify an objective, and then a quantitative measure of the performance of the system under study. The objective in this research is the discrepancy between the experimental results and FEM modeling results. The objective depends on variables $E_1, E_2, G_{12}, G_{23}, \upsilon_{12}$. Our goal is to find values of the variables that optimize the objective. The variables are restricted, or constrained, by the bounds discussed in the last section. The process of identifying the objective, the variables, and the constraints for a given problem is known as modeling.

Once the model has been formulated, an optimization algorithm can be used to find its solution. Usually, the algorithm and model are complicated enough that a computer is needed to implement this process. ANSYS has an optimization package. It is convenient to use ANSYS to implement the optimization consistently, since we have created the FEM models using ANSYS.

No panacea of the algorithms to resolve optimization problems, but, numerous algorithms, each of which is suitable to a particular type of optimization problem. It is designer's responsibility to choose an algorithm that is appropriate for this specific application [12].

Problems with the general form can be classified according to the nature of the objective function and constraints (linear, nonlinear, convex), the number of variables (large or small), and so on [15]. The optimization should be identified and defined first.

The Optimization Techniques Used for This Project

The estimation of stiffness and compliance of a fiber-reinforced composite has been stated in previous section. The stiffness and compliance of composites can be expressed in terms of engineering constants as follows:

$$C_{ijkl} = C_{ijkl}(E_1, E_2, G_{12}, G_{23}, \upsilon_{12}) \tag{4.51}$$

$$S_{ijkl} = S_{ijkl}(E_1, E_2, G_{12}, G_{23}, \upsilon_{12}) \tag{4.52}$$

The geometry, material properties (or stiffness and compliance of materials), and applied loads (forces or displacements) are the dependent variables to determine the reaction forces or displacements on the coupons. Eq. (4.53) depicts this relationship:

$$F_n^r, \delta_n^r = F_n^r, \delta_n^r (C_{ijkl}, g, f, \delta) \tag{4.53}$$

where F_n^r is the response force at node n; δ_n^r is the response displacement at node n; g is a specific geometry of the coupons; f is the applied force on the coupon; and δ is the applied displacements on the coupons.

The reaction forces or displacements at the specific nodes depend on g, f, δ and S_{ijkl}. That means there are three types of variables in this problem, the geometry, applied loads (forces or displacements), and the stiffness characteristic of the composite. The geometry with a notch was selected for this research, and the applied loads (forces or displacements) were also selected for this project. Hence, the only unknown is the stiffness characteristic of the composite. As the geometry and applied loads are known, different composites that have different material properties lead to different results. Moreover, as shown in Eq. (4.51) and Eq. (4.52), for a transversely isotropic composite, the compliance and stiffness characteristics are determined by five engineering constants, E_1, E_2, G_{12}, G_{23}, and υ_{12}. So there exists the relationship

$$F_n^r, \delta_n^r = F_n^r, F_n^r (E_1, E_2, G_{12}, G_{23}, \upsilon_{12}) \tag{4.54}$$

As stated in Chapter 3, upon applying the specified loads (displacements in this project), the reaction forces or displacements, $(F_n^r, \delta_n^r)_{Experiment}$, at the certain points of the coupon can be acquired during IPL tests. Meanwhile, the FEM model can be made to simulate the experimental conditions, where ANSYS is used to create the FEM modeling. By simulating the IPL tests, these models can be used to calculate reaction forces and displacements, $(F_n^r, \delta_n^r)_{Computer}$, at any node in the model of the sample.

According to the theories of micromechanical and macromechanical analysis, the modeling results should agree with the experimental results. Yet, these results usually do not fit well in practical situations. As a result of inaccuracy of the predictions of five engineering constants, the results show the discrepancy between the two approaches, the mathematical modeling and the actual experiments. By minimizing the difference between the experimental data and the computer modeling data, it is possible to optimize the engineering constants.

$$\left|(F_n^r, \delta_n^r)_{Computer} - (F_n^r, \delta_n^r)_{Experiment}\right| = e \tag{4.55}$$

where $(F_n^r, \delta_n^r)_{Computer}$ is the computer result of the reaction forces or displacements at node n; $(F_n^r, \delta_n^r)_{Experiment}$ is the experimental result of the reaction forces and displacements at node n;and e is the error to be minimized.

In fact, Eq. (4.55) represents the objective function in this optimization problem. The five engineering constants, E_1, E_2, G_{12}, G_{23}, and υ_{12}, are the variables, and these variables are restricted by the upper and lower bounds which have been discussed in section 2. These bounds indicate that this is a constrained optimization problem. Now the optimization model has been formulated. In order to find the solutions, the proper optimization algorithms have to be used. It is necessary to choose an algorithm that is appropriate for this specific application.

Optimization Algorithms Used by ANSYS

Understanding the algorithms used in the program is always helpful, and is particularly true in the case of design optimization. In this section, the optimization

theories used by ANSYS are introduced. The details on the following algorithms are presented: steepest descent search method, Newton search method, quasi Newton search method, and conjugate gradient method.

The optimization theories and methods used by the ANSYS optimization program is illustrated in Figure 4.18.

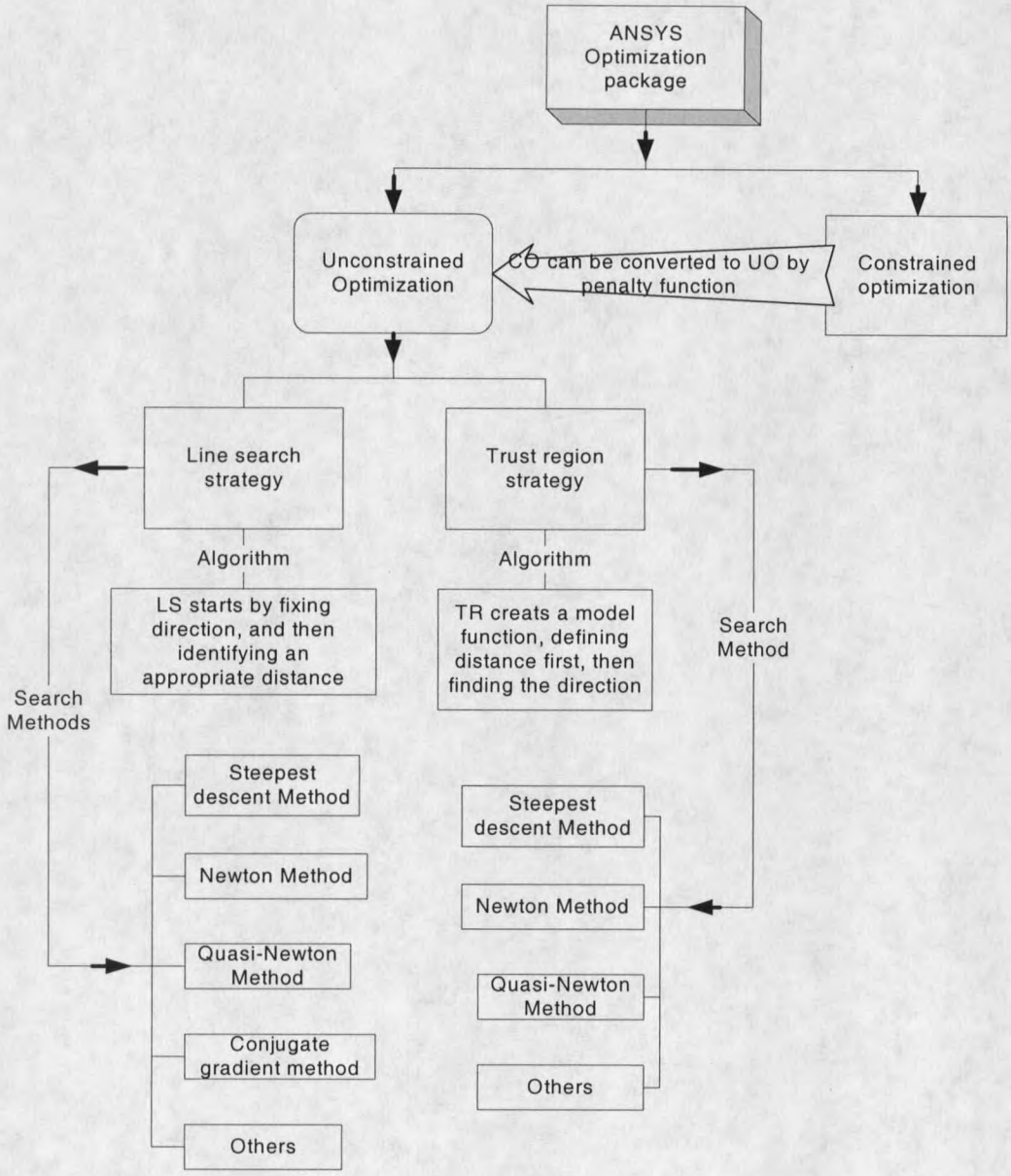

Figure 4.18 Illustration of the theories and methods used by ANSYS program

Although this is a constrained optimization problem, it can be converted to an unconstrained problem by means of penalty functions. Therefore, attention is focused on the unconstrained optimization algorithms rather than constrained ones in this discussion. There are two strategies to resolve this problem, the line search method and trust region method. In a sense, the line search and trust region approaches differ in the order in which they choose the direction and distance of the move to the next iterate [12].

In the line search strategy, the algorithm chooses a direction p_k and searches along this direction from the current iterate x_k for a lower function value. The distance to move along p_k can be found by approximately solving the following one-dimensional minimization problem to find a step length α.

$$\min_{\alpha>0} f(x_k + \alpha p_k) \tag{4.56}$$

At the new point a new search direction and step length are computed, and the process is repeated.

In the second algorithmic strategy, known as trust region, the information gathered about the objective function f is used to construct a model function m_k whose behavior near the current point x_k is similar to that of the actual objective function f. However, the model m_k may not be a good approximation of f when x is far from x_k. In other words, the candidate step p is found by approximately solving the following sub-problem [12]:

$$\min_{p} m_k(x_k + p), \text{ where } x_k + p \text{ lies inside the trust region.} \tag{4.57}$$

The model m_k in Eq.(4.57) is usually defined to be a quadratic function of the form

$$m_k(x_k + p) = f_k + p^T \nabla f_k + \tfrac{1}{2} p^T B_k p, \tag{4.58}$$

where f_k, ∇f_k, and B_k are a scalar, vector and matrix, respectively. The matrix B_k is either the Hessian $\nabla^2 f_k$ or some approximation to it.

Now consider two major issues: choice of the search direction p_k in line research methods, and choice of the Hessian B_k in trust-region methods. These issues are closely related, as will soon be discussed. The following several paragraphs present the optimization search methods.

Steepest Descent Direction. The steepest descent direction ∇f_k that is the gradient of the objective function is the most obvious choice for search direction for a line search method. The steepest descent method is a line search method that moves along $p_k = -\nabla f_k$ at every step. It can choose the step length α_k in a variety of ways. One advantage of the steepest descent direction is that it requires calculation of the gradient ∇f_k but not of second derivatives. However, it can be excruciatingly slow on difficult problems [12], [15].

Newton Direction. Another important search direction, perhaps the most important one of all is the Newton direction. This direction is derived from second order Taylor series approximation to $f(x_k + p)$, which is

$$f(x_k + p) \approx f_k + p^T \nabla f_k + \tfrac{1}{2} p^T \nabla^2 f_k p \overset{def}{=} m_k(p) \tag{4.59}$$

Assuming for the moment that $\nabla^2 f_k$ is positive definite, the Newton direction can be obtained by finding the vector p that minimizes $m_k(p)$. By simply setting the derivative of $m_k(p)$ to zero, the following explicit formula can be obtained:

$$p_k^N = -\nabla^2 f_k^{-1} \nabla f_k \tag{4.60}$$

The Newton direction is reliable when the difference between the true function $f(x_k + p)$ and its quadratic model $m_k(p)$ is not too large. The main drawback of the Newton direction is the need for the Hessian $\nabla^2 f(x)$. Explicit computation of this matrix of second derivatives is sometimes, though not always, a cumbersome, error-prone, and expensive process.

Quasi-Newton Search Directions. provide an attractive alternative in that they do not require computation of the Hessian and yet still attain a super-linear rate of convergence. In place of the true Hessian $\nabla^2 f_k$, an approximation B_k is used, which is updated after each step to take account of the additional knowledge gained during the step [12], [15].

Two of the most popular formulae for updating the Hessian approximation B_k are the symmetric-rank-one (SR1) formula, defined by

$$B_{k+1} = B_k + \frac{(y_k - B_k s_k)(y_k - B_k s_k)^T}{(y_k - B_k s_k)^T s_k} \tag{4.61}$$

and the BFGS formula, named after its inventors, which is defined by

$$B_{k+1} = B_k - \frac{B_k s_k s_k^T B_k}{s_k^T B_k s_k} + \frac{y_k y_k^T}{y_k^T s_k} \tag{4.62}$$

where $B_{k+1} s_k = y_k$, $s_k = x_{k+1} - x_k$, and $y_k = \nabla f_{k+1} - \nabla f_k$.

The quasi-Newton search direction is given by using B_k in place of the exact Hessian, that is,

$$p_k = -B_k^{-1}\nabla f_k \tag{4.63}$$

Conjugate-Direction Methods. The conjugate-direction methods have proved to be highly efficient search techniques. One of the remarkable properties of the conjugate gradient method is its ability to generate, in a very economical fashion, a set of vectors with a property known as conjugacy. They have the form

$$p_k = -\nabla f(x_k) + \beta_k p_{k-1} \tag{4.64}$$

where β_k is a scalar that ensures that p_k and p_{k-1} are conjugate- an important concept in the minimization of quadratic functions. Conjugate gradient methods were originally designed to solve systems of linear equations $Ax = b$, where the coefficient A is symmetric and positive definite. The problem of solving this linear system is equivalent to the problem of minimizing the convex quadratic function defined by

$$\Phi(x) = \tfrac{1}{2}x^T Ax + b^T x \tag{4.65}$$

so it was natural to investigate extensions of these algorithms to more general types of unconstrained minimization problems. In general, nonlinear conjugate gradient directions are much more effective than the steepest descent direction and are almost as simple to compute. These methods do not attain the fast convergence rates of Newton or quasi-Newton methods, but they have the advantage of not requiring storage of matrices. [3]

All of the search directions discussed so far can be used directly in a line search framework. They give rise to the steepest descent, Newton, quasi-Newton, and conjugate

gradient line search methods. All except conjugate gradient have an analogue in the trust-region framework [12].

ANSYS Optimization Package

The ANSYS program provides several optimization methods and tools to accommodate a wide range of optimization problems. The details on the techniques are presented in the following paragraphs: sub-problem approximation, first order, random design generation, sweep generation, factorial evaluation, and gradient evaluation.

The independent variables in an optimization analysis are the design variables. The vector of design variables is indicated by:

$$X = [x_1, x_2, x_3 ..., x_n] \tag{4.66}$$

Design variables are subject to n constraints with the upper and lower limits, that is

$$\underline{x_i} \le x_i \le \overline{x_i} \qquad (i = 1,2,3,...,n) \tag{4.67}$$

where n is number of design variables (note there are total of five variables in this project).

The design variable constraints are often referred to as side constraints and define what is commonly called feasible design space. Now, minimize [6]

$$f = f(X) \tag{4.68}$$

subject to

$$g_i(X) \le \overline{g_i} \qquad (i = 1,2,3,...,m_1) \tag{4.69}$$

$$\underline{h_i} \le h_i(X) \qquad (i = 1,2,3,...,m_2) \tag{4.70}$$

$$\underline{w_i} \le w_i(X) \le \overline{w_i} \qquad (i = 1,2,3,...,m_2) \tag{4.71}$$

where f is the objective function; g_i, h_i, w_i are state variables containing the lower and upper bounds respectively; and $m_1 + m_2 + m_3$ is the number of state variables constraints with various upper and lower limit values.

The state variables can also be referred to as dependent variables in that they vary with the vector X of design variables.

Random Design Generation Tool. A random search for an optimum of $f(X)$ is one in which a given number of values of X are generated at random- within some domain of interest- and the particular X for which $f(X)$ is best is denoted the winner [6].

$$X = X^* = \text{vector generated at random} \tag{4.72}$$

Sweep Generation Tool. The sweep tool is used to scan global design space that is centered on a user-defined, reference design set. Upon execution, a sweep is made in the direction of each design variable while holding all other design variables fixed at there reference values. The state variables and objective function are computed and stored for subsequent display at each sweep evaluation point.

Factorial Evaluation Tool. This is a statistical tool that can be used to sample all extreme points in design space. Factorial search is a search which is conducted over evenly spaced points in a simply connected region of a Euclidean space. Each of the x_i coordinates is assigned a set of evenly spaced points, called grid points, and only the values of x_i at these grid points are used. The function $f(X)$ is evaluated for all possible combinations of the grid points, and the grid value of X which yields the best $f(X)$ is deemed the winner [6].

Gradient Evaluation Tool. The gradient tool computes the gradient of the state variables and the objective function with respect to the design variables. A reference design set is defined as the point of evaluation for the gradient [6].

Sub-Problem Approximation Method. This method of optimization can be described as an advanced, zero-order method in that it requires only the values of the dependent variables (objective function and state variables) and not their derivatives. The dependent variables are first replaced with approximations by means of least squares fitting, and the constrained minimization problem is converted to an unconstrained problem using penalty functions. Minimization is then performed every iteration on the approximated, penalized function until convergence is achieved or termination is indicated. For this method each iteration is equivalent to one complete analysis loop. The trust region strategy is used in this method [6].

First Order Gradient Method. Like the sub-problem approximation method, the first order method converts the problem to an unconstrained one by adding penalty functions to the objective function. However, unlike the sub-problem approximation method, the actual finite element representation is minimized and not an approximation.

The first order method uses gradients of the dependent variables with respect to the design variables. For each iteration, gradient calculations (which may employ a steepest descent or conjugate direction method) are performed in order to determine a search direction, and a line search strategy is adopted to minimize the unconstrained problem.

Thus, each iteration is composed of a number of sub-iterations that include search direction and gradient computations. That is why one optimization iteration for the first order method performs several analysis loops [6].

Optimum for ANSYS Optimization

Now, after reviewing the algorithms provided by the ANSYS optimization package, the sub-problem method and first order method were chosen to carry out this optimization. The sub-problem method is representative of a zeroth order method and the first order is representative of a line search gradient method. These methods were chosen to explore the bounds of convergence of optimization methods. The random design generation contributes to determine the initial design variables, and to provide some pre-conditioning to the design variables for faster convergence. While not comprehensive, this choice of optimization procedures will provide a preliminary understanding of the times involved to obtain the best five elastic design constants variables.

The factorial tool and the sweep tool of ANSYS are involved in non-sequential methods. Furthermore, in the factorial tool, there are only 2 extreme values to be selected for each variable, which are too loose to find the optimum values. The sweep method cannot provide all of the necessary points for analysis. Upon execution, a sweep is made in the direction of each design variable while holding the rest of four design variables fixed at their reference values. Therefore, the iterations are not enough to scan all of the necessary points we need.

Gradient results are useful for studying the sensitivities of the objective function or state variables. Yet the gradient tool is not practical to resolve the actual optimization problem.

Accounting for the comprehensive factors, those tools were not selected as mentioned above, and choose sub-problem approximation, first order gradient methods and random tool to undertake the task of optimization for this project. The first order method is almost the panacea of a general optimization problem. Yet, it has drawbacks as well.

There are special considerations while using sub-problem approximation method and first order method. For the sub-problem approximation, the optimizer initially generates random designs to establish the state variable and objective function approximations. Because these are random designs, convergence may be slow. We can speed up convergence by providing more than one feasible starting design. Simply run a number of random designs and discard all infeasible designs.

Compared to the sub-problem approximation method, the first order method is seen to be more computationally demanding and more accurate. However, high accuracy does not always guarantee the best solution. The first order method is more likely to hit a local minimum. This is because first order starts from one existing point in design space and works its way to the minimum. If the starting point is too near a local minimum, it may find that point instead of the global minimum [12].

The operation procedure of sub-problem approximation and first order method in ANSYS is illustrated in Figure 4.19.

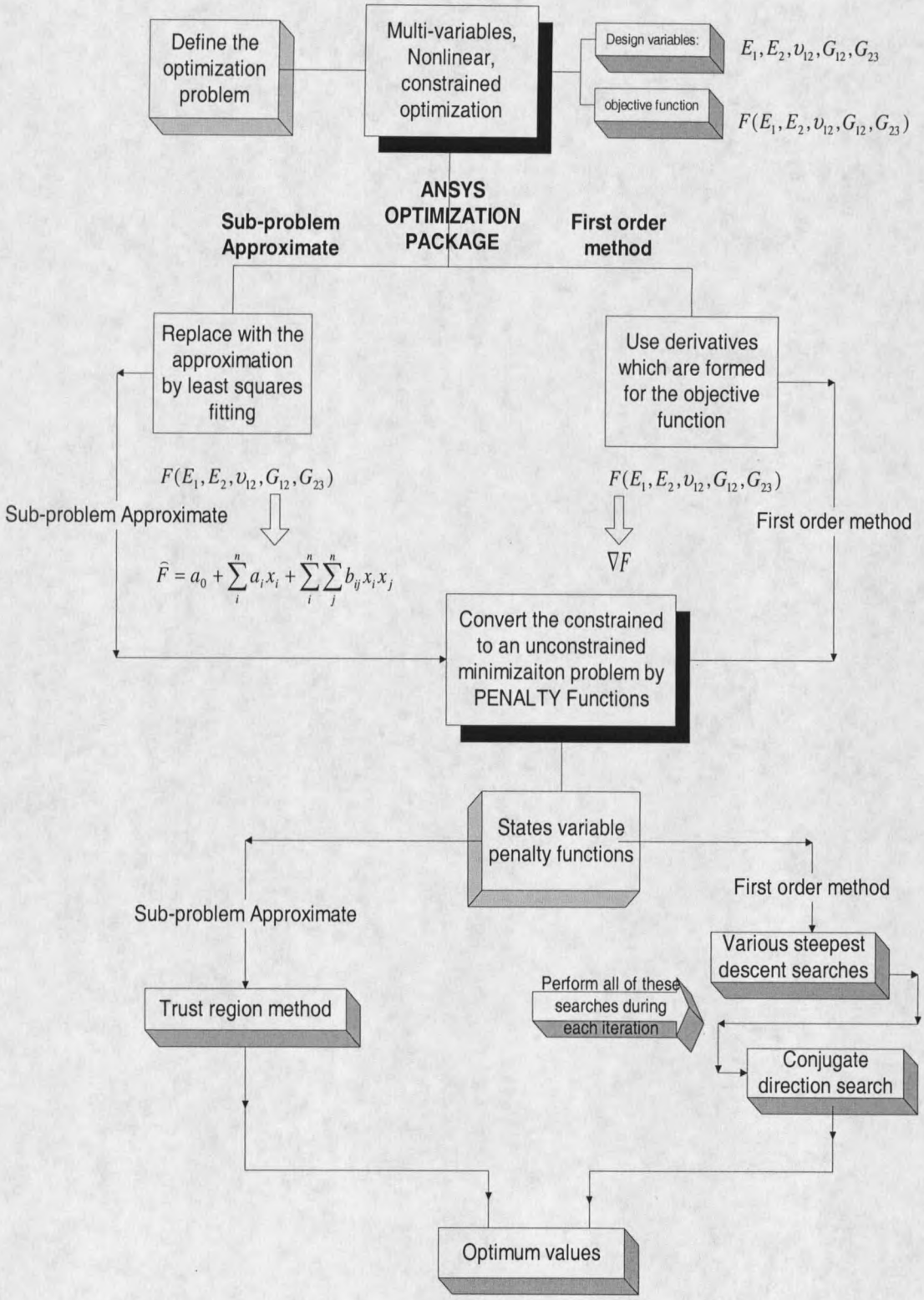

Figure 4.19 Flow chart of sub-problem approximation and first order method

Carrying Out Optimization

For both the sub-problem approximation method and first order method, the program performs a series of analysis-evaluation-modification cycles. That is, an analysis of the initial design is performed, the results are evaluated against specified design criteria, and the design is modified as necessary. This process is repeated until all specified criteria are met. The optimization data flow during an optimization analysis is shown in Figure 4.20. The analysis file must exist as a separate entity [6].

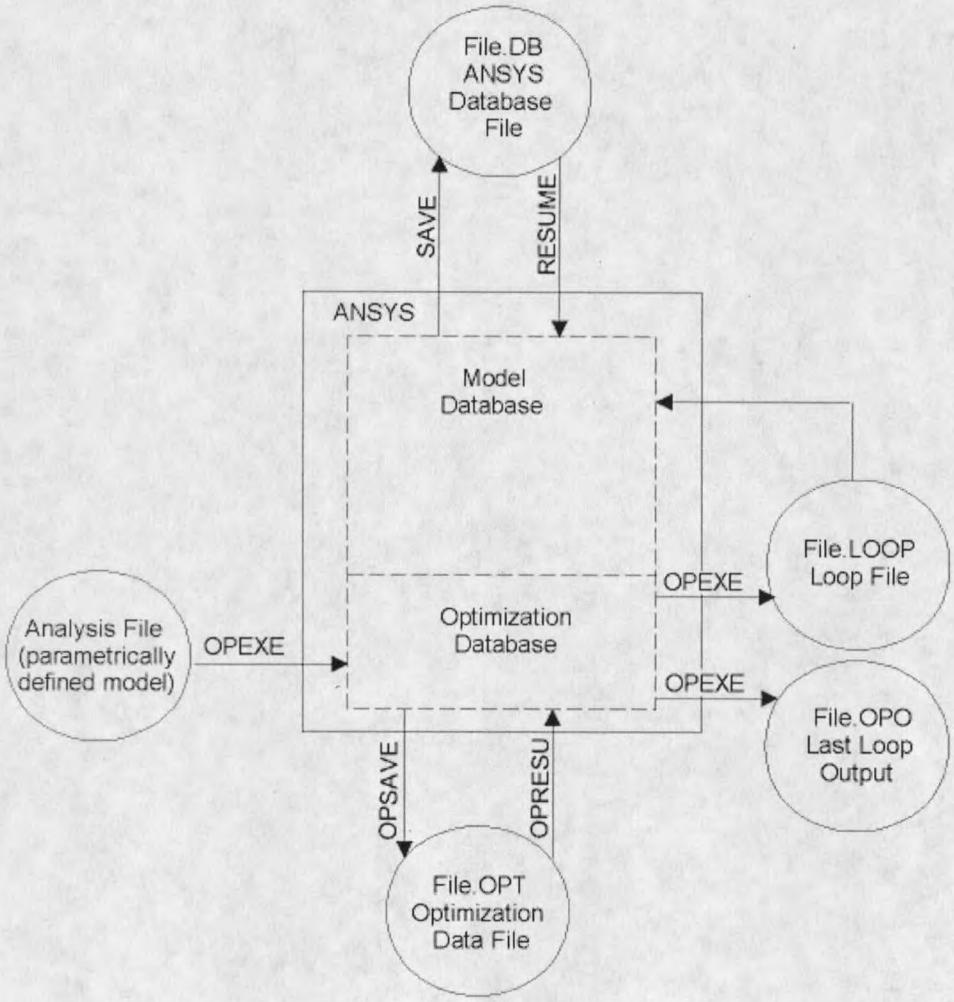

Figure 4.20 Optimization Data Flow

Every optimization method has to be performed by means of computer language, or commands. The commands used for sub-problem approximation method are OPTYPE, OPSUBP, and OPEXE; the commands used for first order method are OPTYPE, OPFRST, and OPEXE (Refer to the Appendix E).

Before performing these methods, we need to define the design variables, state variables and define objective function first.

The command "OPVAR,,DV" is used to define the design variables, the parameters of five variables in this research were listed in the following Table 4.06

Table 4.05 Definition of five design variables

Engineering constants	Value
Longitudinal Modulus E_1	32.354 x 10^9 Pa
Transverse Modulus E_2	8.781 x 10^9 Pa
The major Poisson ratio υ_{12}	0.29
Shear modulus associated with the 1-2 plane G_{12}.	2.021 x 10^9 Pa
Shear modulus associated with the 2-3 plane G_{23}.	1.973 x 10^9 Pa

The command "OPVAR,,SV" is used to define the state variables. The state variables in this case were the reaction forces of the specific point. Refer to Eq.(4.54).

The command "OPVAR,,OBJ" is used to define the objective function. The objective function in this project was the discrepancy between the FEM modeling results and experimental results. Refer to Eq.(4.55). The experimental results were input as the

parameters. These parameters are listed in Chapter 5. Moreover, the tolerance e needs to be defined as well. e =30 was selected for this research.

Note that the detailed macro files of programming are attached in Appendix E and Appendix F, and the optimization results are attached in Appendix H.

The FEM modeling, bounding techniques and optimization techniques have been discussed in this chapter, and the results acquired by employing these numerical methods are presented in the next chapter, Chapter 5.

CHAPTER 5

EXPERIMENTAL RESULTS, NUMERICAL RESULTS AND OPTIMIZATION

The experimental data from the In-Plane Loader were provided and the FEM modeling results were shown in this chapter. Comparing the experimental data and the modeling results, the optimization was carried out. Two optimization methods were used, sub-problem approximation method and first order gradient method. The random generation tool was used to determine the initial constants variables. After acquiring the optimum variables, the optimum engineering constants were input into the program and examined based on whether or not the modeling data agreed with the experimental data. The error analyses were made. The simple tensile load case is elaborated upon in this chapter, including experimental data analysis, numerical data analysis, and optimization. The results of the remaining test cases such as moment, tensile plus shear, and tensile plus shear plus moment were also shown in this chapter, and the detailed data and processes are demonstrated in Appendix G.

The procedure for obtaining optimum material properties was demonstrated in this Chapter. First, standard properties were input to determine grip conditions. Then, the lower and upper bounds of material properties were set via equations mentioned in Chapter 4. Lastly, the optimization of the material properties was carried out by both the sub-problem approximation method and the first order gradient method.

Experimental Results and Data Analysis of Simple Tensile Test Case

Four loading cases were used in the experiments; these were pure tensile, pure rotation, tensile plus shear, and tensile plus shear and plus moment as was presented in Chapter 2. As depicted in Chapter 3, the loads which are displacements in this research were applied at the grips by means of the IPL, and the data of reaction forces at a specific point were collected. Both the experimental data and the corresponding FEM modeling results were analyzed, and then appropriate data was selected to carry out the optimization. Due to the similarity of the procedure of each test loading model, we select the pure tensile test model was selected as a sample to study and discuss in detail. The results of the rest of the test models are shown in the end of this chapter.

The Experimental Results of the Pure Tensile Test

The pure tensile test on the IPL has been conducted; the detailed results of this test are shown in appendix G. The loading paths are shown in Figure 5.01.

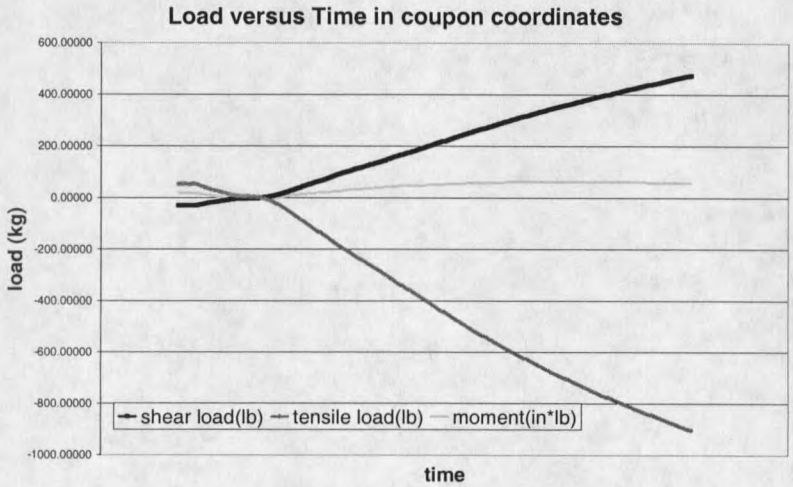

Figure 5.01 Loads of tensile test by the IPL

One may recognize that the shear and moment loads combined with the tensile loads were applied to the coupons during the tensile experiment, although we expected the pure tensile loading model. One of the reasons for this phenomenon is the complexity of the grip condition on the IPL during the tests. The error analysis in the next section provides details about the reasons.

The displacements applied to the coupons are regarded as the loads in this research. Furthermore, the displacements were used as applied loads while modeling in ANSYS. In that case, acquired data for applied displacements was expected during the experiments rather than forces. Yet it is only possible to obtain the original data of applied forces from Figure 5.01. The converted relationship between the force loads and displacements is demonstrated in Figure 5.03; the displacement plot vs time is shown in Figure 5.03.

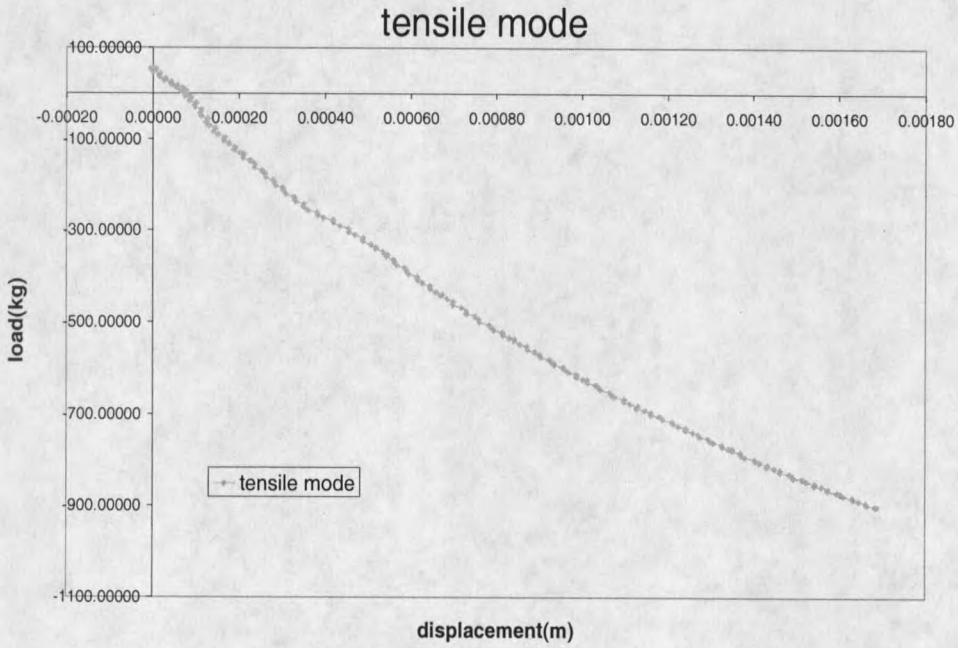

Figure 5.02 Displacement VS loads (Simple Tensile Test)

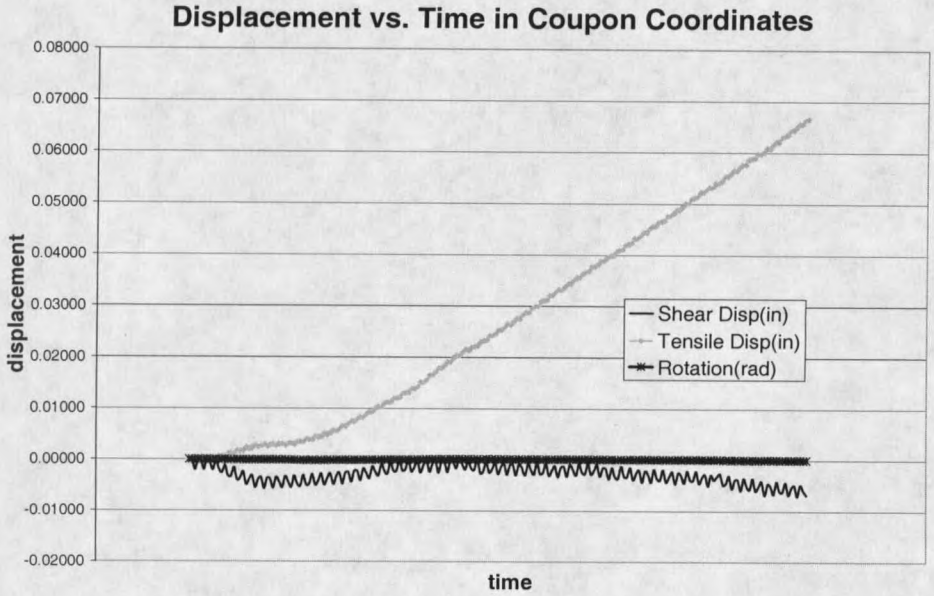

Figure 5.03 Displacements vs Time (Simple Tensile Test)

Screening the Experimental Data. As shown in the Figure 5.01, Figure 5.02 and Figure 5.03, we have obtained a wide range of data of the applied displacements which varies from 0 to 2.052E-3 m. However, not all of the data are used for the further analysis. Only the data which are shown to be in the linear elastic behavior section during the test are used. In other words, the selected data collected before any fracture or failure happened during the tests.

Although the simple tensile loading path was applied in the test, compression was evident at the beginning because of the effects of the grips. The data at the beginning should be ignored. According to the elasticity theory, if the loads applied on the coupon exceed a critical value which is called yield load, the material exhibits nonlinear elastic behavior. As the loads increase, the coupons may display some kinds of nonlinear elastic behaviors. Furthermore, it is difficult to determine the yield loads of the composite

because composites are generally anisotropic, markedly nonlinear, and, unlike metals, usually fail in an extremely complicated spatially diffuse non-catastrophic manner [1]. This difficulty hampers us in determining the exact linear elastic boundary. Yet, we already have a rough idea that the data collected when the applied loads are close to the maximum are not reliable. The selected data need to show linear character and it is usually visualized when the experimental results are plotted with respect to the applied loads. In short, we ignore the data at the beginning and the end. The experimental results and the figures provide some information for determining of the linear elastic boundary.

By analyzing the experimental results, we can see that a part of the section of the plots of experimental data in Figure 5.04 (a) and Figure 5.04 (b) are almost straight lines in the range between 0.02 inches and 0.04 inches, and we can select the experimental data with the displacement range from 0.02 to 0.04 inches, using the selected data for the further analysis.

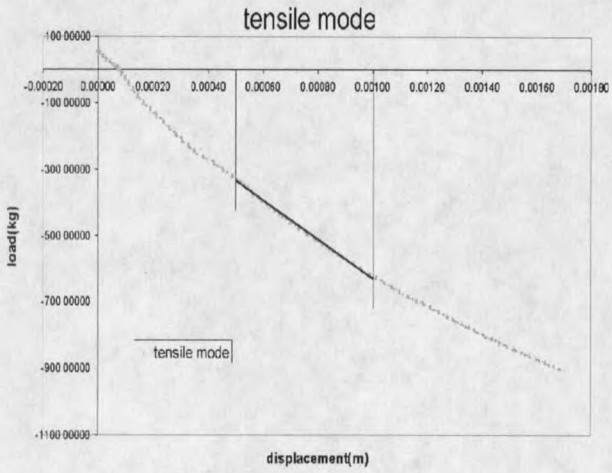

Figure 5.04 (a) Truncation 01

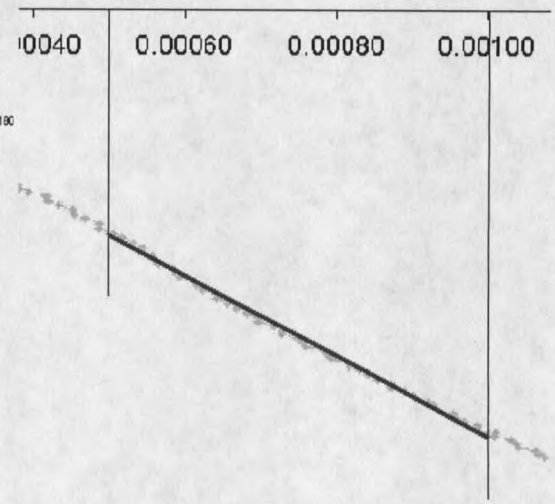

Figure 5.04 (b) The enlarged truncation

Analysis of Experimental Data. Three groups of data were obtained from the IPL tensile test, reaction tensile forces, reaction shear forces, and reaction moments. The details are demonstrated in Appendix H, and a part of the experimental data is shown in table 5.01.

Table 5.01 A part of experimental data from pure tensile test

Shear Load(kg)	Tensile load(kg)	Moment (m*kg)
230.05792	-462.39165	54.76618
261.78446	-522.9106	58.49046
293.0048	-581.2682	60.89728
316.25346	-624.30121	62.34736
339.50376	-666.84306	63.26407
366.86392	-716.13885	63.4843
392.51245	-761.82365	63.17608
415.36549	-801.75661	62.31774

However, one may recognize that the reaction shear forces are higher than was expected. Since it is only a pure tensile test, the reaction shear forces should be much smaller than the tensile forces. The reaction tensile and reaction shear forces are shown in Figure 5.05. We can conclude that there must be some errors during the experiments.

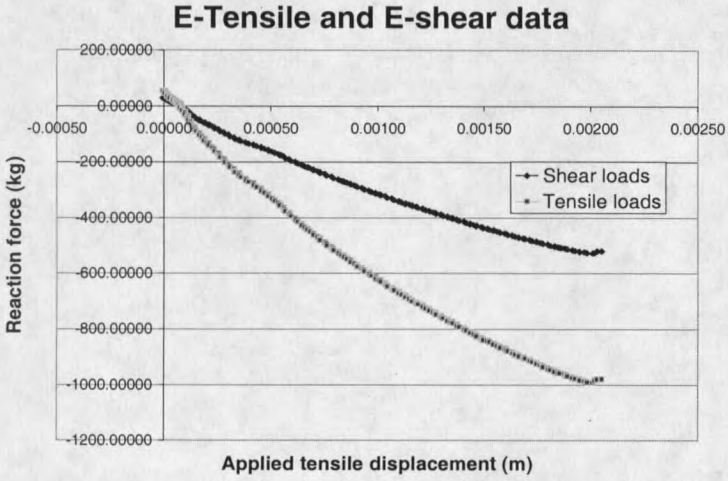

Figure 5.05 The reaction tensile and shear forces

Experimental Error and Tolerant Analysis

To explore the errors, we need to investigate every possible factor, such as facilities error, calculation error, operation error, coupon error and the effects of the grips.

Facility Error. The IPL machine is used to conduct the tensile tests. The structure of the IPL has been introduced in Chapter 3. Errors possibly occurred during the process of parts, fabrication and assembly. These errors are considered facility errors.

Operation Error. The errors occurred during the process in which the coupons are put into position on the IPL. The coupons should be centered on a mark on the IPL. Yet, it is difficult to regulate the center of the magazine. The operation errors can affect the final results.

Calculation Error. Displacements were used as loads in the tests. However, the data obtained are forces; the forces need to be converted to displacements by calculating. This process may bring about errors.

Coupon Error. The errors that may have occurred during the process of manufacturing the composite material and making the coupons with a specific geometry are regarded as the coupon errors.

The Grip Error. The coupons are clamped by the grips during the tests. Slipping was considered during the tensile test. The grips were fastened manually. It is very possible that the grips did not clamp the coupons evenly. This would bring about the errors during application of tensile tests on the coupons.

The grip error appears to be the major error occurring during the test, although there may also be facility error, operation error, and coupon error. Because the surface of composite coupon is very smooth, and the friction ratio is low, no matter how large the forces are that are applied to clamp the coupons, slipping cannot be avoided. The slipping brings about the large shear displacements.

These various kinds of errors may bring about another condition as shown in the following Figure 5.06.

The center of the coupon is supposed to meet the center of the coupon carrier of the IPL (Figure 5.07). Yet, the misalignment makes them deviated; shear forces then become bigger. Furthermore, this misalignment could be a major source for the bigger reaction shear forces during the pure tensile tests.

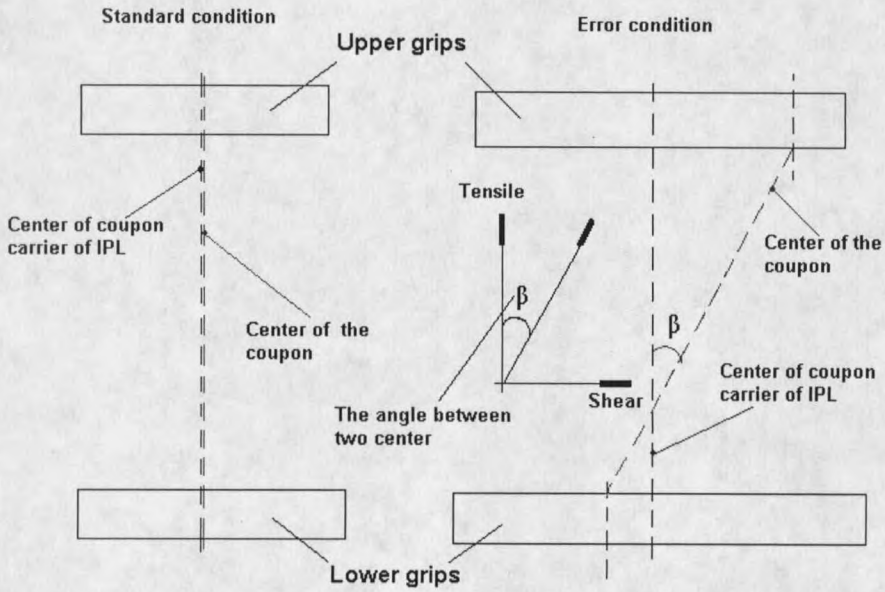

Figure 5.06 Possible error occurred during tensile test.

The moment data obtained by the pure tensile tests are relatively small. Moments were ignored for the mathematical modeling.

Numerical Results of Simple Tensile Loading Model

As elaborated upon in Chapter 4, an ANSYS FEM model was used to simulate the actual test. The pure tensile test is simulated on the computer, and the results are shown and analyzed in this section.

Obtaining the FEM Modeling Results

The initial engineering constants as shown in Table 4.05 are the input parameters. After going through the program, the results were acquired. The results of FEM modeling are shown in Appendix H. The stress distribution on the coupon is demonstrated in Figure 5.07 and Figure 5.08.

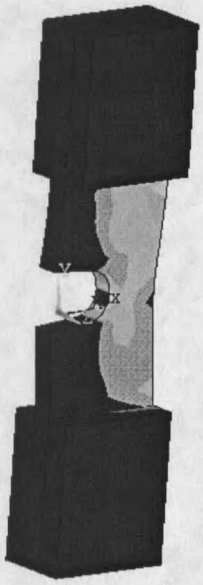

Figure 5.07 Stress distribution by ANSYS

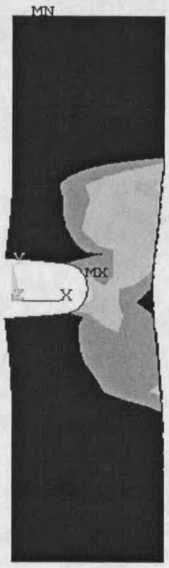

Figure 5.08 Stress distribution on coupon

Node No.59 was selected as the specific point about which forces and moments would be summed to be measured corresponding to the same point in the IPL test (refer to Figure 4.17(a) and Figure 4.17 (b)).

Reaction tensile forces, reaction shear forces, and the moment were obtained from the FEM model. The comparison between experimental data and FEM modeling results is shown in Figure 5.09.

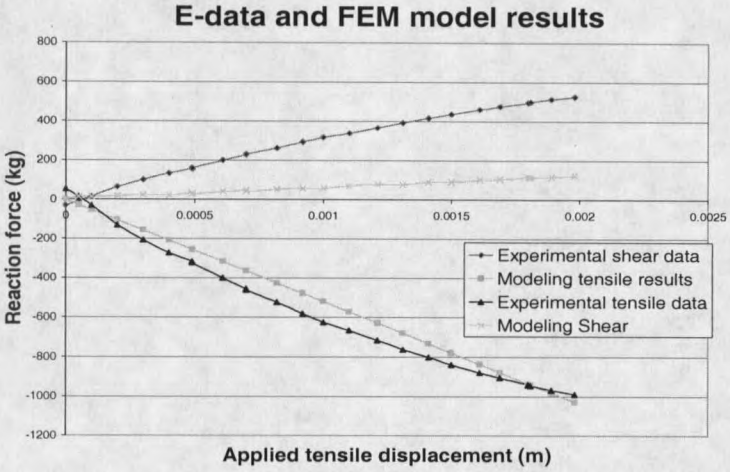

Figure 5.09 The comparison between experimental data and FEM results

One may see that the FEM tensile results from the modeling with the input of the initial engineering constants are close to the experimental data, yet the FEM shear results do not fit the experimental data well. The possible reasons could be the experimental errors which have been discussed in the previous section.

Examining the FEM Modeling Results

Finite Element Analysis is merely a numerical method used to simulate the experimental conditions, and its results are not a substitute for the experimental data.

Hence, the results are approximate rather than the exact ones. However, it is a very efficient way to predict the material behaviors upon the loads. In order to check and examine the accuracy of the FEM modeling, standard engineering constants, taken from the MSU composite database [11] were used as the input. The standard engineering constants are shown in the following table 5.02.

Table 5.02 The standard engineering constants

Engineering constants	Value
Longitudinal Modulus E_1	34 x 10^9 Pa
Transverse Modulus E_2	8. 1 x 10^9 Pa
The major Poisson ratio υ_{12}	0.29
Shear modulus associated with the 1-2 plane G_{12}.	4.48 x 10^9 Pa
Shear modulus associated with the 2-3 plane G_{23}.	3.58 x 10^9 Pa

The FEM modeling results with the input of the standard engineering constants are shown in Figure 5.10.

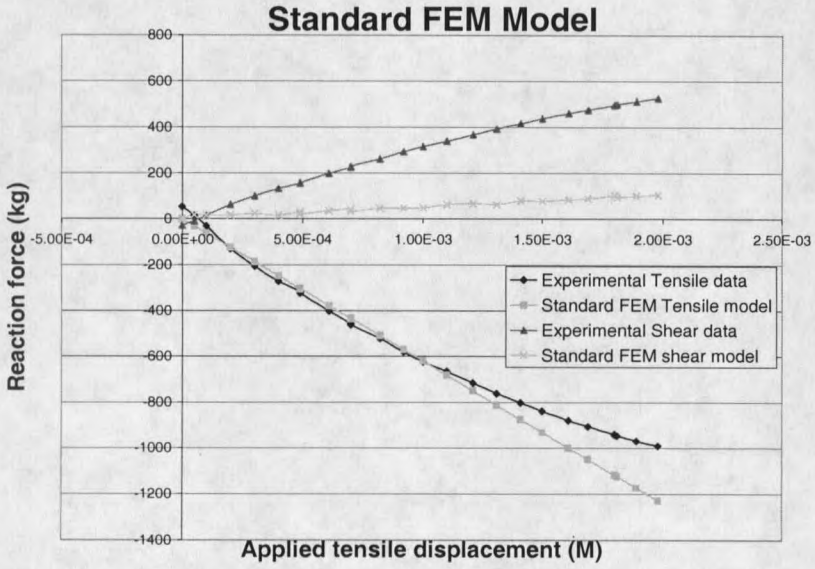

Figure 5.10 Standard FEM Model vs experimental results

It is recognized that the standard FEM results are closer to the experimental results than the results with the initial engineering constants. The comparison among experimental data, standard FEM modeling results, and initial value FEM modeling results is demonstrated in Figure 5.11. Theoretically, the FEM results should agree with the experimental data.

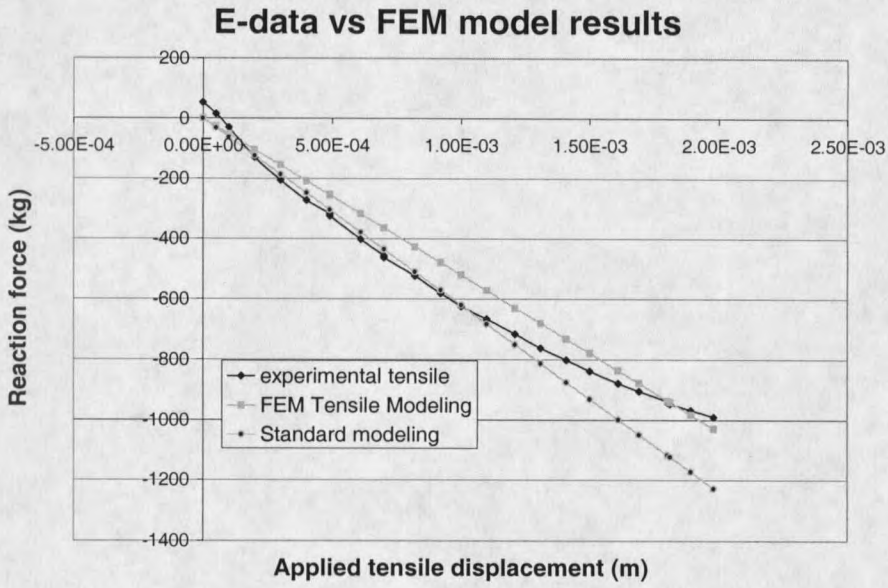

Figure 5.11 Comparison among experimental, standard and initial value FEM results

The standard FEM modeling results meet the experimental data most closely in the selected range, from 0.002 inches to 0.004 inches.

After carefully comparing the FEM tensile results with the experimental tensile data, one can conclude that the FEM modeling tensile results agree with the experimental data. Although the FEM shear results do not fit the experimental data well because of the errors occurred during the tests, the FEM modeling approach is feasible and reasonably accurate in this research.

Our task in this research was to determine unknown composite material properties rather than to check and verify the feasibility of FEM modeling. The known composite properties were used as input and the FEM model executed in order to obtain the modeling results, and then the FEM results were compared with the experimental results. The method is called backward method, and it is a highly efficient way to check and verify the FEM modeling. Yet, the composite material properties need to be refined, and an additional numerical method, the optimization, is required. We input the assumed engineering constants into the FEM program. There may be a discrepancy between the FEM modeling results and the experimental data because of the inaccurate assumption of the initial engineering constants. However, we assume that the experimental data are assumed to be reliable to optimize the engineering constants so that FEM modeling results can meet the experimental results. The optimization procedure and results are elaborated upon in the next section.

Optimization

The optimization theory and computer application have been introduced in Chapter 4. Four aspects affect the results of optimization: initial engineering constants, the optimization algorithms, the grip modeling, and the upper and lower bounds of the engineering constants.

Grip Modeling. Because grip modeling is one of the major factors that affects the FEM results and optimization results, a practical grip model must be developed in order to eliminate some errors.

In ideal conditions, the FEM model result should match the experimental data. FEM modeling results depend on the initial engineering constants, the geometry, and the applied loads. The geometry and applied loads have been determined. Under this circumstance, if we input the standard composite properties or engineering constants to the program, results should agree with the experimental data. However, there is still a discrepancy between the two sets of results. Improper simulation of the grip modeling creates a difference between experimental and FEM modeling results. The method to adjust the grip model has been elaborated upon in Chapter 4. The FEM model was modified to make results agree with the experimental ones by changing the contact element parameters. After going through several iterations, the specific contact element parameters were determined, which made the FEM modeling result meet the experimental ones. The modified grip model was regarded as the standard modeling and was used in every FEM model loading cases, including tensile, moment, tensile plus shear, and tensile plus shear and plus moment.

The standard grip properties are presented in the following Table 5.03.

Table 5.03 The parameter settings of grip modeling

Thickness of grip	Modulus of grip
0.02m	2E+12 Pa

Selecting Specific Loads. A large amount of data has been obtained from IPL tensile tests with different tensile load magnitudes. Yet, it is not necessary to simulate all of the loads by ANSYS. A typical load was selected.

The most efficient way is to acquire the average value of the applied loads in a specific domain, and input this into the program. As mentioned in the previous section, a suitable loads range was selected from 5.08E-4 m to 1.016E-3 m. Over this range, the load (displacement) experimental results were averaged. The averaged data is shown in Table 5.04:

Table 5.04 Average displacement and corresponding experimental results

Displacement (m)	Experimental result (kg) Average		
	Force X	Force Y	Moment Z
0.00074 m	237.20204	-474.85812	54.86889

Load (displacement) as shown in Table 5.04 and the standard contact element settings (see Table 5.03) were input with the initial engineering constants and standard engineering constants, respectively. The corresponding reaction forces are shown in Table 5.05.

Table 5.05 Average displacement and corresponding FEM modeling results

Applied loads (m)	Initial engineering constants results (kg)			Standard engineering constant results (kg)		
	Force X	Force Y	Momt Z	Force X	Force Y	Momt Z
0.00074	37.78127	-459.031	-6.83524	44.3289	-471.206	-7.15739

Comparing Table 5.04 and Table 5.05, it became apparent that the standard engineering constants modeling results were almost the same as the experimental data. Actually, this is the exact result hoped for. The goal is to find the real engineering constant by optimizing the FEM results and experimental data.

Because the experimental shear forces obtained from the IPL test are not accurate, the analysis is focused on the reaction to tensile forces in this project.

The Optimization Settings. Before carrying out the optimization, it is necessary to set the optimization parameters. The details about the optimization parameter settings are tabulated following text. The initial design variables and the upper and lower bounds of the design variables are provided in Table 5.06 and Table 5.07, respectively.

Table 5.06 Initial design variables

Engineering constants	Value
Longitudinal Modulus E_1	32.354 x 10^9 Pa
Transverse Modulus E_2	8.781 x 10^9 Pa
The major Poisson ratio υ_{12}	0.29
Shear modulus associated with the 1-2 plane G_{12}.	2.021 x 10^9 Pa
Shear modulus associated with the 2-3 plane G_{23}.	3.25 x 10^9 Pa

Table 5.07 The upper and lower bounds of the design variables

Engineering constants	Lower and upper bounds
Longitudinal Modulus E_1	$29.119GPa < E_1 < 35.589GPa$
Transverse Modulus E_2	$5.338GPa < E_2 < 9.659GPa$
The major Poisson ratio υ_{12}	$0.261 < \upsilon_{12} < 0.319$
Shear modulus associated with the 1-2 plane G_{12}	$1.61GPa < G_{12} < 5.5GPa$
Shear modulus associated with the 2-3 plane G_{23}	$2.053GPa < G_{23} < 5.5GPa$

Note that the upper bounds of the shear modulus G_{12} and G_{23} have been modified, in order to be more practical for optimization. The state variables and objective function

are defined in Table 5.08. The experimental tensile force to be selected is $(F_n^r)_{experiment} = -474.85812kg$.

Table 5.08 Definition of state variables and objective function

Settings	Equation	Equation code	Corresponding values
State variables	$F_n^r, \delta_n^r = F_n^r, \delta_n^r(C_{ijkl}, g, f, \delta)$	(4.54)	-462.384943 kg
Objective	$\left\|(F_n^r, \delta_n^r)_{Computer} - (F_n^r, \delta_n^r)_{Experiment}\right\| = e$	(4.55)	e=0, F=-474.85812 kg

Two optimization methods and one tool were used: the sub-problem approximation method, the first order gradient method, and the random generation tool. The random method was employed first to search the potential optimums, and then either sub-problem method or first order gradient method was used to obtain more accurate results. Note that initial variables are not required for the random method. The optimums obtained from the random method are the initial design variables used for the sub-problem approximation method and the first order gradient optimization method. The optimization method settings are shown in Table 5.09.

Table 5.09 The optimization method settings

Optimization method	Settings	
Random method	Iteration	30
	Feasible sets	29
Sub-problem	Iteration	100
	Feasible sets	99
First order	Iteration	90
	Percent step pace	5
	Percent forward diff.	1

Optimization results. After going through the optimization program, the optimization results obtained are as shown in Table 5.10, Table 5.11 and Table 5.12.

Table 5.10 The random method optimization results (Unit: Pa)

E_1	E_2	G_{12}	G_{23}	υ_{12}
0.34114E+11	0.77345E+10	0.34677E+10	0.48252E+10	0.30951

Table 5.11 The first order method optimization results (Unit: Pa)

E_1	E_2	G_{12}	G_{23}	υ_{12}
0.34654E+11	0.79627E+10	0.41482E+10	0.49035E+10	0.30965

Table 5.12.The sub-problem method optimization results (Unit: Pa)

E_1	E_2	G_{12}	G_{23}	υ_{12}
0.32824E+11	0.72772E+10	0.53741E+10	0.33664E+10	0.26175

In order to check and examine the accuracy of the optimum results, we input the optimized engineering constants which are used as input for the sub-problem method and the first order method; the results obtained are shown in Figure 5.12.

Comparing the optimization results, it is clear that the results from the first order method are more accurate.

Referring to Figure 5.12 and Figure 5.13, one may recognize that the plot of the reaction tensile results by both the first order method and the sub-problem approximation method are almost the same upon the simple tensile test. The reaction shear results by the two methods are a little different, but neither model result matches the experimental data very

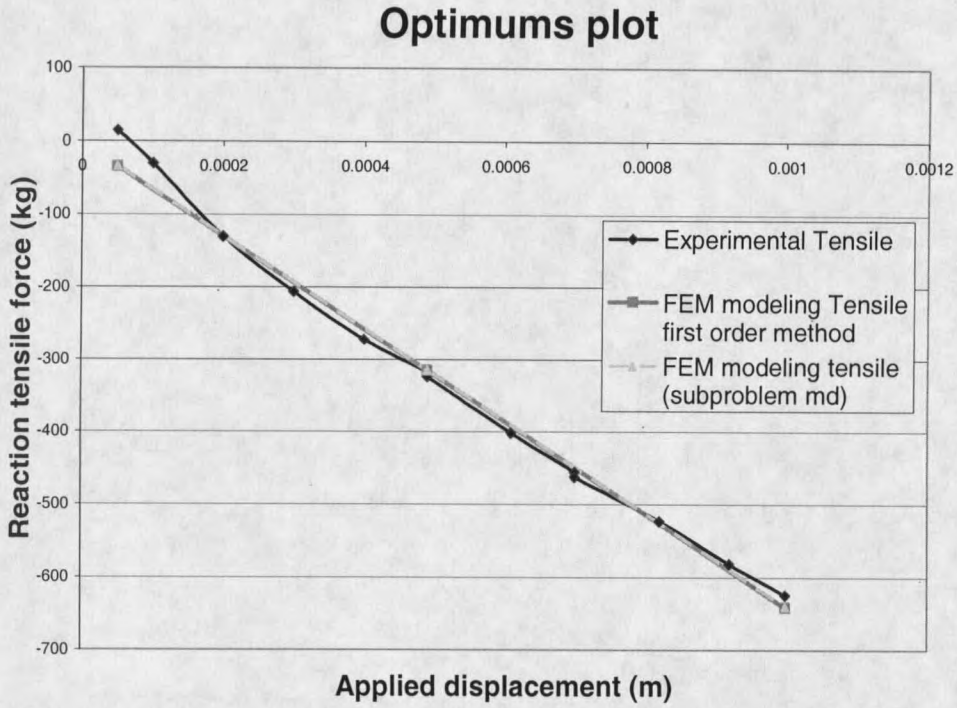

Figure 5.12 Plot of the reaction tensile force with the optimum engineering constants

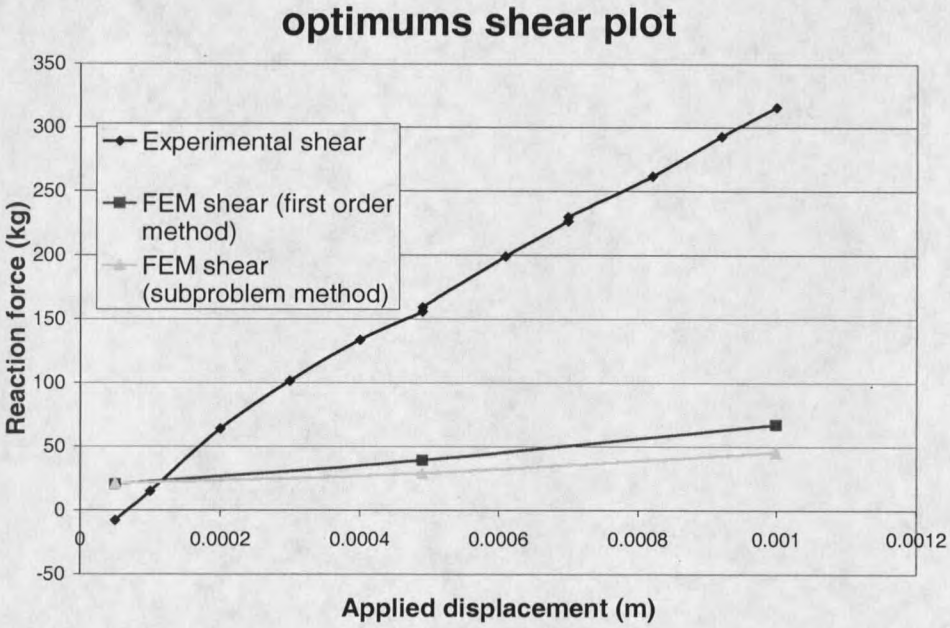

Figure 5.13 Plot of the reaction shear force with the optimum engineering constants

very well. As discussed in the previous section, slipping during the tensile test may increase the shear in the experimental data.

FEM Modeling Error

Optimum engineering constants from both optimization methods are each used as input and the corresponding results obtained. Then the results in the selected loads range were averaged. The average FEM results where compared with corresponding experimental data and the discrepancy were determined. The discrepancy fro the FEM tensile results were: The first order method: 5.574%; The sub-problem method: 7.3%. For the FEM shear results the discrepancies were: The first order method: 77.55%; the sub-problem method: 84.31%.

Recognize that the tensile results are very close to the real experimental data, though the modeling shear results do not agree with experimental data.

Complementary

As mentioned in Chapter 4, the plan was to conduct four different loading cases, and then the results upon each loading cases were used to compare with the corresponding FEM model result in order to carry out the optimization. The remaining loading cases went through the same procedure as the tensile case. The details of the procedure of data analysis are shown in Appendix I.

Results Analysis of the Tensile plus Shear Load Case

The tensile combined with shear load case was used for the coupons in these test.

Experimental Data Analysis

Plot the experimental results of tensile plus shear test, in Figure 5.14 and Figure 5.15.

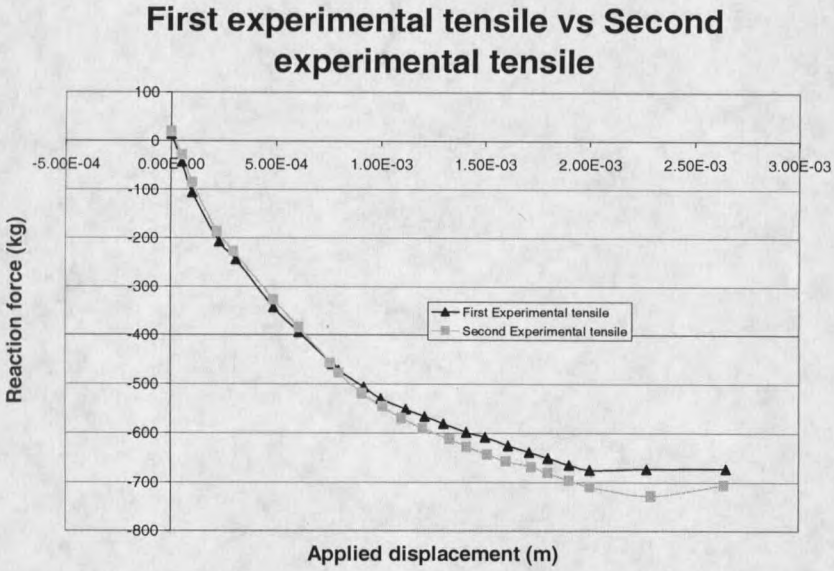

Figure 5.14 Experimental tensile

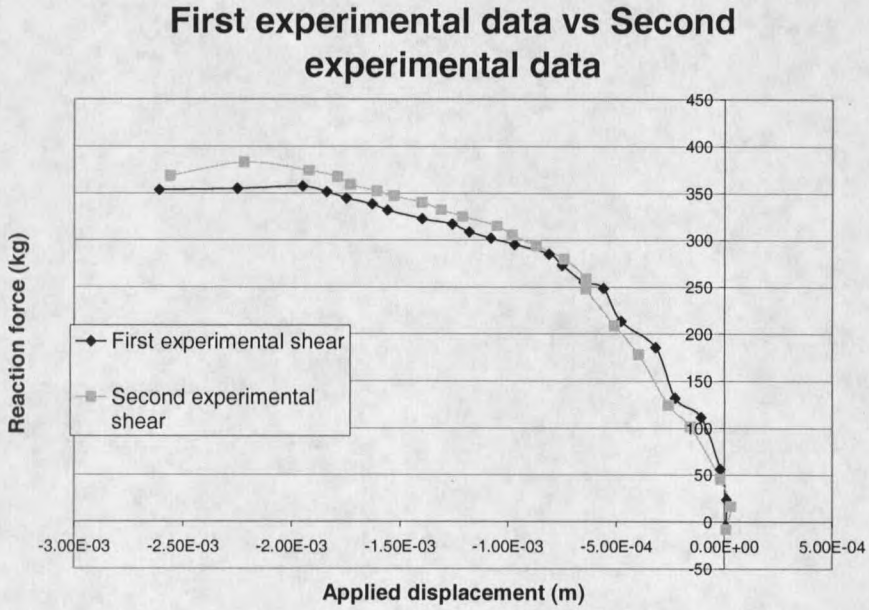

Figure 5.15 Experimental shear

Screening the Experimental Data. After checking the experimental data, the data range from 0.00005 m to 0.00092 m was selected. This range is shown in Figure 5.16 and Figure 5.17.

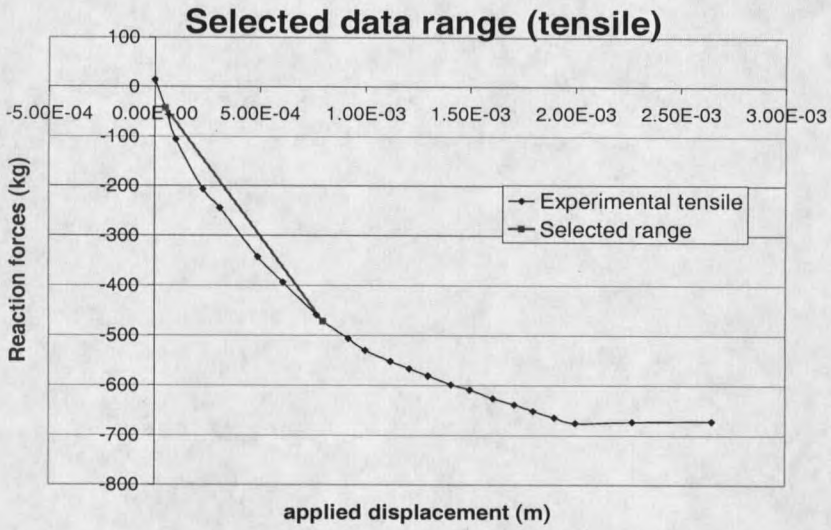

Figure 5.16 Plot the tensile forces in the selected data range

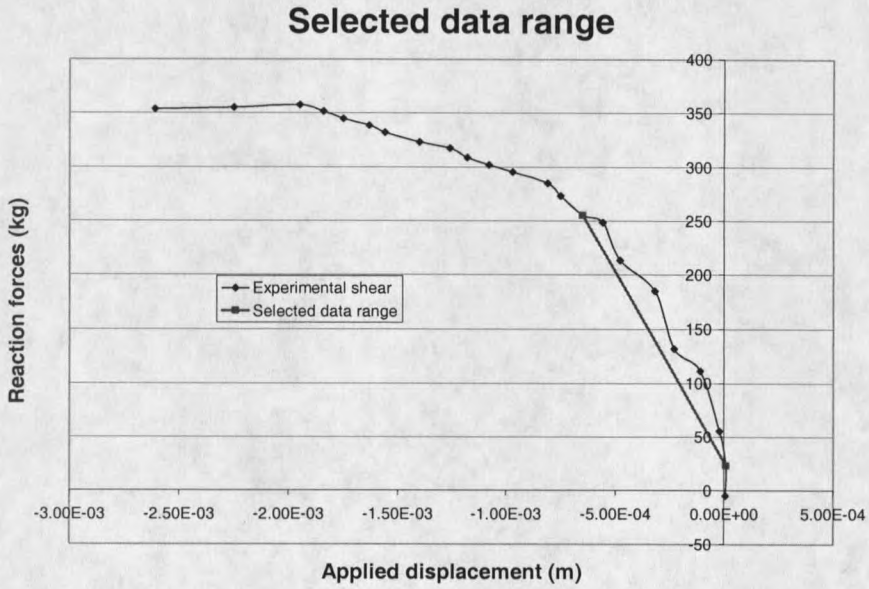

Figure 5.17 Plot the shear forces in the selected data range

Obtaining the Average Experimental Data. As shown in the flow chart (Figure 5.15), in order to compare with the FEM modeling results, the selected experimental data need to be averaged. Furthermore, the first and the second experimental data were also averaged. The results are shown in the following table.

Table 5.13 The average experimental data of the tensile plus shear test

Displacement (m)			Experimental result (kg) Average		
Shear	Tensile	Moment	Force X	Force Y	Moment Z
-0.00034556	0.00047556	0	164.3874772	-303.7400956	-21.02204

FEM Modeling Result Analysis

The standard engineering constants, taken from the MSU composite database, and the loads (displacement) as shown the table 5.11 are used as input in the FEM model. The following results were obtained

Table 5.14 FEM modeling result

Displacement (m)			FEM modeling result (kg) Average		
Shear	Tensile	Moment	Force X	Force Y	Moment Z
-0.00034556	0.00047556	0	81.85859	-299.1452	-5.432

Comparing the results shown in Table 5.13 and Table 5.14, recognize the gaps between the two groups of data. In this case, the grip model parameters must be adjusted so that the two results can fit well. After going through several iterations, the parameters of contact elements were determined. These are shown in Table 5.15

Table 5.15 Parameters of contact elements in the tensile plus shear test.

Thickness of grip	Modulus of grip
0.02m	2E+11 Pa

The adjusted FEM results are shown in Table 5.16

Table 5.16 The adjusted FEM modeling results

Displacement (m)			FEM modeling result (kg) Average		
Shear	Tensile	Moment	Force X	Force Y	Moment Z
-0.00034556	0.00047556	0	81.63753	-303.4788	-5.958

The details of the FEM modeling results are plotted in Figure 5.18 and Figure 5.19.

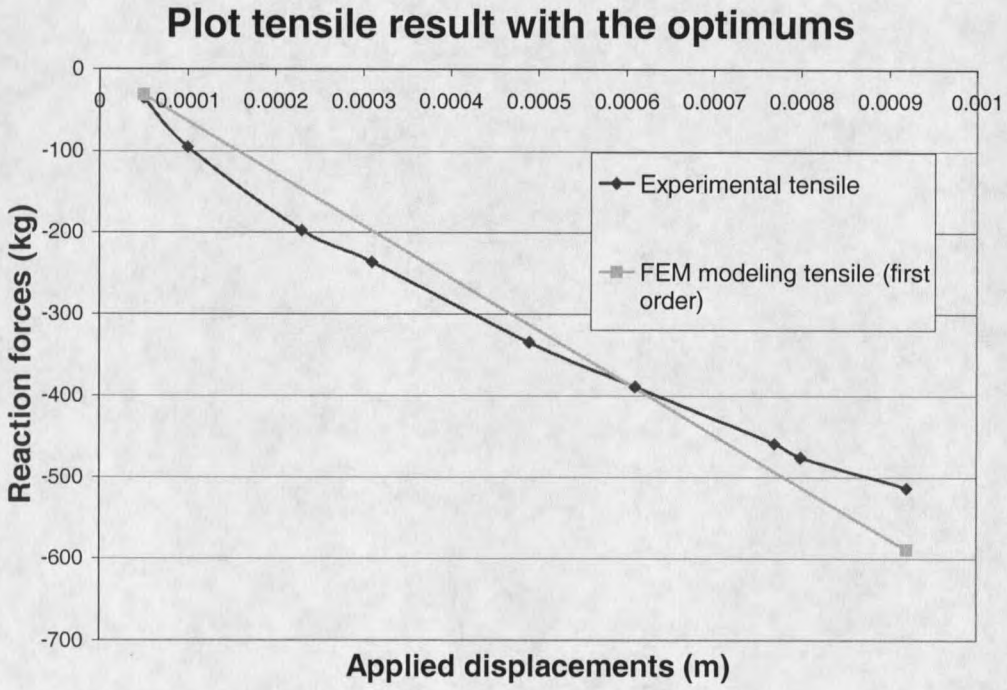

Figure 5.18 FEM tensile plot (tensile plus shear load case)

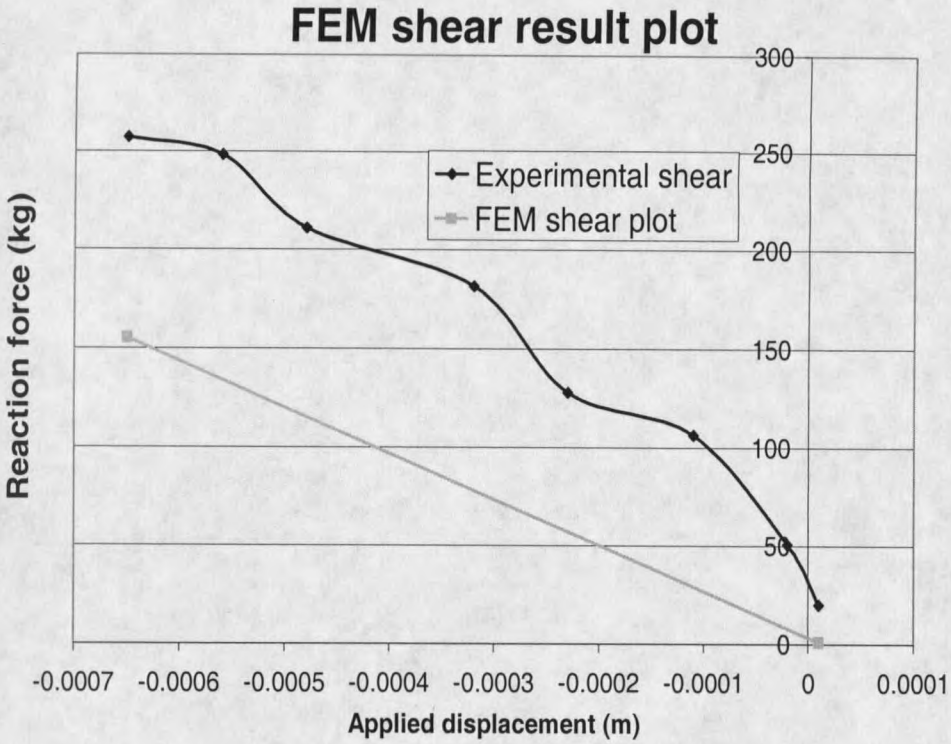

Figure 5.19 FEM shear plot (tensile plus shear load case)

Error Analysis

After analyzing both experimental data and the corresponding FEM modeling results as shown in Figure 5.18 and Figure 5.19, it is clear that there is a large discrepancy between the experimental shear and the FEM reaction shear, although the tensile data fit well.

The suspected reason is that the grips on the IPL machine did not work well with the coupons. The slipping was a big obstacle that prevented acquisition of accurate experimental shear results.

Errors were also possibly induced by other factors, as mentioned in the previous section.

Implementation of the Optimization

The definition of the design variables, state variables, and the objective function was the same as those in the pure tensile test.

First, the random method was used to find an initial set of design variables. Then the first order gradient method was employed for further optimization. The results of the random method, the first order gradient method and the sub-problem method are shown in Table 5.17, Table 5.18 and Table 5.19, respectively.

Table 5.17 The results of the random method (Unit: Pa)

E_1	E_2	G_{12}	G_{23}	υ_{12}
0.31348E+11	0.90079E+10	0.4526E+10	0.362E+10	0.31381

Table 5.18 The results of the first order method (Unit: Pa)

E_1	E_2	G_{12}	G_{23}	υ_{12}
0.34542E+11	0.88839E+10	0.40883E+10	0.3515E+10	0.31371

Table 5.19 The results of the sub-problem method (Unit: Pa)

E_1	E_2	G_{12}	G_{23}	υ_{12}
0.30984E+11	0.87433E+10	0.48805E+10	0.54752E+10	0.26946

Inputting the optimums back into the FEM model, the following results yielded. The results plots of tensile and shear are shown in Figure 5.20 and Figure 5.21.

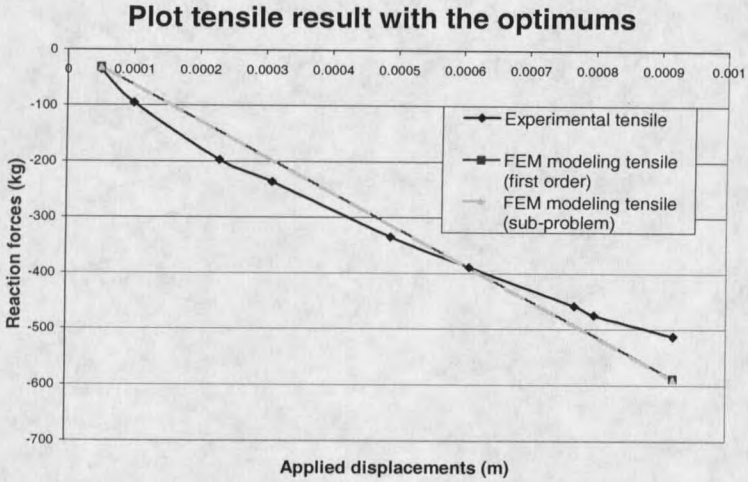

Figure 5.20 Optimization tensile plot (tensile plus shear load case)

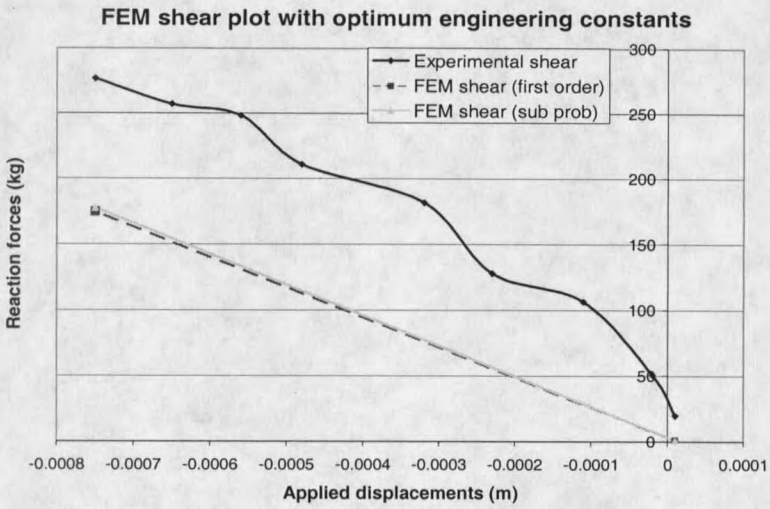

Figure 5.21 Optimization shear plot (tensile plus shear load case)

<u>Error of FEM Modeling Tensile Results:</u>

The error of the FEM tensile results by first order method is 2.0668%

The error of the FEM tensile results by sub-problem method is 2.4091%

The error of the FEM shear results by first order method is 46.5%

The error of the FEM shear results by sub-problem method is 45.7%

The Data Analysis of the Pure Moment Load Case

The pure rotation was applied to the coupons in this test. Two tests were conducted, and the results are illustrated in the following paragraphs.

Experimental Data Analysis

The results of the pure rotation load case were plotted in Figure 5.22

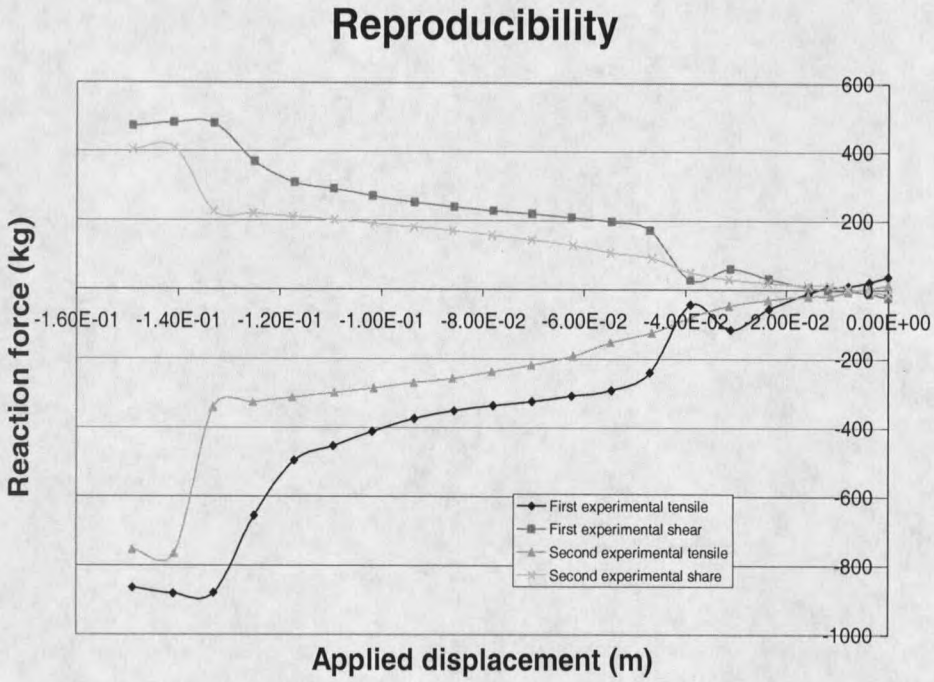

Figure 5.22 Plot of the first and second experimental data

Screening the Experimental Data. After checking the experimental data, the data range which is from -0.0008 m to -0.0015 m with criteria of elastic behaviors was selected. This range is shown in Figure 5.23.

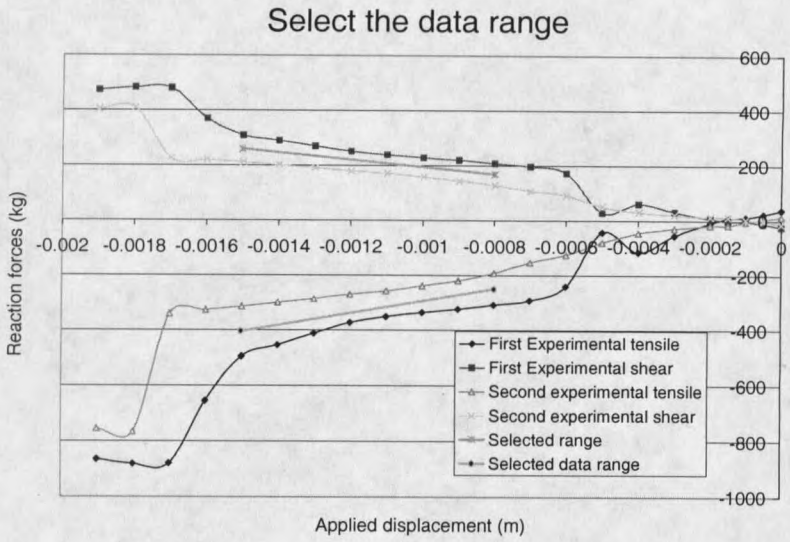

Figure 5.23 The selected data range

Obtaining the Average Experimental Data. As shown in the flow chart (Figure 5.15), in order to compare with the FEM modeling results, the selected experimental data need to be averaged. Furthermore, the first and the second experimental data were also averaged. The average values are shown in the following table.

Table 5.20 The average experimental data of the pure rotation test

Displacement (m)			Experimental result (kg) Average		
Shear	Tensile	Moment	Force X	Force Y	Moment Z
-0.00361125	-0.00051	-0.00115	212.856605	-320.272664	-18.75373667

FEM Modeling Results Analysis

The standard engineering constants, taken from the MSU composite database, and the loads (displacement) as shown in table 5.20 were used as input fro the FEM model fro the pure moment load case. The following results were obtained..

Table 5.21 FEM modeling results

Displacement (m)			FEM modeling result (kg) Average		
Shear	Tensile	Moment	Force X	Force Y	Moment Z
0	0	-0.00115	36.1104787	-292.29013	-3.845985625

Comparing the results shown in table 5.20 and table 5.21, recognize the gaps between the two groups of data. This gap indicates the grip model parameters must be adjusted. After going through several iterations, the parameters of grip model were determined, as shown in Table 5.22

Table 5.22 Parameters of contact elements in the pure rotation test.

Thickness of grip	Modulus of grip
0.01m	3E+11 Pa

The adjusted FEM results are shown in the table 5.23

Table 5.23 The adjusted FEM modeling results

Displacement (m)			FEM modeling result (kg) Average		
Shear	Tensile	Moment	Force X	Force Y	Moment Z
0	0	-0.00115	38.3324949	-320.472473	-5.027569303

The details of the FEM modeling results are plotted in Figure 5.24 and Figure 5.25

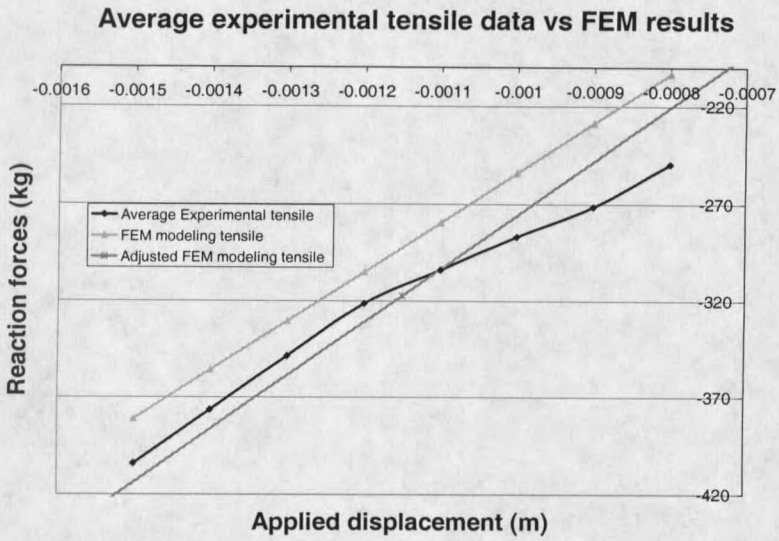

Figure 5.24 FEM modeling tensile plot (rotation load case)

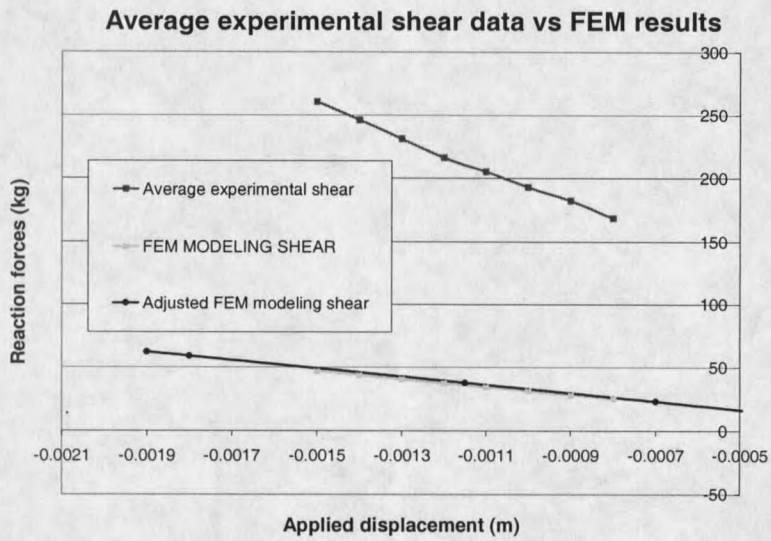

Figure 5.25 FEM modeling shear plot (rotation load case)

Carrying Out Optimization

The definition of the design variables, state variables and the objective function were the same as those in the pure tensile test.

First, the random method was used to find an initial set of design variables. Then the first order gradient method was employed for further optimization. The results of random method and consequent first order gradient method are shown in Table 5.24 and Table 5.25 respectively.

Table 5.24 The results of the random method (Unit: Pa)

E_1	E_2	G_{12}	G_{23}	υ_{12}
0.32394E+11	0.71308E+10	0.40014E+10	0.39001E+10	0.2938

Table 5.25 The results of the first order method (Unit: Pa)

E_1	E_2	G_{12}	G_{23}	υ_{12}
0.3307E+11	0.74045E+10	0.48057E+10	0.40486E+10	0.29388

Inputting the optimums back to the FEM model, the results are shown in Figure 5.26.

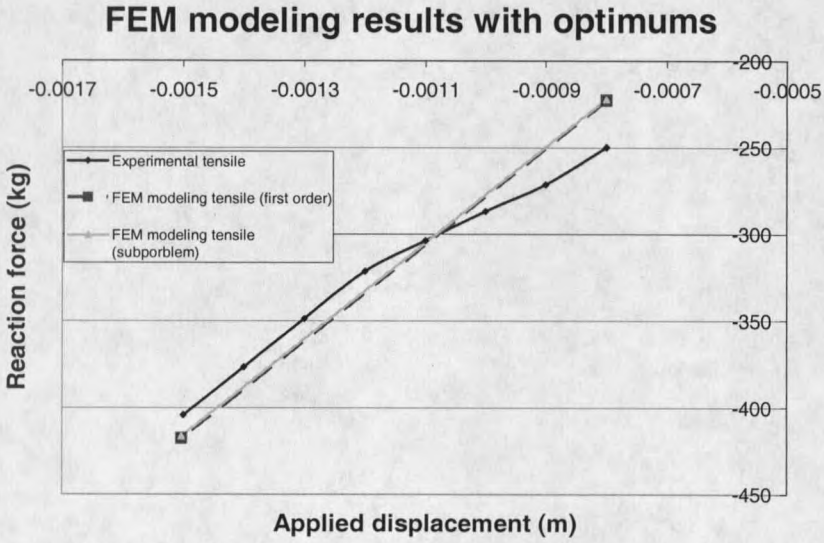

Figure 5.26 Optimization tensile Plot (rotation load case)

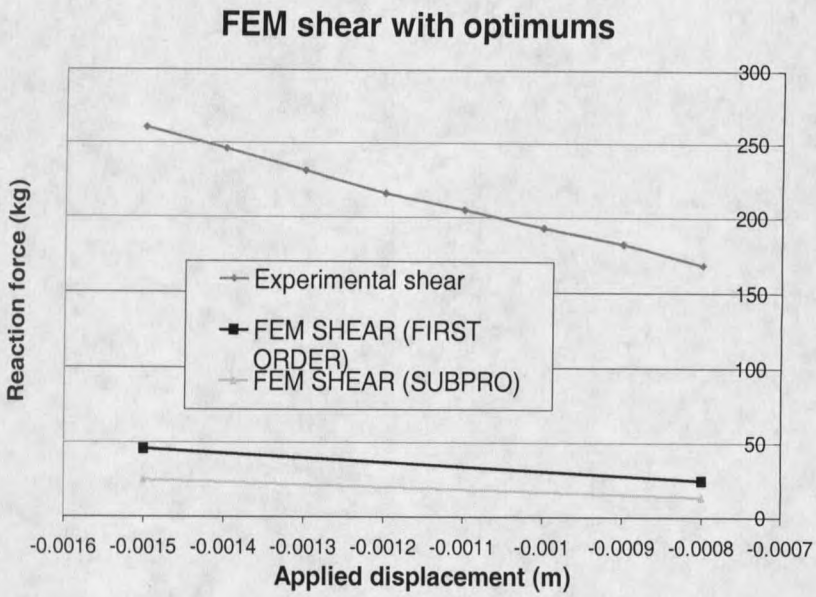

Figure 5.27 Optimization shear plot (rotation case)

The Error of FEM Modeling

The discrepancy between FEM model results by the first order methods is 0.0063%; and it is 0.3352% for the sub-problem method. The error of the FEM modeling shear result by the first order method is 83.47%; it is 91% by the sub-problem method.

The Results Analysis of Tensile, Shear and Rotation Test Case

The tensile and shear displacement and a rotation were applied to the coupons during this test. Because this test is complicated and slippage occurred in the grips, the experimental results obtained were not very accurate. The test results are plotted, and the experimental data are analyzed in the next paragraphs.

Experimental Data Analysis

Plot of the experimental results

The tensile results and shear results are plotted in Figure 5.28 and Figure 5.29.

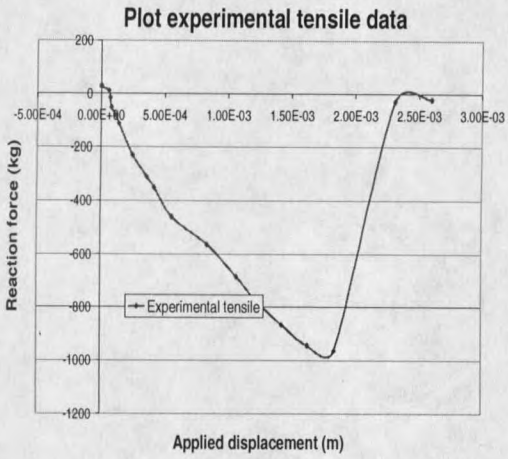

Figure 5.28 Plot experimental tensile results

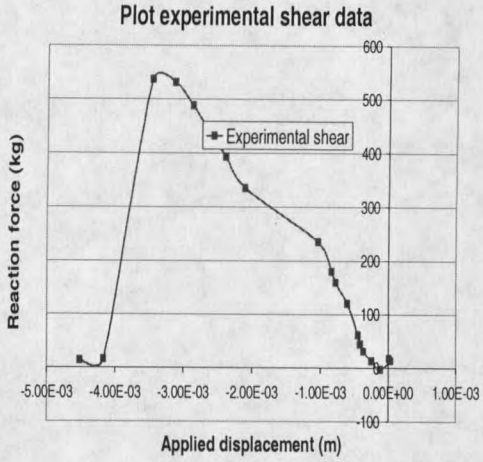

Figure 5.29 Plot experimental shear results

Screening the Experimental Data. After checking the experimental data, we selected the data range from 0.00025 m to 0.00163 m was selected. This range is shown in Figure 5.30 and Figure 5.31.

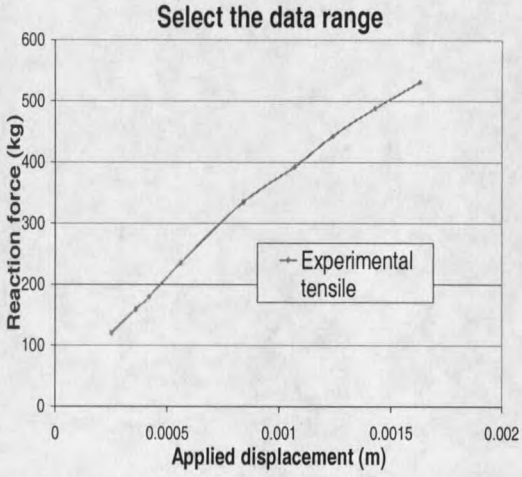

Figure 5.30 Tensile results in selected range

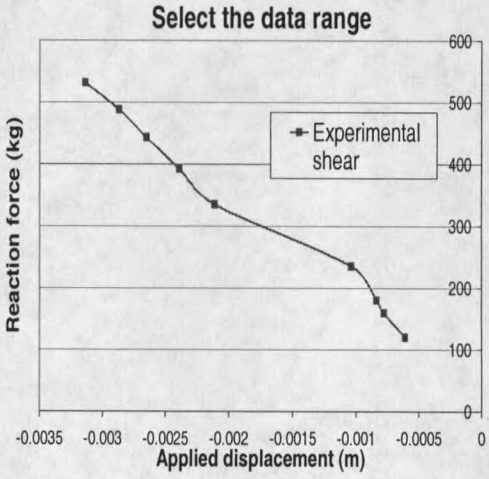

Figure 5.31 Shear results in selected range

Obtaining the Average Experimental Data. As shown in the flow chart (Figure 5.15), in order to compare with the FEM modeling results, the selected experimental data need to be averaged. Furthermore, the first and the second experimental data were also averaged. The average values are shown in the following table.

Table 5.26 The average experimental data of the pure rotation test

Displacement (m)			Experimental result (kg) Average		
Shear	Tensile	Moment	Force X	Force Y	Moment Z
-0.00059	0.00023	-0.00027	103.57339	--19768568	12.51167

FEM Modeling Results Analysis

The standard engineering constants, taken from the MSU composite database, and the loads (displacement) as shown in table 5.26, were used in the FEM model for this load case. The results obtained are as follows.

Table 5.27 FEM modeling result

Displacement (m)			Experimental result (kg) Average		
Shear	Tensile	Moment	Force X	Force Y	Moment Z
-0.00059	0.00023	-0.00027	-12.9542537	--197.7414	-2.205238

Comparing the results shown in table 5.26 and table 5.27, again, recognize the gaps between the two groups of data. The parameters of the grip model are determined, after several iterations. These are shown in Table 5.28

Table 5.28 Parameters of grip model in the pure rotation test.

Thickness of grip	Modulus of grip
0.005m	1.14E+9 Pa

The adjusted FEM results are shown in the table 5.29

Table 5.29 The adjusted FEM modeling results

Displacement (m)			FEM modeling result (kg) Average		
Shear	Tensile	Moment	Force X	Force Y	Moment Z
-0.00059	0.00023	-0.00027	-12.9542537	--197.7414	-2.205238

The details of the FEM modeling results are plotted in Figure 5.32 and Figure 5.33.

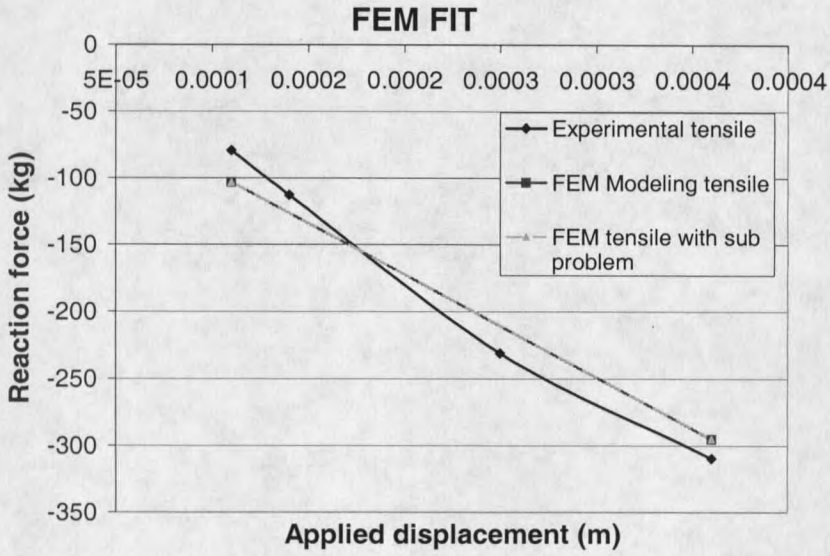

Figure 5.32 FEM tensile results (combined load case)

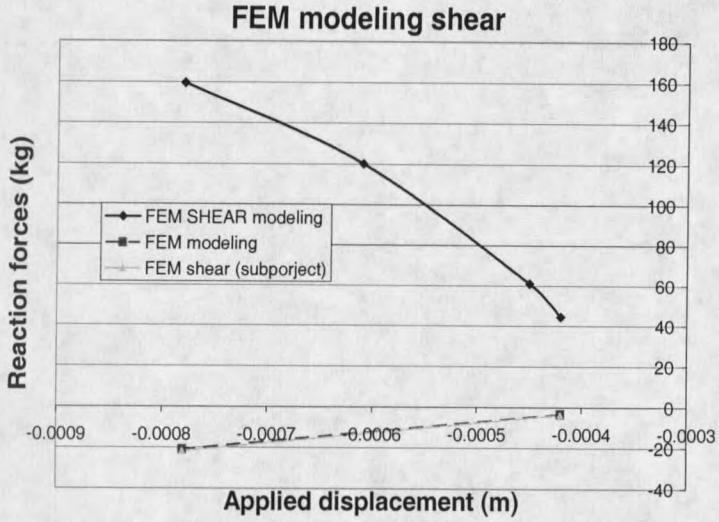

Figure 5.33 FEM shear results (combined load case)

Carrying Out Optimization

The definition of the design variables, state variables and the objective function was the same as those for the pure tensile test.

First, the random method was used to find an initial set of design variables. Then the first order gradient method was employed for further optimization. The results of random method and consequent first order gradient method are shown in table 5.30 and table 5.31 respectively.

Table 5.30 The results of the first order method (Unit: Pa)

E_1	E_2	G_{12}	G_{23}	υ_{12}
0.34301E+11	0.78143E+10	0.44139E+10	0.47313E+10	0.26682

Table 5.31 The results of the sub-problem method (Unit: Pa)

E_1	E_2	G_{12}	G_{23}	υ_{12}
0.35371E+11	0.71355E+10	0.44535E+10	0.2906E+10	0.28724

Inputting the optimums back to the FEM modeling, the results which were plot in Figure 5.34 and Figure 5.35 were obtained.

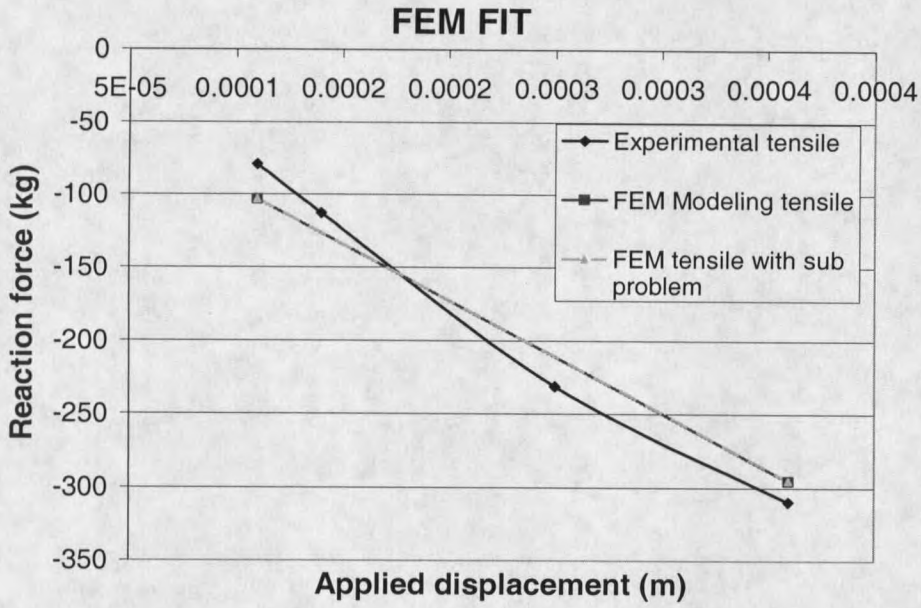

Figure 5.34 Optimization tensile result plot (combined load case)

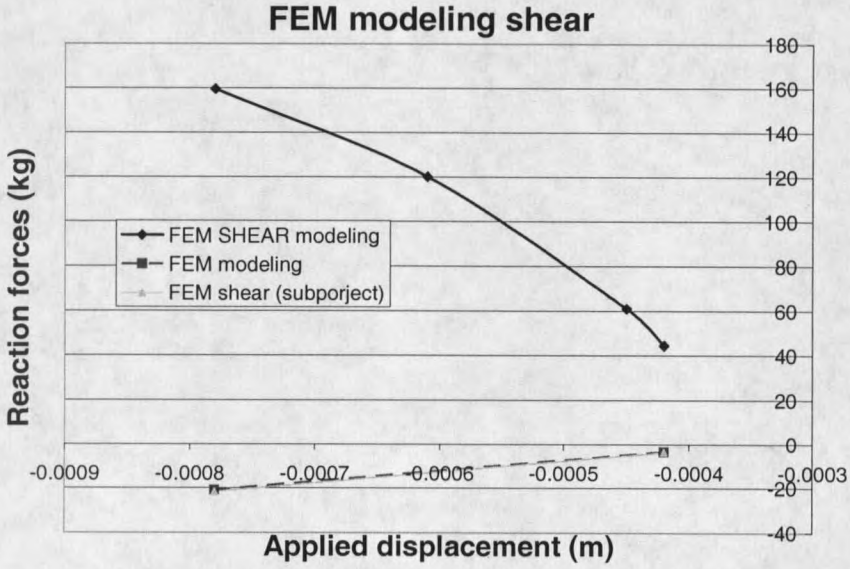

Figure 5.35 Optimization shear result plot (combined load case)

The Error of FEM Modeling

The discrepancy between FEM model results by the first order methods is 8.747%; and it is 8.762% for the sub-problem method. The discrepancy of the FEM model shear result by both methods is very large. The experimental data are questionable as a result of grip slippage in this test.

The conclusion and future work are presented in the next Chapter.

CHAPTER 6

CONCLUSIONS AND FUTURE WORK

The results from the IPL tests and FEM modeling are summarized and the optimum engineering constants are compared with the standard values, taken from the MSU composite database, in this chapter. This methodology is discussed in the terms of accuracy, feasibility, efficiency, and cost. Secondly, the potential problems that occurred during the experiments and analyses are reviewed. Lastly, the suggested future work items are presented in the final section.

Analysis of the Results

As described in Chapter 5, optimization was carried out based on the experimental data from the IPL tests and the FEM model results. The comparison of the optimization results with the standard engineering constants [11] is provided in Table 6.01.

Comparing the optimum engineering constants to the standard and predicted engineering constants in Table 6.01, one should recognize that the optimum values are very close to the standard ones. This indicates that this methodology for determining the constitutive law of the composite is feasible and practical.

The estimated values of the longitudinal Young's modulus E_1, the transverse modulus E_2, and the major Poisson ratio υ_{12} are very close to the standard values. Hence, the method of estimation for of E_1, E_2, and υ_{12} can be used in practical analysis. If those

elastic parameters that are estimated reliably by the micromechanics approach were eliminated from the optimization set, it would be easier to determine other engineering constants such as shear modulus.

Table 6.01 Comparison optimization results

The initial predicted engineering constants				
E_1	E_2	G_{12}	G_{23}	υ_{12}
0.32354E+11	0.8781E+10	0.2021E+10	1.973E+10	0.29
The optimums from the tensile test case (Unit: Pa)				
0.34654E+11	0.79627E+10	0.41482E+10	0.49035E+10	0.30965
The optimums from the tensile plus shear test case (Unit: Pa)				
0.34542E+11	0.88839E+10	0.40883E+10	0.3515E+10	0.31371
The optimum engineering constants from pure rotation test case (Unit: Pa)				
0.3307E+11	0.74045E+10	0.48057E+10	0.40486E+10	0.29388
The optimum constants from tensile, shear and rotation combined test case (Unit: Pa)				
0.34301E+11	0.78143E+10	0.44139E+10	0.47313E+10	0.26682
The standard engineering constants, taken from the MSU Database (Unit: Gpa)				
32.677±1.8	8.437±0.72	3.803±1.11	3.504±0.67	0.285±0.02

As two methods were selected to carry out optimization in this project, the sub-problem approximation method and the first order gradient method, the comparison of these two methods was made also, and the comparison results in terms of time, iteration, and accuracy are shown in Table 6.02.

One of the reasons to select two methods is to obtain a reference, which provides the comparison. This comparison helps to identify the global or local optimums.

Table 6.02 Comparison between sub-problem method and first order method

Sub-problem Approximation Method				
Terms / Test cases	Parameter	Time of Opt.	Accuracy (kg)	
	Iterations	Hours	Opt.Accuracy	Result plot
Pure tensile	16	0.1667	0.8	7.3%
T+S	20	0.21	0.6	2.4091%
Pure rotation	16	0.1667	1.06	0.3352%
T+S+R	16	0.1667	0.0325	8.762%
First Order Gradient Method				
Terms / Test cases	Parameter	Time of Opt.	Accuracy (kg)	
	Iterations	Hours	Opt.Accuracy	Result plot
Pure tensile	10	1.5	0.1E-03	5.574%
T+S	5	0.75	0.123E-06	2.0668%
Pure rotation	9	1.4	0.2	0.0063%
T+S+R	15	2.3	0.44E-05	8.747%

It is indicated that the first order gradient method provide more accurate optimization result than the sub-problem method. However, for each iteration, the first order method takes much longer time than the sub-problem method at least 4 or 5 times longer than sub-problem method.

It is necessary to know that the random tool is an important tool to find the proper initial values. The random tool provides good initial values to both sub-problem approximation method and the first order gradient method, so that the optimization time for each method was decreased dramatically. Furthermore, the optimization results are more precise than the ones without using the random tool. An example provides a clear picture of importance of the random method for preconditioning. The statistic data in terms of iteration, time and optimization accuracy are shown in Table 6.03.

Table 6.03 Comparison on iteration times with and without random tool preconditioning

First Order Gradient Method			
	Iteration	Time(hours)	Opt. Accuracy
Using Random	5-15	1	0.1E-5
No Random	70-100	5-6	0.1E-2
Sub-problem Approximation Method			
	Iteration	Time(hours)	Opt. Accuracy
Using Random	5-15	0.05-0.15	0.1E-1
No Random	70-100	0.5-1	1-10

The typical features of this methodology are relatively low cost, high efficiency, easy operation, and reliability. It is noted in Table 6.03 that the first-order method requires much more time for adequate convergence compared to the sub-problem domain. This is because the first order method is rather general compared to the sub-problem domain method as was discussed in Chapter 4. Based on the results presented in Table 6.02, the experimental errors, and the limitations of the as assumptions stated in Chapters 1 and 2, the application of the first order method is probably not warranted in this case, and the sub problem domain method is the best choice.

Compared with conventional methods for finding material properties, which usually require thousands of tedious experiments and which are also labor intensive, this methodology is very simple. Only 10 simple experiments were conducted during the course. These tests were performed on the In-Plane Loader (IPL), which is a highly automated machine. The comparison between this methodology and other conventional methods are illustrated in Table 6.04.

Table 6.04 Comparison between the current methodology and conventional ones

Methods / Items	Current method	Conventional method
Quantity of tests	10-100	1,000-1,000,0000
Laborers	1-2	10-100
Cost	$2,000-$5,000	$200,000-$1,000,000
Efficiency	Obtain results in hours	Obtain results in months or years
Accuracy	In the same level	In the same level
Consistency	Consistent	inconsistent

The IPL can apply the loads for the selected load cases, via computer control. Therefore, no additional care is required, nor labor additional needed. It is almost a foolproof machine, and easy to operate.

Conducting one single experiment on the IPL takes only a few minutes, including loading and clamping the coupons and it requires only a few tests. Hence, this methodology provides an opportunity to find the material properties in a short time.

Potential Problems of the Current Research

Although we have gained some satisfactory results during this research, there are problems. The summary of the problems of this research are presented in the following paragraphs.

The IPL Experiment

As stated in Chapter 2, the IPL machine is new, and this is the first study to provide experimental/numerical correlations. Consequently, there are some potential sources of errors from the experimental data. These will be identified here, with some suggested methods of resolution in the Future Work section of this chapter.

The first potential problem is in the operation of the IPL machine. Data are input via the digital control system of the IPL. It was noted that there were some deviations between the input and the measured output. This is not a large problem for this study, since the measured output data were used for the optimization results. The facility could also have some errors as a consequence of dimensional tolerances in the machine. The includes placement and location of the specimen in the grips. The calculation of displacements could also be a source of error. In calculating the equivalent u_x, u_y and ω, a nonlinear kinematics program is required for data reduction. This needs to be verified to determine the accuracy of data reduction. The test specimens are manufactured with a diamond saw, and the notches are inserted with a router bit. Any deviations from the as-modeled specimen could affect results.

The slipping of the grip is deemed to the largest source of error during the IPL tests as was illustrated in the experimental results presented in Chapter 5. Since the composite coupon's surfaces are very smooth, it is difficult for the grips to clamp the coupons tightly without sliding during the tests. This was especially true in the pure shear test; which did not yield satisfactory data. However, in tests where the slippage was minimal, the grip modeling method of determining pseudo equivalent grip parameters is adequate as verified in Table 6.02 above.

Optimization

ANSYS was used to carry out the optimization. The ANSYS optimization package could only provide general solutions, not specific ones as discussed in Chapter 4. The optimization problem in this project had total of five variables. Because of the multi-variables, up to 120 sets of design variables satisfied one objective function. Decision regarding which one was most appropriate.

A more robust solution would be to create an optimization program specially for this problem, allowing the user to change the settings and apply more constraints to the optimization. In such a case better optimization results could most likely be obtained.

Future Work

For this project, optimization was constrained to linear elastic behavior. Also the selected composite was deemed a transversely isotropic material. This assumption leads to the reduction of the engineering constants to be determined. In this case, five engineering constants were determined rather than nine.

Actually, the composite behavior is more complicated, and it is typically not a transversely isotropic material. To find properties of composites with higher accuracy, a total of nine engineering constants must be determined.

The next step of this research would be the study of composite nonlinear behavior. At relatively low extensional strains ($\varepsilon \cong 0.005$), the lamina has fiber/matrix splitting and the equivalent constitutive response is nonlinear. The In- Plane Loader machine is still a significant tool in the research.

The sources of error should be quantified and/or eliminated. With respect to the control system of the IPL, the discrepancy between the input and output needs to be resolved. First, the discrepancy needs to be quantified with independent displacement measurements. Then, the discrepancy needs to be minimized. Since the IPL utilizes Labview^{tm} as the tool for both the control and data acquisition, it is conceivable that a feedback control scheme could be implemented. However, this error was accounted for in this research because the as-measured displacements and loads were used for optimization. The facility errors need to be quantified and taken into account. Load cells on the linear actuators are used to determine the loads in the grips of the IPL via measurements and the geometric configuration. Independent measurements of the in-plane forces and moment at the grip need to be conducted to verify this procedure. The displacement calculations need to be verified with additional measurements. This will help to validate and calibrate the kinematical relationships used for grip displacements. The influence of manufacturing and specimen placement in the grips can be easily quantified by performing tests with specimens with manufacturing variances, and by placing specimens in the IPL with orientations within specified limits. The results of these data will be useful for isolating variances due to testing versus material variances.

The major source of error is speculated to be due to uncertainties in the grips. This was adequately accommodated for by the grip modeling procedure as demonstrated in Table 6.02, but improvements are necessary for more accurate data. First, elimination of slippage is required for accurate modeling and development of constitutive response. Then, accurate contact modeling can be accomplished to eliminate the need "pseudo" grip properties discussed in Chapters 3 and 4. Given the quantification and elimination of

these errors, the methodology developed herein shows promise for determining the constitutive response of a wide variety of composite materials over the applied mechanical loadings in complicated structures.

REFERENCES CITED

REFERENCES CITED

1 P.W. Mast, G.E. Nash, J.G. Michopoulos, R. Thomas, R. Badaliance, I. Wolock, Characterization of strain-induced damage in composite based on the dissipated energy density, 22 (1995) 71-96, Theoretical and Applied Fracture Mechanics

2 Robert M.JONES., Mechanics of Composite Materials, 1975 by Scripta Book Company.

3 Irving H.Shames and Francis A.Cozzarelli, Elastic and Inelastic Stress Analysis, 1997 Taylor & Francis.

4 Daniel David Samborsky, Fatigue of E-Glass Fiber Reinforced Composite Materials and Substructures, M.S. thesis of Civil Engineering of Montana State University (1999)

5 Ever J. BARBERO., Introduction to Composite Material Design, 1999 Taylor & Francis. Master of Science Thesis, Civil Engineering Department, Montana state University (1999).

6 ANSYS V7.1 manual, SAS IP, Inc (2002).

7 Halpin, J., and Tsai, S. W., Effects of Environmental Factors on Composite Materials, Air Force Materials Lab-Technical Report 67-423, Department of Defense, USA (1969).

8 Luciano, R., and Barbero, E.J., Formulas for the stiffness of composites with periodic microstructure, I.J. Solids Structures, 31, 2933-2944 (1994).

9 Hashin, Z., and Rosen, B. W., The elastic Moduli of Fiber-Reinforced materials, J.Applied Mechanics, June, 223-230 (1964).

10 Eric Booth, In- Plane Loader machine Progress Report. Mechanical Engineering Department, Montana State University (2002).

11 MSU Composite Database

12 Jorge NOCEDAL, Stephen J. Wright., Numerical Optimization, 1999 Springer-Verlag New York, Inc.

13 B. Paul, Prediction of Elastic Constants of Multiphase Materials, 36-Volum 218, February 1960-37, Transaction of the metallurgical society of AIME

14 C S Krishnamoorty, Finite Element Analysis Theory and Programming, 1994, Tata McGraw-Hill Publishing company Limited

15 Donald A. Pierre, Optimization Theory with Application, 1969 by John Wiley & Sons, Inc.

16 Erik Larsen, Douglas Cairns, John Mandell, and Daniel Samborsky, Investigation of a two-stage injection process to reduce the effects of in-plane resin flow, AIAA-2002-0026

17 Mase, G.E., and Mase, G.T., Continuum Mechanics for Engineers, CRC press, Boca Raton, FL (1992)

18 Tsai.S.W., and Hahn, H.T., Introduction to Composite Materials, Technomic, Lancaster, PA (1980).

19 Hull, D., An Introduction to Composite Materials, Cambridge University Press, Cambridge (1981)

20 Halpin, J., and Pagano, N.J., The Laminate Approximation for Random Oriented Composite, J. Composite Materials, 3, 720-724 (1969).

21 Agarwal, B.D., and Broutman L. J., Analysis and Performance of Fiber Composite, 2ND Ed., John Wiley & Sons, New York (1990).

22 Barbero, E.J., Prediction of Compressive Strength of Polymer Matrix Composite, J. Composite Materials, 32, 483-502 (1997).

23 Tsai, Stephen W.: Mechanics of Composite Material, Part II, Theoretical Aspects, Air Force Material Laboratory Tech. Rept. AFML-TR-66-149, November, 1966.

24 Jones, Robert M.: Stiffness of Orthotropic Materials and Laminated Fiber-Reinforced Composites, AIAA Journal, January, 1974, pp.112-114.

25 Chamis, C.C. and G.P. Sendeckyj: Critique on Theories Predicting Thermoelastic Properties of Fibrous Composites, J. Composite Materials, July, 1968, pp.332-358.

26 Hashin, Zvi: The Elastic Moduli of Heterogeneous Materials, J.Appl. Mech., March, 1962, pp 143-150.

27 Hashin, Zvi, and B.Walter Rosen: The Elastic Moduli of Fiber-Reinforced Materials, J. Appl. Mech. June, 1964, pp. 223-232. Errata, March, 1965, P. 219.

28 Tsai, Stephen W.: Structural Behavior of Composite Materials, NASA CR-71, July, 1964.

29 Adams, D.F., and D.R. Doner: Transverse Normal Loading of a Unidirectinal Composite, J. Composite Materials, January, 1967, pp.4-17.

30 Hewitt, R.L., and M.C. de Malherbe: An Approximation for the Longitudinal Shear Modulus of Continuous Fiber Composites, J. Composite Materials, April, 1970, pp.280-282.

APPENDICES

APPENDICES

APPENDIX A

Rotation Programming

```
theta = Pi / 4;
ev[1] = {1, 0, 0};
ev[2] = {0, 1, 0};
ev[3] = {0, 0, 1};
evp[1] = {Cos[theta], -Sin[theta], 0};
evp[2] = {Sin[theta], Cos[theta], 0};
evp[3] = {0, 0, 1};

Clear[Q]
Q = Table[ev[i].evp[j], {i, 1, 3}, {j, 1, 3}]
```

$$\left\{\left\{\frac{1}{\sqrt{2}}, \frac{1}{\sqrt{2}}, 0\right\}, \left\{-\frac{1}{\sqrt{2}}, \frac{1}{\sqrt{2}}, 0\right\}, \{0, 0, 1\}\right\}$$

```
Q[[2, 1]]

clear[Cm]
Cm = Table[C[i, j, k, l], {i, 1, 3}, {j, 1, 3}, {k, 1, 3}, {l, 1, 3}]
```

{{{{C[1, 1, 1, 1], C[1, 1, 1, 2], C[1, 1, 1, 3]}, {C[1, 1, 2, 1],
C[1, 1, 2, 2], C[1, 1, 2, 3]}, {C[1, 1, 3, 1], C[1, 1, 3, 2],
C[1, 1, 3, 3]}}, {{C[1, 2, 1, 1], C[1, 2, 1, 2],
C[1, 2, 1, 3]}, {C[1, 2, 2, 1], C[1, 2, 2, 2],
C[1, 2, 2, 3]}, {C[1, 2, 3, 1], C[1, 2, 3, 2],
C[1, 2, 3, 3]}}, {{C[1, 3, 1, 1], C[1, 3, 1, 2],
C[1, 3, 1, 3]}, {C[1, 3, 2, 1], C[1, 3, 2, 2],
C[1, 3, 2, 3]}, {C[1, 3, 3, 1], C[1, 3, 3, 2],
C[1, 3, 3, 3]}}}, {{{C[2, 1, 1, 1], C[2, 1, 1, 2],
C[2, 1, 1, 3]}, {C[2, 1, 2, 1], C[2, 1, 2, 2],
C[2, 1, 2, 3]}, {C[2, 1, 3, 1], C[2, 1, 3, 2],
C[2, 1, 3, 3]}}, {{C[2, 2, 1, 1], C[2, 2, 1, 2],
C[2, 2, 1, 3]}, {C[2, 2, 2, 1], C[2, 2, 2, 2],
C[2, 2, 2, 3]}, {C[2, 2, 3, 1], C[2, 2, 3, 2],
C[2, 2, 3, 3]}}, {{C[2, 3, 1, 1], C[2, 3, 1, 2],
C[2, 3, 1, 3]}, {C[2, 3, 2, 1], C[2, 3, 2, 2],
C[2, 3, 2, 3]}, {C[2, 3, 3, 1], C[2, 3, 3, 2],
C[2, 3, 3, 3]}}}, {{{C[3, 1, 1, 1], C[3, 1, 1, 2],
C[3, 1, 1, 3]}, {C[3, 1, 2, 1], C[3, 1, 2, 2],
C[3, 1, 2, 3]}, {C[3, 1, 3, 1], C[3, 1, 3, 2],
C[3, 1, 3, 3]}}, {{C[3, 2, 1, 1], C[3, 2, 1, 2],
C[3, 2, 1, 3]}, {C[3, 2, 2, 1], C[3, 2, 2, 2],
C[3, 2, 2, 3]}, {C[3, 2, 3, 1], C[3, 2, 3, 2],
C[3, 2, 3, 3]}}, {{C[3, 3, 1, 1], C[3, 3, 1, 2],
C[3, 3, 1, 3]}, {C[3, 3, 2, 1], C[3, 3, 2, 2],
C[3, 3, 2, 3]}, {C[3, 3, 3, 1], C[3, 3, 3, 2], C[3, 3, 3, 3]}}}}

```
For[i = 1, i < 4, i++ , Block[{},
      For[j = 1, j < 4, j++ , Block[{},
        For[k = 1, k < 4, k++ , Block[{},
          For[l = 1, l < 4, l++ , Block[{},
            Cm[[i, j, k, l]] = 0 ]


      ]
     ]
    ]
   ]]]]
Cm[[1, 1, 2, 2]] = C12;
Cm[[1, 1, 3, 3]] = C12;
Cm[[2, 2, 1, 1]] = C12;
Cm[[2, 2, 2, 2]] = C22;
Cm[[2, 2, 3, 3]] = C23;
Cm[[3, 3, 1, 1]] = C12;
Cm[[3, 3, 2, 2]] = C23;
Cm[[3, 3, 3, 3]] = C22;
Cm[[2, 3, 2, 3]] = 1/2*(C22 - C23);
Cm[[3, 2, 3, 2]] = 1/2*(C22 - C23);
Cm[[1, 3, 1, 3]] = C66;
Cm[[3, 1, 3, 1]] = C66;
Cm[[1, 2, 1, 2]] = C66;
Cm[[2, 1, 2, 1]] = C66;
Cm[[2, 1, 1, 2]] = C66;
Cm[[1, 2, 2, 1]] = C66;
Cm[[3, 1, 1, 3]] = C66;
Cm[[1, 3, 3, 1]] = C66;
Cm[[2, 3, 3, 2]] = 1/2*(C22 - C23);
Cm[[3, 2, 3, 2]] = 1/2*(C22 - C23);
```

$$C[1,1,1,1] = \frac{1}{8}\,(2\,C11 - 4\,C12 + 3\,C22 - C23 + 2\,C66)$$

$$C[1,1,1,2] = \frac{1}{8}\,(2\,C11 - C22 - C23 - 2\,C66)$$

$$C[1,1,1,3] = \frac{C12 - C23}{2\sqrt{2}}$$

$$C[1,1,2,1] = \frac{1}{8}\,(2\,C11 - 4\,C12 + C22 + C23 - 2\,C66)$$

$$C[1,1,2,2] = \frac{1}{8}\,(2\,C11 - 3\,C22 + C23 + 2\,C66)$$

$$C[1,1,2,3] = \frac{C12 - C23}{2\sqrt{2}}$$

$$C[1,1,3,1] = -\frac{C22 - C23 + 2\,C66}{4\sqrt{2}}$$

$$C[1,1,3,2] = \frac{-C22 + C23 + 2\,C66}{4\sqrt{2}}$$

$$C[1,1,3,3] = 0$$

$$C[1,2,1,1] = \frac{1}{8}\,(2\,C11 - C22 - C23 - 2\,C66)$$

$$C[1,2,1,2] = \frac{1}{8}\,(2\,C11 + 4\,C12 + 3\,C22 - C23 + 2\,C66)$$

$$C[1,2,1,3] = \frac{C12 + C23}{2\sqrt{2}}$$

$$C[1,2,2,1] = \frac{1}{8}\,(2\,C11 - 3\,C22 + C23 + 2\,C66)$$

$$C[1,2,2,2] = \frac{1}{8}\,(2\,C11 + 4\,C12 + C22 + C23 - 2\,C66)$$

$$C[1,2,2,3] = \frac{C12 + C23}{2\sqrt{2}}$$

$$C[1,2,3,1] = \frac{-C22 + C23 + 2\,C66}{4\sqrt{2}}$$

$$C[1,2,3,2] = -\frac{C22 - C23 + 2\,C66}{4\sqrt{2}}$$

$$C[1,2,3,3] = 0$$

$$C[1,3,1,1] = \frac{C12 - C23}{2\sqrt{2}}$$

$$C[1,3,1,2] = \frac{C12 + C23}{2\sqrt{2}}$$

$$C[1,3,1,3] = \frac{C22 + C66}{2}$$

$$C[1,3,2,1] = \frac{C12 - C23}{2\sqrt{2}}$$

$$C[1,3,2,2] = \frac{C12 + C23}{2\sqrt{2}}$$

$$C[1,3,2,3] = \frac{C22 - C66}{2}$$

$$C[1,3,3,1] = 0$$

$$C[1,3,3,2] = 0$$

$$C[1,3,3,3] = -\frac{C66}{\sqrt{2}}$$

$$C[2,1,1,1] = \frac{1}{8}(2\,C11 - 4\,C12 + C22 + C23 - 2\,C66)$$

$$C[2,1,1,2] = \frac{1}{8}(2\,C11 - 3\,C22 + C23 + 2\,C66)$$

$$C[2,1,1,3] = \frac{C12 - C23}{2\sqrt{2}}$$

$$C[2,1,2,1] = \frac{1}{8}(2\,C11 - 4\,C12 + 3\,C22 - C23 + 2\,C66)$$

$$C[2,1,2,2] = \frac{1}{8}(2\,C11 - C22 - C23 - 2\,C66)$$

$$C[2,1,2,3] = \frac{C12 - C23}{2\sqrt{2}}$$

$$C[2,1,3,1] = \frac{C22 - C23 + 2\,C66}{4\sqrt{2}}$$

$$C[2,1,3,2] = \frac{C22 - C23 - 2\,C66}{4\sqrt{2}}$$

$$C[2,1,3,3] = 0$$

$$C[2,2,1,1] = \frac{1}{8}(2\,C11 - 3\,C22 + C23 + 2\,C66)$$

$$C[2,2,1,2] = \frac{1}{8}(2\,C11 + 4\,C12 + C22 + C23 - 2\,C66)$$

$$C[2,2,1,3] = \frac{C12 + C23}{2\sqrt{2}}$$

$$C[2,2,2,1] = \frac{1}{8}\,(2\,C11 - C22 - C23 - 2\,C66)$$

$$C[2,2,2,2] = \frac{1}{8}\,(2\,C11 + 4\,C12 + 3\,C22 - C23 + 2\,C66)$$

$$C[2,2,2,3] = \frac{C12 + C23}{2\sqrt{2}}$$

$$C[2,2,3,1] = \frac{C22 - C23 - 2\,C66}{4\sqrt{2}}$$

$$C[2,2,3,2] = \frac{C22 - C23 + 2\,C66}{4\sqrt{2}}$$

$$C[2,2,3,3] = 0$$

$$C[2,3,1,1] = \frac{C12 - C23}{2\sqrt{2}}$$

$$C[2,3,1,2] = \frac{C12 + C23}{2\sqrt{2}}$$

$$C[2,3,1,3] = \frac{C22 - C66}{2}$$

$$C[2,3,2,1] = \frac{C12 - C23}{2\sqrt{2}}$$

$$C[2,3,2,2] = \frac{C12 + C23}{2\sqrt{2}}$$

$$C[2,3,2,3] = \frac{C22 + C66}{2}$$

$$C[2,3,3,1] = 0$$

$$C[2,3,3,2] = 0$$

$$C[2,3,3,3] = \frac{C66}{\sqrt{2}}$$

$$C[3,1,1,1] = -\frac{C66}{2\sqrt{2}}$$

$$C[3,1,1,2] = \frac{C66}{2\sqrt{2}}$$

$$C[3,1,1,3] = 0$$

$$C[3,1,2,1] = \frac{C66}{2\sqrt{2}}$$

$$C[3,1,2,2] = -\frac{C66}{2\sqrt{2}}$$

$$C[3,1,3,1] = \frac{1}{4}(C22 - C23 + 2\,C66)$$

$$C[3,1,3,2] = \frac{1}{4}(C22 - C23 - 2\,C66)$$

$$C[3,1,3,3] = 0$$

$$C[3,2,1,1] = \frac{C66}{2\sqrt{2}}$$

$$C[3,2,1,2] = -\frac{C66}{2\sqrt{2}}$$

$$C[3,2,1,3] = 0$$

$$C[3,2,2,1] = -\frac{C66}{2\sqrt{2}}$$

$$C[3,2,2,2] = \frac{C66}{2\sqrt{2}}$$

$$C[3,2,2,3] = 0$$

$$C[3,2,3,1] = \frac{1}{4}(C22 - C23 - 2\,C66)$$

$$C[3,2,3,2] = \frac{1}{4}(C22 - C23 + 2\,C66)$$

$$C[3,2,3,3] = 0$$

$$C[3,3,1,1] = 0$$

$$C[3,3,1,2] = 0$$

$$C[3,3,1,3] = -\frac{C66}{\sqrt{2}}$$

$$C[3,3,2,1] = 0$$

$$C[3,3,2,2] = 0$$

$$C[3,3,2,3] = \frac{C66}{\sqrt{2}}$$

$$C[3,3,3,1] = 0$$

$$C[3,3,3,2] = 0$$

$$C[3,3,3,3] = C66$$

APPENDIX B

Estimation of Engineering Constants

Prediction of Engineering constants

The modulus unit is Gpa

$E_f := 73.1$ $G_f := 29.959$ $\nu_f := 0.22$ $V_f := 0.417$ $V_m := 0.583$

$E_m := 3.21$ $G_m := 0.96$ $\nu_m := 0.34$

Thickness of the coupon $t := 3.98 \cdot 10^{-3} m$

Thickness of each layer $t_1 := 4.975 \cdot 10^{-4} m$

Layup [0/+45/90/-45/-45/90/+45/0]

Longtituinal modulus E1

$E_1 := E_f \cdot V_f + E_m \cdot V_m$ $E_1 = 32.354$

Transverse modulus E2

$\zeta := 2$

$$\eta := \frac{\frac{E_f}{E_m} - 1}{\frac{E_f}{E_m} + \zeta}$$

$$E_2 := E_m \cdot \left(\frac{1 + \zeta \cdot \eta \cdot V_f}{1 - \eta \cdot V_f} \right)$$ $E_2 = 8.781$

$$E_{2'} := \frac{E_m \cdot E_f}{V_m \cdot E_f + V_f \cdot E_m}$$ $E_{2'} = 5.338$

Poissons 's ratio

$\nu_{12} := \nu_f \cdot V_f + \nu_m \cdot V_m$ $\nu_{12} = 0.28996$

Shear modulus associated with the plane 2-3

Shear modulus associated with the plane 2-3

$$S_3 := 0.49247 - 0.47603 V_f - 0.02748 V_f^2$$

$$G_{12} := G_m \cdot \left[1 + \frac{V_f \cdot \left(1 - \frac{G_m}{G_f}\right)}{\frac{G_m}{G_f} + S_3 \cdot \left(1 - \frac{G_m}{G_f}\right)} \right] \qquad G_{12} = 2.202$$

$$G_{12'} := \frac{1}{\frac{V_m}{G_m} + \frac{V_f}{G_f}} \qquad G_{12'} = 1.61$$

Shear modulus associated with the plane 2-3

$$\eta_{23} := \frac{3 - 4 \cdot \nu_m + \frac{G_m}{G_f}}{4 \cdot \left(1 - \nu_m\right)}$$

$$G_{23} := G_m \cdot \frac{V_f + \eta_{23} \cdot \left(1 - V_f\right)}{\eta_{23} \cdot \left(1 - V_f\right) + V_f \cdot \frac{G_m}{G_f}} \qquad G_{23} = 1.973$$

$$\nu_{23} := \frac{\tilde{E}_{2'}}{2G_{23}} - 1 \qquad \nu_{23} = 0.353$$

$$G_{13} := G_{12}$$

$$\nu_{13} := \nu_{12}$$

APPENDIX C

Verification of the Assumed Engineering Constants

Restriction on values of materials constant

For orthotropic materials, the relations between elastic constants are very complex. Those relations must be investigated with rigor in order to avoid the pitfalls of an intuition built up on the basis of working with isotropic materials. First, the product of a stress component and the corresponding strain components must be positive in order to avoid the creation of energy. This latter condition provides a thermodynamic constraint on the values of the elastic constants. The matrices relating stress to strain are required to be positive definite, i.e., to have positive principal values or invariants. Thus, both the stiffness and compliance matrices must be positive definite.
Thus, having the following restrict condition

$S_{11}, S_{22}, S_{33}, S_{44}, S_{55}, S_{66} > 0$ or $C_{11}, C_{22}, C_{33}, C_{44}, C_{55}, C_{66} > 0$

Then $E_1, E_2, E_3, G_{23}, G_{31}, G_{12} > 0$

The values E_1, E_2, E_3, G_{23}, G_{31}, G_{12} have be estimated in the previous section as

$E_1 := 32.354$ $E_2 := 8.781$ $E_3 := 8.781$ $G_{12} := 2.021$

$G_{13} := 2.021$ $G_{23} := 1.973$

These values are all biger than zero, thus satisfying the constraint above

$$\left(1 - \nu_{23} \cdot \nu_{32}\right), \left(1 - \nu_{13} \cdot \nu_{31}\right), \left(1 - \nu_{12} \cdot \nu_{21}\right) > 0$$

and

$$\Delta = 1 - \nu_{12} \cdot \nu_{21} - \nu_{13} \cdot \nu_{31} - \nu_{23} \cdot \nu_{32} - 2 \cdot \nu_{21} \cdot \nu_{32} \cdot \nu_{13} > 0$$

By use of the condition of symmetry of complains $\frac{\nu_{ij}}{E_i} = \frac{\nu_{ji}}{E_j}$ $i, j = 1, 2, 3$

The restrict conditions can be written as:

$E_1 := 32.354$ $E_2 := 8.781$ $E_3 := E_2$

$$\left|\nu_{32}\right| < \left(\frac{E_3}{E_2}\right)^{\frac{1}{2}} \qquad \left|\nu_{23}\right| < \left(\frac{E_2}{E_3}\right)^{\frac{1}{2}} \qquad \left|\nu_{32}\right| < 1 \qquad \left|\nu_{23}\right| < 1$$

$$\left|\nu_{13}\right| < \left(\frac{E_1}{E_3}\right)^{\frac{1}{2}} \qquad \left|\nu_{31}\right| < \left(\frac{E_3}{E_1}\right)^{\frac{1}{2}} \qquad \left|\nu_{13}\right| < 1.92 \qquad \left|\nu_{31}\right| < 0.521$$

As we have determined the values of ν_{21} and ν_{12} in the previous section, then we can investigate whether the values we established are satisfied the restrict conditions.

$\nu_{12} := 0.29$ $\qquad$ $\nu_{21} := 0.08$

It is obvious that the the values ν_{21} and ν_{12} estimated in previous section are satisfied the restrict conditions. In the same manner, we recognized that ν_{13} and ν_{31} are also within the constraint range.

Substitute Poission's ratios estimated

$\nu_{23} := 0.354$ $\qquad$ $\nu_{32} := 0.354$ $\qquad$ $\nu_{13} := 0.29$ $\qquad$ $\nu_{31} := 0.08$

$$1 - \nu_{12}\cdot\nu_{21} - \nu_{13}\cdot\nu_{31} - \nu_{23}\cdot\nu_{32} - 2\cdot\nu_{21}\cdot\nu_{32}\cdot\nu_{13} = 0.812$$

Then obtaining

$$1 - \nu_{12}\cdot\nu_{21} - \nu_{13}\cdot\nu_{31} - \nu_{23}\cdot\nu_{32} - 2\cdot\nu_{21}\cdot\nu_{32}\cdot\nu_{13} > 0$$

<u>Thus, we can conclude that all the values of the initially estimated engineering constants satisfy the restrictions, and the assumption is reasonable.</u>

APPENDIX D

Calculation of the Lower and Upper Bounds of Engineering Constants

Calculation of upper and lower bounds of engineering constants

The Unit is Gpa

$E_f := 73.1$ $\nu_f := 0.22$ $G_f := 29.959$ $V_f := 0.417$

$E_m := 3.21$ $\nu_m := 0.34$ $G_m := 0.96$ $V_m := 0.583$

Lower and upper bounds of the Young's Modulus E

1. Estimate the lower and upper bounds of the Young's Modulus E1

$E_1 := E_f \cdot V_f + E_m \cdot V_m$ $E_1 = 32.354$

Lower bound of Young's Modulus E1 $E_{1lower} := (1 - 0.1)E_1$ $E_{1lower} = 29.119$

Upperr bound of Young's Modulus E1 $E_{1upper} := (1 + 0.1)E_1$ $E_{1upper} = 35.59$

Obtaining the lower and upper bounds of E1 $29.119 < E_1 < 35.589$

2. Estimate the lower and upper bounds of the Young's Modulus E2

Two forms of the strain energy will be employed in order to estimate the Young's Modulus E2

The stress state Strain Energy $U = \frac{1}{2} \cdot \frac{\sigma^2}{E} \cdot V$

The strain state Strain Energy $U = \frac{1}{2} \cdot E \cdot \varepsilon^2 V$

The stress-strain relations of the isotropic materials are as follows:

$$\sigma_x = \frac{\nu E}{(1+\nu)(1-2\nu)}\left(\varepsilon_x + \varepsilon_y + \varepsilon_z\right) + \frac{E}{(1+\nu)}\varepsilon_x$$

$$\sigma_y = \frac{\nu E}{(1+\nu)(1-2\nu)}\left(\varepsilon_x + \varepsilon_y + \varepsilon_z\right) + \frac{E}{(1+\nu)}\varepsilon_y$$

$$\sigma_z = \frac{\nu E}{(1+\nu)(1-2\nu)}\left(\varepsilon_x + \varepsilon_y + \varepsilon_z\right) + \frac{E}{(1+\nu)}\varepsilon_z$$

$$\tau_{xy} = G \cdot \gamma_{xy} = \frac{E}{2(1+\nu)} \cdot \gamma_{xy}$$

$$\tau_{xz} = G \cdot \gamma_{xz} = \frac{E}{2(1+\nu)} \cdot \gamma_{xz}$$

$$\tau_{yz} = G \cdot \gamma_{yz} = \frac{E}{2(1+\nu)} \cdot \gamma_{yz}$$

To find a lower bound on the apparent Young's modulus, E load the basic unianial test specimen with normal stress on the ends. The internal stress field that satisfies this loading and the stress equations of equilibrium is:

$$\sigma_x^{\,o} = \sigma \qquad \sigma_y^{\,o} = \sigma_z^{\,o} = \tau_{xy}^{\,o} = \tau_{yz}^{\,o} = \tau_{zx}^{\,o} = 0$$

$$U^0 = \frac{1}{2} \cdot \int_V \frac{\left(\sigma_x^{\,0}\right)^2}{E} dV = \frac{\sigma^2}{2} \cdot \int_V \frac{1}{E} dV$$

$$\int_V \frac{1}{E} dV = \frac{V_m \cdot V}{E_m} + \frac{V_f \cdot V}{E_f}$$

$$U^o = \frac{\sigma^2}{2}\left(\frac{V_m}{E_m} + \frac{V_f}{E_f}\right)V$$

$$\frac{1}{2}\frac{\sigma^2}{E} V \le \frac{\sigma^2}{2}\left(\frac{V_m}{E_m} + \frac{V_f}{E_f}\right)V$$

or

$$\frac{1}{E} < \frac{V_m}{E_m} + \frac{V_f}{E_f}$$

$$E > \frac{E_m \cdot E_f}{V_m \cdot E_f + V_f \cdot E_m} \qquad \frac{E_m \cdot E_f}{V_m \cdot E_f + V_f \cdot E_m} = 5.338$$

Obtaining $E_2 > 5.338$

To find an upper bound on the apparent Young's modulus, E, subjected to the bas uniaxial test specimen to an elongation εL where ε is the average strain and L is the specimen length, the internal strain field that corresponds to the average strain at tl boundaries of the specimen is:

$$\varepsilon_x = \varepsilon \qquad \varepsilon_y = \varepsilon_z = -\nu \cdot \varepsilon \qquad \gamma_{xy} = \gamma_{xz} = \gamma_{yz} = 0$$

$$\sigma_{xm} = \frac{1 - \nu_m - 2\nu_m \cdot \nu}{1 - \nu_m - 2\nu_m^2} \cdot E_m \cdot \varepsilon$$

$$\sigma_{ym} = \sigma_{zm} = \frac{\nu_m - \nu}{1 - \nu_m - 2\nu_m^2} \cdot E_m \cdot \varepsilon$$

$$\gamma_{xym} = \gamma_{xzm} = \gamma_{yzm} = 0$$

$$\sigma_{xf} = \frac{1 - \nu_f - 2\nu_f \cdot \nu}{1 - \nu_f - 2\nu_f^2} \cdot E_f \cdot \varepsilon$$

$$\sigma_{yf} = \sigma_{zf} = \frac{\nu_f - \nu}{1 - \nu_f - 2\nu_f^2} \cdot E_f \cdot \varepsilon$$

$$\gamma_{xyf} = \gamma_{xzf} = \gamma_{yzf} = 0$$

The strain engergy expression:

$$U' = \frac{1}{2} \cdot \int \left(\sigma_x \cdot \varepsilon_x + \sigma_y \cdot \varepsilon_y + \sigma_z \cdot \varepsilon_z + \tau_{xy} \cdot \gamma_{xy} + \tau_{yz} \cdot \gamma_{yz} + \tau_{xz} \cdot \gamma_{xz}\right) dV$$

$$U' = \frac{\varepsilon^2}{2} \cdot \int_{V_f \cdot V} \frac{1 - \nu_f - 4 \cdot \nu_f \cdot \nu + 2 \cdot \nu^2}{1 - \nu_f - 2\nu_f^2} \cdot E_f \, dV + \frac{\varepsilon^2}{2} \cdot \int_{V_m \cdot V} \frac{1 - \nu_m - 4 \cdot \nu_m \cdot \nu + 2 \cdot \nu^2}{1 - \nu_m - 2\nu_m^2} \cdot E_m \, dV$$

$$\frac{1}{2} \cdot E \cdot \varepsilon^2 \cdot V < \frac{\varepsilon^2}{2} \cdot \left(\frac{1 - \nu_f - 4 \cdot \nu_f \nu + 2\nu^2}{1 - \nu_f - 2\nu_f^2} \cdot E_f \cdot V_f + \frac{1 - \nu_m - 4 \cdot \nu_m \nu + 2\nu^2}{1 - \nu_m - 2\nu_m^2} \cdot E_m \cdot V_m \right) \cdot V$$

$$E < \frac{1 - \nu_f - 4 \cdot \nu_f \nu + 2\nu^2}{1 - \nu_f - 2\nu_f^2} \cdot E_f \cdot V_f + \frac{1 - \nu_m - 4 \cdot \nu_m \nu + 2\nu^2}{1 - \nu_m - 2\nu_m^2} \cdot E_m \cdot V_m$$

$$\nu := \frac{\left(1 - \nu_m - 2\nu_m^2\right) \cdot \nu_f \cdot E_f \cdot V_f + \left(1 - \nu_f - 2\nu_f^2\right) \nu_m \cdot E_m \cdot \left(1 - V_f\right)}{\left(1 - \nu_m - 2\nu_m^2\right) \cdot E_f \cdot V_f + \left(1 - \nu_f - 2\nu_f^2\right) E_m \cdot \left(1 - V_f\right)} \qquad \nu = 0.231$$

$$\frac{1 - \nu_f - 4 \cdot \nu_f \nu + 2\nu^2}{1 - \nu_f - 2\nu_f^2} \cdot E_f \cdot V_f + \frac{1 - \nu_m - 4 \cdot \nu_m \nu + 2\nu^2}{1 - \nu_m - 2\nu_m^2} \cdot E_m \cdot V_m = 32.469 \qquad E_2 < 32.469$$

Obtaining the upper and lower bounds of E2 $5.338 < E_2 < 32.469$

The value of Poisson's ratio ν, for the composite material is unknow at this stage of analysis so the upper bound on E is inspecific. In accordance with the principle of minimı potential energy, the expression for the strain energy U' must be minimized with respect the umspecified constant ν to specify the bound on E. The minimization procedure consis of determining where:

$$\frac{d}{d\nu}U' = 0 \qquad \frac{d^2}{d\nu^2}U' > 0$$

$$\frac{d}{d\nu}U' = \frac{\varepsilon^2 V}{2}\cdot\left(\frac{-4\nu_f + 4\nu}{1-\nu_f-2\nu_f^2}\cdot E_f\cdot V_f + \frac{-4\nu_m + 4\nu}{1-\nu_m-2\nu_m^2}\cdot E_m\cdot V_m\right)$$

$$\nu = \frac{\left(1-\nu_m-2\nu_m^2\right)\cdot\nu_f\cdot E_f\cdot V_f + \left(1-\nu_f-2\nu_f^2\right)\cdot\nu_m\cdot E_m\cdot V_m}{\left(1-\nu_m-2\nu_m^2\right)\cdot E_f\cdot V_f + \left(1-\nu_f-2\nu_f^2\right)\cdot E_m\cdot V_m}$$

$$\frac{d^2}{d\nu^2}U' = \frac{\varepsilon^2\cdot V}{2}\left(\frac{4E_f\cdot V_f}{1-\nu_f-2\nu_f^2} + \frac{4E_m\cdot V_m}{1-\nu_m-2\nu_m^2}\right)$$

$\frac{d^2}{d\nu^2}U'$ **always positive**

Lower and upper bounds of Shear Modulus G

1. Estimate the lower and upper bounds of Shear Modulus G12

To find a lower bound on the apparent Shear modulus, G12, load the pure shear stress test specimen with shear stress on 1-2 plane. The internal stress field that satisfies this loading and the stress equations of equilibrium is:

$$\sigma_x^{\,o} = \sigma_y^{\,o} = \sigma_z^{\,o} = \tau_{yz}^{\,o} = \tau_{zx}^{\,o} = 0 \qquad \tau_{xy}^{\,o} = \tau$$

$$U^0 = \frac{1}{2}\cdot\int_V \frac{\left(\tau_{xy}^{\,0}\right)^2}{G}\,dV = \frac{\tau^2}{2}\cdot\int_V \frac{1}{G}\,dV = \frac{\tau^2}{2}\cdot\left(\int_{V_m}\frac{1}{G_m}\,dV + \int_{V_f}\frac{1}{G_f}\,dV\right)$$

$$U^o = \frac{\tau^2}{2}\left(\frac{V_f}{G_f} + \frac{V_m}{G_m}\right)\cdot V$$

$$U = \frac{1}{2}\frac{\tau^2}{G}\cdot V$$

$$\frac{1}{G} < \frac{V_f}{G_f} + \frac{V_m}{G_m}$$

or

$$G > \frac{G_m\cdot G_f}{V_f\cdot G_m + V_m\cdot G_f} \qquad \frac{G_m\cdot G_f}{V_f\cdot G_m + V_m\cdot G_f} = 1.61$$

The lower bounds of G12 $G_{12} > 1.61$

To find an upper bound on the apparent shear modulus,G, subjecte the pure shear test specimen to an elongation εL where ε is the average strain and L is the specimen length, the internal strain field that corresponds to the average strain at the boundaries of the specimen is:

$$\varepsilon_x = \varepsilon_y = \varepsilon_z = \gamma_{xz} = \gamma_{yz} = 0 \qquad \gamma_{xy} = \gamma$$

$$\sigma_{xm} = \sigma_{ym} = \sigma_{zm} = \tau_{xzm} = \tau_{yzm} = 0 \qquad \tau_{xym} = G \cdot \gamma$$

$$U' = \frac{1}{2} \cdot \int G \cdot \gamma^2 \, dV = \frac{\gamma^2}{2} \cdot \int G \, dV$$

$$U' = \frac{\gamma^2}{2} \cdot \left(G_m \cdot V_m + G_f \cdot V_f\right) \cdot V$$

$$U = \frac{\gamma^2}{2} \cdot G \cdot V$$

$$G \le G_m \cdot V_m + G_f \cdot V_f \qquad G_m \cdot V_m + G_f \cdot V_f = 13.053$$

Obtaining the lower and upper bounds: $1.61 < G_{12} < 13.053$

2. Estimate the lower and upper bounds of the Shear Modulus G23

In order to be aware of the shear modulus of G23 of 2-3 plane, the poisson ratio in 2 direction $\nu 23$ has to be known first.

Assumption of $\nu 23$

$$\left|\nu_{23}\right| < \left(\frac{E_2}{E_3}\right)^{\frac{1}{2}}$$

The lower bounds of $\nu 23$

$$\left(\left|\nu_{23}\right|\right)^{lower} < \left(\frac{E_2^{\,lower}}{E_3^{\,upper}}\right)^{\frac{1}{2}}$$

The upper bounds of $\nu 23$

$$\left(\left|\nu_{23}\right|\right)^{upper} < \left(\frac{E_2^{\,upper}}{E_3^{\,lower}}\right)^{\frac{1}{2}}$$

Obtaining $\left(\left|\nu_{23}\right|\right)^{lower} = 0.405 \qquad \left(\left|\nu_{23}\right|\right)^{upper} = 2.466$

Obtaining $\left(\left|\nu_{23}\right|\right)^{lower} = 0.405$ $\left(\left|\nu_{23}\right|\right)^{upper} = 2.466$

Shear Modulus of 2-3 plane: $G_{23} = \dfrac{E_2}{2\left(1+\nu_{23}\right)}$

The upper bound of G23 $G_{23}^{upper} = \dfrac{E_2^{upper}}{2\left(1+\nu_{23}^{lower}\right)}$

The lower bound of G23 $G_{23}^{lower} = \dfrac{E_2^{lower}}{2\left(1+\nu_{23}^{upper}\right)}$

$G_{23}^{lower} = 0.769$ $G_{23}^{upper} = 11.555$

Obtaining the lower and upper bounds: $0.769 < G_{23} < 11.555$

Lower and upper bounds of Poisson ratio ν12

The lower and upper bound ν12. Having determined approximate valu for ν21, one may then approximate ν12 by the well-known relationship

$\nu_{12} := 0.29$

The lower bound of ν12 $\nu_{12}^{lower} = \nu_{12}\cdot(1-10\%)$ $\nu_{12}^{lower} = 0.261$

Modification of Transverse Modulus

$E_2 \cdot (1 + 10\%) = 9.659$ where $E_2 = 8.781$

Obtaining the modified transverse Modulus

$5.338 < E_2 < 9.659$

Modification of shear Modulus G23

The lower bound $G_{23}^{lower} = \dfrac{E_2^{lower}}{2(1 + \nu_{23})}$ Assumed $\nu_{23} := 0.3$

The upper bound $G_{23}^{upper} = \dfrac{E_2^{upper}}{2(1 + \nu_{23})}$

$\dfrac{32.469}{2(1 + 0.3)} = 12.488$ $G_{23}^{lower} = 2.053$

$\dfrac{5.338}{2(1 + 0.3)} = 2.053$ $G_{23}^{upper} = 12.488$

Obtaining the modified shear modulus G23

$2.053 < G_{23} < 12.488$

APPENDIX E

Basic FEM Modeling

```
/BATCH

! Parameters of material property
EXX=34.114E+09          !Input material parameters
EYY=7.7345E+09
EZZ=EYY
PRXYY=0.30951
PRYZZ=0.34
PRXZZ=PRXYY
GXYY=3.4677E+09
GYZZ=4.8252E+09
GXZZ=GXYY
t=3.98e-3               !Input the thickness of the coupon
tl=t/8                  !The thickness of each layer
L0=12.6E-03
r=3.2E-03
w1=19.2E-03
W=25.6E-03
h1=7.2E-03
h2=25.4E-03
H=50.8E-03
ASIZE1=3.5E-03          !Mesh size
ASIZE2=3.5E-03
ASIZE3=3.5E-03
testdata=-474.85812
/UNITS,SI

/PREP7

k,1000,L0,0,0,          !Define the keypoint
k,1001,L0+r,0,0,
k,1002,w1,0,0,
k,1003,W,0,0,
k,1004,0,r,0,
k,1005,L0,r,0,
k,1006,0,h1,0
k,1007,w1,h1,0,
k,1008,W,h1,0,
k,1009,0,h2,0,
k,1010,w1,h2,0,
k,1011,W,h2,0,
k,1012,0,H,0,
k,1013,w1,H,0,
k,1014,W,H,0,

k,3004,0,-r,0,
k,3005,L0,-r,0,
k,3006,0,-h1,0,
k,3007,w1,-h1,0,
k,3008,W,-h1,0,
k,3009,0,-h2,0,
k,3010,w1,-h2,0,
k,3011,W,-h2,0,
k,3012,0,-H,0,
k,3013,w1,-H,0,
k,3014,W,-H,0,


larc,1005,1001,1000,r   !Define the lines by connecting the keypoints
```

```
l,1004,1005
l,1001,1002
l,1002,1003
l,1006,1007
l,1007,1008
l,1009,1010
l,1010,1011
l,1012,1013
l,1013,1014
l,1004,1006
l,1005,1007
l,1002,1007
l,1003,1008
l,1006,1009
l,1007,1010
l,1008,1011
l,1012,1009
l,1010,1013
l,1014,1011

l,3004,3005
larc,3005,1001,1000,r
l,3006,3007
l,3007,3008
l,3009,3010
l,3010,3011
l,3012,3013
l,3013,3014
l,3004,3006
l,3005,3007
l,3006,3009
l,1002,3007
l,3007,3010
l,1003,3008
l,3008,3011
l,3009,3012
l,3010,3013
l,3011,3014

al,11,2,12,5            !Define the areas
al,12,1,3,13
al,13,4,14,6
al,15,5,16,7
al,16,6,17,8
al,18,7,19,9
al,19,8,20,10


al,21,29,23,30
al,22,30,32,3
al,32,24,34,4
al,31,25,33,23
al,24,33,26,35
al,36,27,37,25
al,37,28,38,26


! INPUT MATERIAL PROPERTY
MP, EX,1,EXX            !Define the material properties of the composite
MP, EY,1,EYY
MP,EZ,1,EZZ
```

```
MP,PRXY,1,PRXYY
MP,PRYZ,1,PRYZZ
MP,PRXZ,1,PRXZZ
MP,GXY,1,GXYY
MP,GXZ,1,GXYY
MP,GYZ,1,GYZZ

MP,EX,2,2E13            !Define the grip properties
MP,PRXY,2,0.3

! MESHING
ET,1,MESH200            !Select element type MESH200
KEYOPT,1,1,6
KEYOPT,1,2,0
ET,2, SOLID46
!KEYOPT,1,1,6
!KEYOPT,1,2,0
KEYOPT,2,8,1
R,1                     !Define the real constants
RMODIF,1,1,8,0,0,0
RMODIF,1,7,0
RMODIF,1,13,1,0,tl,1,+45,tl,   !Define the thickness of each layer of the composite
RMODIF,1,19,1,90,tl,1,-45,tl,
RMODIF,1,25,1,-45,tl,1,90,tl,
RMODIF,1,31,1,+45,tl,1,0,tl,
ET,13,SOLID45

AESIZE,1,ASIZE1         ! Mesh selected areas
MSHAPE,0,2D
MSHKEY,1
AMESH,1
AESIZE,2,ASIZE2
MSHAPE,0,2D
MSHKEY,1
AMESH,2
AESIZE,3,ASIZE2
MSHAPE,0,2D
MSHKEY,1
AMESH,3
AESIZE,4,ASIZE1
MSHAPE,0,2D
MSHKEY,1
AMESH,4
AESIZE,5,ASIZE1
MSHAPE,0,2D
MSHKEY,1
AMESH,5
AESIZE,6,ASIZE1
MSHAPE,0,2D
MSHKEY,1
AMESH,6
AESIZE,7,ASIZE1
MSHAPE,0,2D
MSHKEY,1
AMESH,7
AESIZE,8,ASIZE1
MSHAPE,0,2D
MSHKEY,1
AMESH,8
AESIZE,9,ASIZE2
MSHAPE,0,2D
```

```
MSHKEY,1
AMESH,9
AESIZE,10,ASIZE2
MSHAPE,0,2D
MSHKEY,1
AMESH,10
AESIZE,11,ASIZE1
MSHAPE,0,2D
MSHKEY,1
AMESH,11
AESIZE,12,ASIZE1
MSHAPE,0,2D
MSHKEY,1
AMESH,12
AESIZE,13,ASIZE1
MSHAPE,0,2D
MSHKEY,1
AMESH,13
AESIZE,14,ASIZE1
MSHAPE,0,2D
MSHKEY,1
AMESH,14

K,2014,W,H,-t
L,1014,2014
EXTOPT,ACLEAR,1              !Mesh the volume
TYPE, 2
VDRAG,ALL,,,,,,39
EXTOPT,ACLEAR,0
!/ESHAPE, 1
!/DSCALE, 1, AUTO

!Build up the grips
BLOCK,0 ,W,h2,H,0,5E-3       !Model the grip's geometry
BLOCK,0 ,W,h2,H,-t,-5E-03-t
BLOCK,0,W,-h2,-H,0,5E-03
BLOCK,0,W,-h2,-H,-t,-5E-03-t
ESIZE,ASIZE3,1
MAT, 2
TYPE,13
VMESH,15,16
VMESH,17,18

!Contact ELement
ASEL, ,,,13,14,,1      !Define and Select the contact surface.
CM,TARGET1,NODE
ALLS
ASEL, ,,,79,,,1
CM,CONTACT1,NODE
ALLS
ASEL, ,,,63,66,66-63,1
CM,TARGET2,NODE
ALLS
ASEL, ,,,86,,,1
CM,CONTACT2,NODE
ALLS
ASEL, ,,,38,41,41-38,1
CM,TARGET3,NODE
ALLS
ASEL, ,,,74,,,1
CM,CONTACT3,NODE
```

```
ALLS
ASEL, ,,,6,7,,1
CM,TARGET4,NODE
ALLS
ASEL, ,,,67,,,1
CM,CONTACT4,NODE
ALLS
/COM, CONTACT PAIR CREATION - START
CM,_NODECM,NODE
CM,_ELEMCM,ELEM
CM,_LINECM,LINE
CM,_AREACM,AREA
/GSAV,cwz,gsav,,temp
MP,MU,1,0.2
MAT,1
MP,EMIS,1,7.88860905221e-31
R,3
REAL,3
ET,14,170
ET,15,174
R,3,,,1.0,0.1,0,
RMORE,,,1.0E20,0.0,1.0,
RMORE,0.0,0,1.0,,1.0,0.5
RMORE,0,0.5,1.0,0.0,
KEYOPT,15,2,0
KEYOPT,15,4,0
KEYOPT,15,5,0
KEYOPT,15,7,0
KEYOPT,15,8,0
KEYOPT,15,9,0
KEYOPT,15,10,0
KEYOPT,15,11,0
KEYOPT,15,12,5
! Generate the target surface
NSEL,S,,,TARGET1
CM,_TARGET,NODE
TYPE,14
ESLN,S,0
ESURF,ALL
CMSEL,S,_ELEMCM
! Generate the contact surface
NSEL,S,,,CONTACT1
CM,_CONTACT,NODE
TYPE,15
ESLN,S,0
ESURF,ALL
ALLSEL
ESEL,ALL
ESEL,S,TYPE,,14
ESEL,A,TYPE,,15
ESEL,R,REAL,,3
/PSYMB,ESYS,1
/PNUM,TYPE,1
/NUM,1
EPLOT
ESEL,ALL
ESEL,S,TYPE,,14
ESEL,A,TYPE,,15
ESEL,R,REAL,,3
CMSEL,A,_NODECM
CMDEL,_NODECM
```

```
CMSEL,A,_ELEMCM
CMDEL,_ELEMCM
CMSEL,S,_LINECM
CMDEL,_LINECM
CMSEL,S,_AREACM
CMDEL,_AREACM
/GRES,cwz,gsav
CMDEL,_TARGET
CMDEL,_CONTACT
/COM, CONTACT PAIR CREATION - END
/COM, CONTACT PAIR CREATION - START
CM,_NODECM,NODE
CM,_ELEMCM,ELEM
CM,_LINECM,LINE
CM,_AREACM,AREA
/GSAV,cwz,gsav,,temp
MP,MU,1,0.2
MAT,1
MP,EMIS,1,7.88860905221e-31
R,4
REAL,4
ET,16,170
ET,17,174
R,4,,,1.0,0.1,0,
RMORE,,,1.0E20,0.0,1.0,
RMORE,0.0,0,1.0,,1.0,0.5
RMORE,0,0.5,1.0,0.0,
KEYOPT,17,2,0
KEYOPT,17,4,0
KEYOPT,17,5,0
KEYOPT,17,7,0
KEYOPT,17,8,0
KEYOPT,17,9,0
KEYOPT,17,10,0
KEYOPT,17,11,0
KEYOPT,17,12,5
! Generate the target surface
NSEL,S,,,TARGET2
CM,_TARGET,NODE
TYPE,16
ESLN,S,0
ESURF,ALL
CMSEL,S,_ELEMCM
! Generate the contact surface
NSEL,S,,,CONTACT2
CM,_CONTACT,NODE
TYPE,17
ESLN,S,0
ESURF,ALL
ALLSEL
ESEL,ALL
ESEL,S,TYPE,,16
ESEL,A,TYPE,,17
ESEL,R,REAL,,4
/PSYMB,ESYS,1
/PNUM,TYPE,1
/NUM,1
EPLOT
ESEL,ALL
ESEL,S,TYPE,,16
ESEL,A,TYPE,,17
```

```
ESEL,R,REAL,,4
CMSEL,A,_NODECM
CMDEL,_NODECM
CMSEL,A,_ELEMCM
CMDEL,_ELEMCM
CMSEL,S,_LINECM
CMDEL,_LINECM
CMSEL,S,_AREACM
CMDEL,_AREACM
/GRES,cwz,gsav
CMDEL,_TARGET
CMDEL,_CONTACT
/COM, CONTACT PAIR CREATION - END
/COM, CONTACT PAIR CREATION - START
CM,_NODECM,NODE
CM,_ELEMCM,ELEM
CM,_LINECM,LINE
CM,_AREACM,AREA
/GSAV,cwz,gsav,,temp
MP,MU,1,0.2
MAT,1
MP,EMIS,1,7.88860905221e-31
R,5
REAL,5
ET,18,170
ET,19,174
R,5,,,1.0,0.1,0,
RMORE,,,1.0E20,0.0,1.0,
RMORE,0.0,0,1.0,,1.0,0.5
RMORE,0,0.5,1.0,0.0,
KEYOPT,19,2,0
KEYOPT,19,4,0
KEYOPT,19,5,0
KEYOPT,19,7,0
KEYOPT,19,8,0
KEYOPT,19,9,0
KEYOPT,19,10,0
KEYOPT,19,11,0
KEYOPT,19,12,5
! Generate the target surface
NSEL,S,,,TARGET3
CM,_TARGET,NODE
TYPE,18
ESLN,S,0
ESURF,ALL
CMSEL,S,_ELEMCM
! Generate the contact surface
NSEL,S,,,CONTACT3
CM,_CONTACT,NODE
TYPE,19
ESLN,S,0
ESURF,ALL
ALLSEL
ESEL,ALL
ESEL,S,TYPE,,18
ESEL,A,TYPE,,19
ESEL,R,REAL,,5
/PSYMB,ESYS,1
/PNUM,TYPE,1
/NUM,1
EPLOT
```

```
ESEL,ALL
ESEL,S,TYPE,,18
ESEL,A,TYPE,,19
ESEL,R,REAL,,5
CMSEL,A,_NODECM
CMDEL,_NODECM
CMSEL,A,_ELEMCM
CMDEL,_ELEMCM
CMSEL,S,_LINECM
CMDEL,_LINECM
CMSEL,S,_AREACM
CMDEL,_AREACM
/GRES,cwz,gsav
CMDEL,_TARGET
CMDEL,_CONTACT
/COM, CONTACT PAIR CREATION - END
/COM, CONTACT PAIR CREATION - START
CM,_NODECM,NODE
CM,_ELEMCM,ELEM
CM,_LINECM,LINE
CM,_AREACM,AREA
/GSAV,cwz,gsav,,temp
MP,MU,1,0.2
MAT,1
MP,EMIS,1,7.88860905221e-31
R,6
REAL,6
ET,20,170
ET,21,174
R,6,,,1.0,0.1,0,
RMORE,,,1.0E20,0.0,1.0,
RMORE,0.0,0,1.0,,1.0,0.5
RMORE,0,0.5,1.0,0.0,
KEYOPT,21,2,0
KEYOPT,21,4,0
KEYOPT,21,5,0
KEYOPT,21,7,0
KEYOPT,21,8,0
KEYOPT,21,9,0
KEYOPT,21,10,0
KEYOPT,21,11,0
KEYOPT,21,12,5
! Generate the target surface
NSEL,S,,,TARGET4
CM,_TARGET,NODE
TYPE,20
ESLN,S,0
ESURF,ALL
CMSEL,S,_ELEMCM
! Generate the contact surface
NSEL,S,,,CONTACT4
CM,_CONTACT,NODE
TYPE,21
ESLN,S,0
ESURF,ALL
ALLSEL
ESEL,ALL
ESEL,S,TYPE,,20
ESEL,A,TYPE,,21
ESEL,R,REAL,,6
/PSYMB,ESYS,1
```

```
/PNUM,TYPE,1
/NUM,1
EPLOT
ESEL,ALL
ESEL,S,TYPE,,20
ESEL,A,TYPE,,21
ESEL,R,REAL,,6
CMSEL,A,_NODECM
CMDEL,_NODECM
CMSEL,A,_ELEMCM
CMDEL,_ELEMCM
CMSEL,S,_LINECM
CMDEL,_LINECM
CMSEL,S,_AREACM
CMDEL,_AREACM
/GRES,cwz,gsav
CMDEL,_TARGET
CMDEL,_CONTACT
/COM, CONTACT PAIR CREATION - END


!Apply Loads
/SOL
DA,81,ALL,0
DA,87,ALL,0
!forcey=5.1816E+03
displacement=0.00074
place=-0.00004
alls
vsel, ,,,15,16,,1
cp,NEXT,all,all

/com,applying specified constraint on the master node
*get,numn,node,0,num,min     ! Finding the first node number on the list
D,numn,UY,displacement
D,numn,UX,place
D,numn,UZ,0
alls

!Step loads
/AUTOTS,ON
/SOLCONTROL, OFF
DELTIM,1,1,5

/STATUS,SOLU
EQSLV,PCG
SOLV

/POST1
PLNSOL, S, EQV
VSEL,,LOC,Y,-100, KY(30),,1
NFORCE                      ! Sums and prints, in each component
                            !direction for each selected node,
                            !the nodal force and moment
                            ! contributions of the selected
                            !elements attached to the node.
NSEL,,,,59
ESLN,r,0                    !Selects those elements attached to
                            !the selected nodes
FSUM                        !Sums the nodal force and moment
                            !contributions of elements
```

```
*GET, FORCEY, FSUM,,ITEM,FY   !Obtain the tensile force
*GET, FORCEX, FSUM,,ITEM,FX   !Obtain the shear force
*GET, MOMENT, FSUM,,ITEM,MZ   !Obtain the moment
Objective=abs(FORCEY-testdata)
```

APPENDIX F

Optimization modeling using ANSYS

```
! Optimization
/OPT
OPANL,'amodeltensile','inp',''
OPVAR,EXX,DV,29.119E+09,35.589E+09     ! Define the design variable
OPVAR,EYY,DV,5.338E+09,9.659E+09
OPVAR,GXYY,DV,1.61E+09,5.5E+09
OPVAR,GYZZ,DV,2.053E+09,5.5E+09
OPVAR,PRXYY,DV,0.261,0.319
OPVAR,FORCEY,SV,-1.2E+4,0              ! Define the state variable
OPVAR,Objective,OBJ,,,0                ! Define the objective function

! RUN THE OPTIMIZATION
OPKEEP,ON

!Random method
OPTYPE,RAND
OPRAND,30,29

!First order gradient method
OPTYPE,FIRS
OPFRST,91,5,1,

!Sub-problem approximation method
OPTYPE,SUBP
OPSUBP,100,99
OPEQN,0,0,0,0,0
OPSAVE,'amodeltensile','opt0',''
OPEXE

! REVIEW RESULTS
OPLIST,ALL,,,1
PLVAROP,EXX,EYY,GXYY,GYZZ,PRXYY
PLVAROPT,FORCEY
PLVAROPT,Objective
FINISH
```

APPENDIX G

Parameters from MSU Database

Table Physical 3-D Constants of Material D155, Vf=36% and 44%

Physical constants of Material D155, Vf=36%			
Property and test plan	Test Values	Average	Standard Deviation
El, Gpa (LT plane)	28.1, 27.0, 29.8	28.3	1.4
El, Gpa (LZ plane)	28.0, 28.3, 27.6	28.0	0.4
Et, Gpa (TZ plane)	8.00, 7.31, 7.93	7.75	0.38
Ez, Gpa (ZX plane)	7.10, 7.65, 7.38	7.38	0.28
NUlt	0.329, 0.320, 0.301	0.32	0.01
NUlz	0.305, 0.338, 0.331	0.33	0.02
NUtz	0.466, 0.395, 0.449	0.44	0.04
Glt, GPa	3.31, 3.35, 3.23	3.30	0.06
Glz, GPa	3.03, 2.72, 2.70	2.82	0.19
Gtz, GPa	2.78, 3.12, 1.76	2.55	0.71
Physical constants of Material D155, Vf=44%			
Property and test plan	Test Values	Average	Standard Deviation
El, Gpa (LT plane)	31.9, 35.4, 33.6	33.6	1.8
El, Gpa (LZ plane)	34.5, 34.3, 34.5	34.4	0.1
Et, Gpa (TZ plane)	8.14, 8.96, 7.52	8.21	0.72
Ez, Gpa (ZX plane)	7.58, 8.00, 8.00	7.86	0.24
NUlt	0.289, 0.291, 0.290	0.29	0.01
NUlz	0.302, 0.314, 0.308	0.31	0.01
NUtz	0.373, 0.371, 0.366	0.37	0.01
Glt, GPa	5.76, 3.94, 3.74	4.48	1.11
Glz, GPa	3.88, 4.40, 3.07	3.78	0.67
Gtz, GPa	2.96, 2.70, 2.20	2.62	0.39

APPENDIX H

Optimization Results

The pure tensile test, sub-problem approximation method

LIST OPTIMIZATION SETS FROM SET 1 TO SET 18 AND SHOW ONLY OPTIMIZATION PARAMETERS. (A "*" SYMBOL IS USED TO INDICATE THE BEST LISTED SET)

	SET 13 (FEASIBLE)	SET 14 (FEASIBLE)	SET 15 (FEASIBLE)	*SET 16* (FEASIBLE)
FORCEY (SV)	-453.18	-463.01	-494.84	-474.06
EXX (DV)	0.32720E+11	0.32595E+11	0.33477E+11	0.32824E+11
EYY (DV)	0.57299E+10	0.74039E+10	0.89478E+10	0.72772E+10
GXYY (DV)	0.49676E+10	0.54898E+10	0.54900E+10	0.53741E+10
GYZZ (DV)	0.35571E+10	0.22311E+10	0.31761E+10	0.33664E+10
PRXYY (DV)	0.28016	0.27507	0.30764	0.26175
OBJECTIVE(OBJ)	21.675	11.847	19.987	0.79334

The pure tensile test, first order gradient method

LIST OPTIMIZATION SETS FROM SET 1 TO SET 11 AND SHOW ONLY OPTIMIZATION PARAMETERS. (A "*" SYMBOL IS USED TO INDICATE THE BEST LISTED SET)

	SET 9 (FEASIBLE)	*SET 10* (FEASIBLE)	SET 11 (FEASIBLE)
FORCEY (SV)	-472.91	-474.86	-474.86
EXX (DV)	0.34610E+11	0.34654E+11	0.34654E+11
EYY (DV)	0.79442E+10	0.79627E+10	0.79627E+10
GXYY (DV)	0.40956E+10	0.41482E+10	0.41482E+10
GYZZ (DV)	0.48969E+10	0.49035E+10	0.49035E+10
PRXYY (DV)	0.30964	0.30965	0.30965
OBJECTIVE(OBJ)	1.9499	0.99700E-04	0.28825E-03

The tensile plus shear test, sub-problem approximation method

LIST OPTIMIZATION SETS FROM SET 1 TO SET 7 AND SHOW ONLY OPTIMIZATION PARAMETERS. (A "*" SYMBOL IS USED TO INDICATE THE BEST LISTED SET)

	SET 5 (FEASIBLE)	SET 6 (FEASIBLE)	SET 7 (FEASIBLE)
FORCEY (SV)	-303.74	-303.74	-303.74
EXX (DV)	0.34542E+11	0.34542E+11	0.34542E+11
EYY (DV)	0.88839E+10	0.88839E+10	0.88839E+10
GXYY (DV)	0.40883E+10	0.40883E+10	0.40882E+10

GYZZ (DV)	0.35150E+10	0.35150E+10	0.35150E+10
PRXYY (DV)	0.31371	0.31371	0.31371
OBJECTIVE(OBJ)	0.12403E-06	0.16959E-04	0.34042E-04

The tensile plus shear test, the first order gradient method

LIST OPTIMIZATION SETS FROM SET 1 TO SET 7 AND SHOW ONLY OPTIMIZATION PARAMETERS. (A "*" SYMBOL IS USED TO INDICATE THE BEST LISTED SET)

	SET 5 (FEASIBLE)	SET 6 (FEASIBLE)	SET 7 (FEASIBLE)
FORCEY (SV)	-303.74	-303.74	-303.74
EXX (DV)	0.34542E+11	0.34542E+11	0.34542E+11
EYY (DV)	0.88839E+10	0.88839E+10	0.88839E+10
GXYY (DV)	0.40883E+10	0.40883E+10	0.40882E+10
GYZZ (DV)	0.35150E+10	0.35150E+10	0.35150E+10
PRXYY (DV)	0.31371	0.31371	0.31371
OBJECTIVE(OBJ)	0.12403E-06	0.16959E-04	0.34042E-04

The pure rotation test, the sub-problem approximation method

LIST OPTIMIZATION SETS FROM SET 1 TO SET 26 AND SHOW ONLY OPTIMIZATION PARAMETERS. (A "*" SYMBOL IS USED TO INDICATE THE BEST LISTED SET)

	SET 9 (FEASIBLE)	SET 10 (FEASIBLE)	SET 11 (FEASIBLE)	SET 12 (FEASIBLE)
FORCEY (SV)	-319.21	-326.46	-250.31	-294.31
EXX (DV)	0.34078E+11	0.35219E+11	0.30139E+11	0.31487E+11
EYY (DV)	0.59795E+10	0.70584E+10	0.54764E+10	0.61554E+10
GXYY (DV)	0.54832E+10	0.54903E+10	0.26354E+10	0.39802E+10
GYZZ (DV)	0.25151E+10	0.21722E+10	0.21836E+10	0.47103E+10
PRXYY (DV)	0.26334	0.26169	0.26948	0.26619
OBJECTIVE(OBJ)	1.0620	6.1825	69.959	25.958

The pure rotation test, first order gradient method

LIST OPTIMIZATION SETS FROM SET 1 TO SET 17 AND SHOW ONLY OPTIMIZATION PARAMETERS. (A "*" SYMBOL IS USED TO INDICATE THE BEST LISTED SET)

	SET 13 (FEASIBLE)	SET 14 (FEASIBLE)	SET 15 (FEASIBLE)	*SET 16* (FEASIBLE)
FORCEY (SV)	-317.42	-318.36	-319.24	-320.08
EXX (DV)	0.32971E+11	0.33006E+11	0.33039E+11	0.33070E+11
EYY (DV)	0.73637E+10	0.73779E+10	0.73915E+10	0.74045E+10

GXYY (DV)	0.46902E+10	0.47307E+10	0.47692E+10	0.48057E+10
GYZZ (DV)	0.40260E+10	0.40339E+10	0.40414E+10	0.40486E+10
PRXYY (DV)	0.29387	0.29387	0.29388	0.29388
OBJECTIVE(OBJ)	2.8480	1.9162	1.0316	0.19190

The superposed test, first order gradient method

LIST OPTIMIZATION SETS FROM SET 1 TO SET 17 AND SHOW ONLY OPTIMIZATION PARAMETERS. (A "*" SYMBOL IS USED TO INDICATE THE BEST LISTED SET)

	SET 13 (FEASIBLE)	SET 14 (FEASIBLE)	*SET 15* (FEASIBLE)	SET 16 (FEASIBLE)
FORCEY (SV)	-608.44	-608.53	-610.65	-610.65
EXX (DV)	0.31939E+11	0.31942E+11	0.32068E+11	0.32068E+11
EYY (DV)	0.83700E+10	0.83713E+10	0.84344E+10	0.84344E+10
GXYY (DV)	0.49644E+10	0.49662E+10	0.49662E+10	0.49662E+10
GYZZ (DV)	0.23737E+10	0.23741E+10	0.23924E+10	0.23924E+10
PRXYY (DV)	0.30650	0.30650	0.30657	0.30657
OBJECTIVE(OBJ)	2.2132	2.1244	0.43678E-05	0.18206E-04

The superposed test, sub-problem method

LIST OPTIMIZATION SETS FROM SET 1 TO SET 19 AND SHOW ONLY OPTIMIZATION PARAMETERS. (A "*" SYMBOL IS USED TO INDICATE THE BEST LISTED SET)

	SET 13 (FEASIBLE)	SET 14 (FEASIBLE)	SET 15 (FEASIBLE)	*SET 16* (FEASIBLE)
FORCEY (SV)	-198.98	-204.18	-198.79	-197.65
EXX (DV)	0.35370E+11	0.35520E+11	0.35521E+11	0.35371E+11
EYY (DV)	0.70474E+10	0.72956E+10	0.73504E+10	0.71355E+10
GXYY (DV)	0.45303E+10	0.48685E+10	0.44163E+10	0.44535E+10
GYZZ (DV)	0.33346E+10	0.45126E+10	0.32508E+10	0.29060E+10
PRXYY (DV)	0.31768	0.31863	0.27260	0.28724
OBJECTIVE(OBJ)	1.2956	6.4945	1.0998	0.32522E-01

APPENDIX I

Flow Chart of Data Analysis

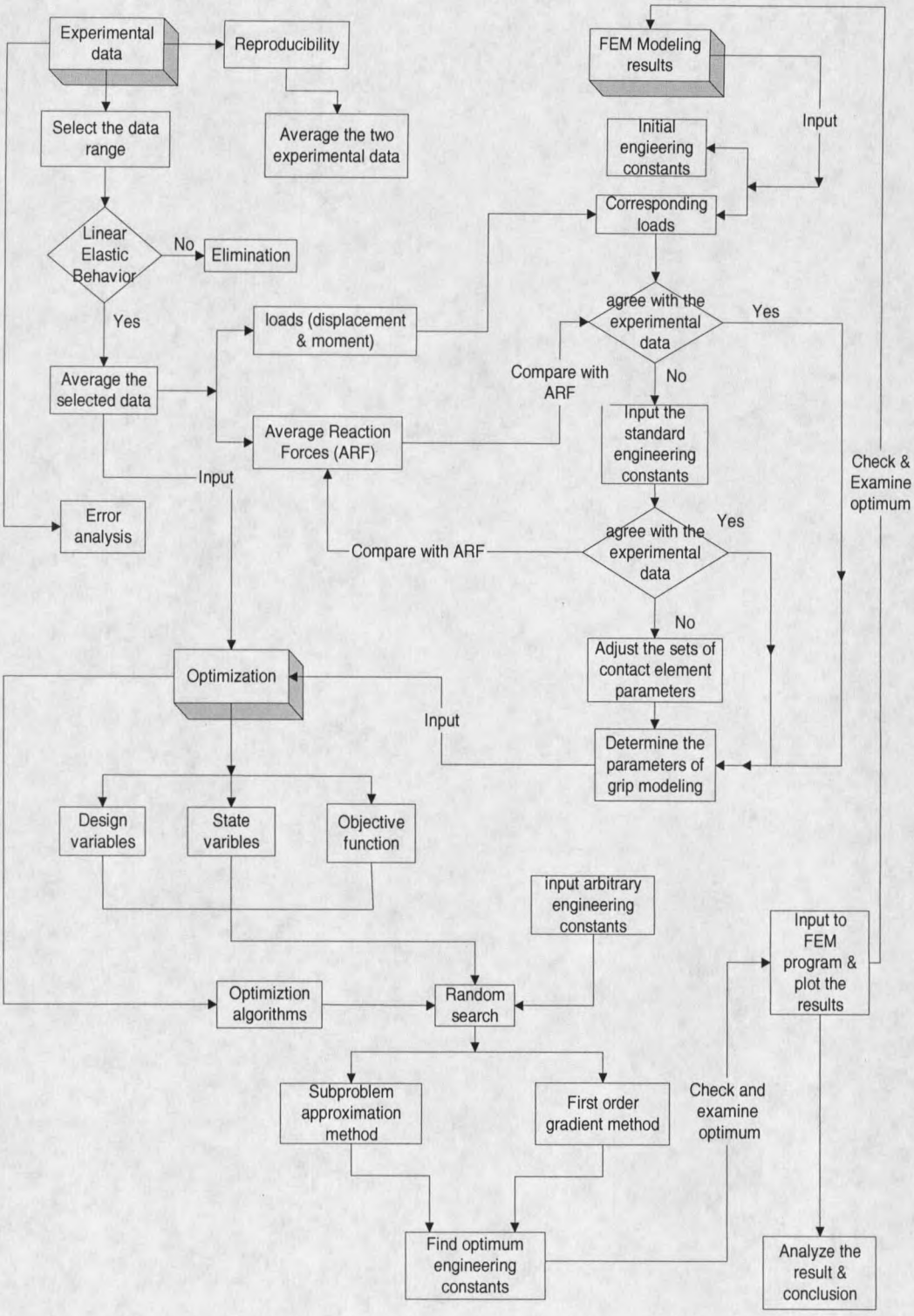
Experimental data
Reproducibility
Select the data range
Average the two experimental data
Linear Elastic Behavior
No
Elimination
Yes
Average the selected data
loads (displacement & moment)
Average Reaction Forces (ARF)
Input
Error analysis
Compare with ARF
FEM Modeling results
Input
Initial engieering constants
Corresponding loads
agree with the experimental data
Yes
No
Input the standard engineering constants
agree with the experimental data
Yes
No
Compare with ARF
Adjust the sets of contact element parameters
Determine the parameters of grip modeling
Check & Examine optimum
Optimization
Input
Design variables
State varibles
Objective function
input arbitrary engineering constants
Optimiztion algorithms
Random search
Subproblem approximation method
First order gradient method
Find optimum engineering constants
Check and examine optimum
Input to FEM program & plot the results
Analyze the result & conclusion